SEISMIC RETROFIT OF REINFORCED CONCRETE SHEAR WALLS USING FIBRE REINFORCED POLYMER COMPOSITES

Hossam El-Sokkary

A Thesis

in

The Department of

Building, Civil and Environmental Engineering

Presented in Partial Fulfillment of the Requirements

For the Degree of

Doctor of Philosophy (Civil Engineering) at

CONCORDIA UNIVERSITY

Montréal, Québec, Canada

July 2012

CONCORDIA UNIVERSITY

School of Graduate Studies

This is to certify that the thesis prepared

By: Hossam El-Sokkary

Entitled: **Seismic Retrofit of Reinforced Concrete Shear Walls using Fibre Reinforced Polymer Composites**

and submitted in partial fulfillment of the requirements for the degree of

Doctor of Philosophy (Civil Engineering)

complies with the regulations of the University and meets the accepted standards with respect to originality and quality.

Signed by the final examining committee:

_____ Chair
Dr. R. Raut

_____ External Examiner
Dr. S. Rizkalla

_____ External to Program
Dr. M. Pugh

_____ Examiner
Dr. A. Bagchi

_____ Examiner
Dr. L. Tirca

_____ Thesis Supervisor
Dr. K. Galal

Approved by

_____
Dr. Maria Elektorowicz, GPD
Department of Building, Civil and Environmental Engineering

_____
Dr. R. Drew, Dean
Faculty of Engineering and Computer Science

Date _____

ABSTRACT

SEISMIC RETROFIT OF REINFORCED CONCRETE SHEAR WALLS USING FIBRE REINFORCED POLYMER COMPOSITES

Hossam El-Sokkary, Ph.D.
Concordia University, 2012.

In the past few decades, there have been considerable advancements in the design of reinforced concrete (RC) shear walls for new construction, such as performance-based seismic design and capacity design principles. These advancements have resulted in a concurrent need for upgrading the seismic performance of existing RC shear walls so that they can meet the safety requirements of modern seismic design codes. As such, there is a need to retrofit existing RC structural shear walls to increase their capacity at locations of higher seismic demands. These upgrades could be at the plastic hinge zone at the base of a wall, or at higher stories due to the effects of higher modes of vibration.

This research aims to evaluate the effectiveness of using externally bonded carbon fibre-reinforced polymers (CFRP) in the seismic retrofit of RC shear walls. The research program comprises three phases. First, the testing of two 8-storey RC shear walls rehabilitated using CFRP composites under dynamic excitation. The walls were designed according to the NBCC 2005 and the CSA-A23.3-04. The walls were first tested under a simulated earthquake excitation using the shake table at the École Polytechnique de Montréal, where they experienced higher demands and nonlinearity at the sixth storey panel due to the effect of higher modes of vibrations. The tested walls were rehabilitated at the ground and at the sixth-storey level and retested on the shake table when subjected to several levels of ground motion excitation. In the second phase, three RC shear wall

panels were tested under cyclic lateral excitation at the Structures Laboratory of Concordia University. The tested wall panels represent the control wall and two FRP-retrofitted panels using two different retrofit schemes. All three wall panels had reinforcement details similar to those of the sixth-storey panel of the code-designed 8-storey shear walls from the first phase. The walls were tested when subjected to a constant axial load along with synchronized cyclic moment and shear force at the top of the tested panel. The main purpose of the FRP-retrofit schemes was to increase the flexural and shear capacities of the tested wall panels and to assess the effectiveness of the FRP-retrofit schemes up to failure. In the third phase, a numerical macro-model was proposed to simulate the behaviour of the control and the retrofitted wall panels tested under cyclic loading.

The experimental test results of the FRP-retrofit schemes used in the two 8-storey RC shear walls and the three RC wall panels showed a satisfactory performance with improved flexural strength; the testing showed that the main retrofit objectives were achieved. The nonlinear numerical macro-model was able to simulate the monotonic and cyclic behaviour of the wall panels tested under cyclic loading.

ACKNOWLEDGEMENTS

I would like to express my sincere gratitude to my supervisor, Dr. Khaled Galal, for his continued guidance, support, encouragement and helpful advice throughout my Masters and Ph.D. research. His efforts in reviewing and correcting this dissertation drafts are greatly appreciated.

The financial support of Le fonds Québécois de la recherche sur la nature et les technologies (FQRNT) through the Team research project led by Professor Pierre Léger of École Polytechnique de Montréal, and the Natural Science and Engineering Research Council (NSERC) of Canada are greatly appreciated. Fyfe Co. LLC is also acknowledged for donating the FRP composite material used for this research. Encouraging awards from Concordia University are also acknowledged.

I would like to thank everyone who helped me during my experimental program, namely: Hany, Mossab, Arash, Mohamed, Ricky, Bassem, Michael, David, Abdallah, Ali Aljassim. I wish also to thank Dr. Mohamed Elnady for his valuable advice during the cyclic tests.

Finally, I dedicate this thesis to my parents, my brother and my sister for their invaluable support during my study. Their presence really encouraged me to achieve my goals and to work hard on my research.

To my beloved parents

TABLE OF CONTENTS

LIST OF FIGURES

LIST OF TABLES

LIST OF SYMBOLS

A_i	Area represented by the spring
A_{frp}	Fibre cross sectional area
A/V	Peak ground acceleration-to-peak ground velocity ratio
E_{frp}	Modulus of elasticity for fibre composite material
E_i	Material's modulus of elasticity
f_c'	Concrete characteristic strength
f_t	Concrete tensile strength
f_y	Steel yield strength
h	Wall height
H_m	Height of the model
H_p	Height of the prototype
K_o	Initial stiffness of spring
K_e	Wall stiffness at yield
K_{pp}	Post-peak degradation stiffness
L_o	Clear length of the member
ℓ_u	Wall unsupported height
M	Storey overturning moment or moment demand
M_f	Factored moment demand
M_n	Nominal flexural resistance
M_r	Factored flexural resistance
M/VL	Moment-to-shear ratio
R	Force resultant in the FRP anchor

R_d	Ductility-related force modification factor
R_o	Overstrength-related force modification factor
S_E	Similitude ratio for modulus of elasticity
S_F	Similitude ratio for force
S_L	Similitude ratio for length
S_M	Similitude ratio for mass
S_T	Similitude ratio for time
V	Storey shear force
V_c	Concrete contribution to the nominal shear strength
V_d	Wall design load capacity
V_e	Elastic lateral load
V_u	Ultimate load capacity
α	Parameter for curvature variation along the wall height
β	Post-yielding parameter
Δ	Wall displacement
Δ_{ep}	Wall idealized yield displacement
Δ_s	Wall shear displacement
Δ_y	Wall yield displacement
$\Delta_{0.8u}$	Wall displacement corresponding to 20% strength degradation
ε_c	Concrete material strain
ε_{frp}	FRP strain
ε_{net}	Equivalent net strain of the FRP strips
ε_s	Steel material strain
ε_{sy}	Steel material yield strain

Φ	Parameter to direct the unloading
Φ_{frp}	FRP material resistance factor
γ	Unloading stiffness degradation parameter
η	Ratio of the plastic zone length to the member clear length
λ	Post-peak residual strength-to-maximum compressive strength ratio
μ	ultimate strain-to-strain at maximum compressive strength ratio
μ_{Δ}	Displacement ductility
μ_{θ}	Rotational ductility
$\boldsymbol{\nu}, \boldsymbol{\kappa}$	Skeleton curve parameters for steel model
θ	Unloading control parameter, rotational demand, or wall top rotation
σ_c	Concrete material compressive strength
σ_{sy}	Steel material yield stress
τ	Tension descending part after tension crack

CHAPTER 1

INTRODUCTION

1.1 GENERAL

Reinforced concrete (RC) walls are classified according to the Canadian Standard CSA-A23.3 (2004) as bearing walls, non-bearing walls, shear walls, flexural shear walls, and squat shear walls. Shear walls are part of the lateral force resisting system that carry vertical loads, bending moments about the wall strong axis, and shear forces parallel to the wall length. RC shear walls are widely used in medium- to high-rise buildings to provide the lateral strength, stiffness and energy dissipation capacity required to resist lateral loads arising from wind or earthquakes. In the past few decades, there has been considerable advancement in the design of RC walls for new construction. The newly adopted performance evaluation methodology and capacity design principles are examples of these important advancements in seismic engineering. Therefore, there is an urgent need to upgrade existing RC shear wall buildings that were designed according to older design codes so that their seismic performance can meet the requirements of modern seismic design codes.

Tremblay et al. (2001) indicated the importance of higher mode effects for slender high-rise shear walls that result in higher shear forces and bending moments in the upper regions of a wall. Their analytical study showed that these higher demands would lead to the formation of a plastic hinge at that upper region. Similar conclusions were reported by

Bachmann and Linde (1995), Priestley and Amaris (2002), and Panneton et al. (2006). For experimental validation, two identical scaled (1:0.429) 8-storey RC shear walls were constructed and tested on the shake table of the École Polytechnique de Montréal (EPM). The tests aimed to investigate the higher mode effects on multi-storey RC shear walls subjected to Eastern North America ground motions, which are expected to be rich in high frequencies (Ghorbanirenani et al. 2012). The walls were built with a total height of 9.0 m and designed according to the National Building Code of Canada NBCC (2005) and the Canadian Standard CSA-A23.3 (2004) as moderately ductile walls. These walls were designed based on the codes' regulations that a single plastic hinge would form at the wall base. However, the nonlinear dynamic analysis of the code-designed walls predicted inelastic response at higher levels of the wall. The shake table tests on the original walls showed the formation of another plastic hinge at the sixth storey level in addition to the one at the wall base. These findings indicate that there is a need to retrofit RC walls that are susceptible to increased demands at their higher level.

1.2 OBJECTIVES AND SCOPE

The main objective of the research program is to investigate experimentally the effectiveness of externally bonded carbon fibre-reinforced polymer (CFRP) composite sheets in increasing the flexural and shear capacities of RC shear walls that are susceptible to increased demands due to higher-mode effects or due to changes in the design codes. The study also aims to propose a numerical model to simulate the behaviour of the original and the FRP-retrofitted walls.

To achieve the stated research objectives, the following work plan was designed and performed:

1- An experimental program was conducted to examine the effectiveness of CFRP composites in upgrading the seismic performance of multi-storey RC shear walls that are susceptible to increased demands at higher stories due to higher-mode effects. The test involved shake table testing of two 8-storey RC walls retrofitted using CFRP composite sheets.

2- The experimental program was continued by testing three RC shear wall panels under cyclic loading up to failure. The tested walls represent a control wall and two FRP-retrofitted walls using two different retrofit schemes.

3- Evaluation of the retrofit schemes was carried out by comparing the behaviour of the tested walls.

4- A nonlinear macro-model of the tested walls under cyclic loading before and after the FRP-retrofit was developed.

1.3 THESIS ORGANIZATION

The thesis is divided into 8 chapters. Chapter 1 is an introduction describing the objectives and scope of the research. Chapter 2 is a literature review of the different failure modes of RC shear walls, different retrofit techniques used for RC walls, and the numerical macro-models used for the simulation of their seismic behaviour. Chapter 3 describes the details of the shake table tests: the test setup, wall specimen design and construction, and the FRP-rehabilitation scheme used. Chapter 4 presents the results of the shake table tests and provides a comparison between the tested walls. Chapter 5

describes the details of the cyclic tests, whereas their test results are presented in Chapter 6. The proposed numerical macro-model of the tested walls under cyclic loading is described in Chapter 7. The summary of the research project, the main contributions and conclusions, and the recommendations for future work are presented in Chapter 8.

CHAPTER 2

LITERATURE REVIEW

2.1 INTRODUCTION

Many of the existing RC buildings with shear wall system that are located in seismically active zones were designed according to older design codes. These buildings are considered to be seismically deficient according to the new codes due to lack of strength and/or ductility. Therefore, retrofitting such buildings becomes a necessity and can not be overlooked. Several retrofit techniques of RC shear walls using different materials are reported in the literature. These included using steel, concrete, fiber-reinforced polymers, and shape memory alloys as retrofitting materials. The expected mode of failure for a certain deficient existing wall indicates the appropriate retrofitting technique that should be used for that wall. Generally, retrofitting techniques would aim to improve the wall strength, stiffness, ductility, or a combination of these. Increasing the wall energy dissipation capacity is also a main goal for an effective retrofit, mainly due to the dynamic nature of ground motion excitations. Control of the wall permanent deformations is another important target, which can be achieved by using re-centering materials such as shape memory alloys (SMA). Most of the tests conducted on RC shear walls identify their existing and retrofitted performance using roof displacement-base shear, moment-rotation, energy dissipated, and displacement time history relationships. Figure 2.1 shows different wall characteristics that can be improved by retrofit.

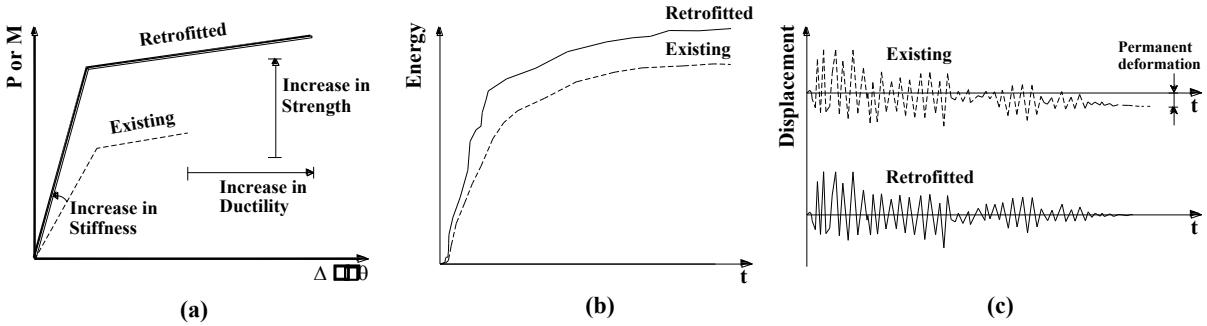

Figure 2.1 Different characteristics to be improved by retrofit (a) Stiffness, Strength, and/or ductility (b) Energy dissipation capacity (c) Permanent deformation control.

Predicting the performance of RC walls under lateral loads requires enhanced numerical tools that are calibrated using controlled experimental tests. These tools should take into account most of the important factors that could affect the response of RC walls. Hence, modeling of RC walls involves several challenges in representing the combined effects of moment, shear and axial forces, in addition to bar slip, buckling, damping, boundary conditions, as well as retrofit method, if any. Different modeling techniques were used by researchers for simulating the seismic behaviour of RC shear walls. These range from macro-models such as lumped plasticity, multi-axial spring models, combined models, up to micro-models such as finite element and fibre models.

This chapter presents a literature survey of different retrofit techniques that were used to enhance the seismic performance of RC shear walls. This will be presented through some of the previous experimental work done by researchers on the retrofit of RC walls. The chapter will also discuss different modes of failure of RC shear walls that were observed from post-earthquake events' reconnaissance or reported from controlled experimental

research work. The expected mode of failure for a specific existing RC wall will determine the appropriate retrofitting technique that should be used for that wall. The chapter also summarizes different modeling techniques that were used to simulate both the local and global behaviour of RC shear walls.

2.2 MODES OF FAILURE OF RC SHEAR WALLS

2.2.1 Flexural failure

In this mode of failure, considerable flexure cracks appear near the bottom part of the tensile zone of the wall, yielding of tensile steel or compression steel may occur, crushing of concrete in the compression zone could happen at the ultimate stages. The compression steel also might buckle if the concrete cover in the compression zone spalled off. This type of failure occurs when the flexural capacity of the RC wall is lower than its shear capacity. Figure 2.2 shows the crack pattern for a wall failed in a flexure manner (Greifenhagen and Lestuzzi 2005).

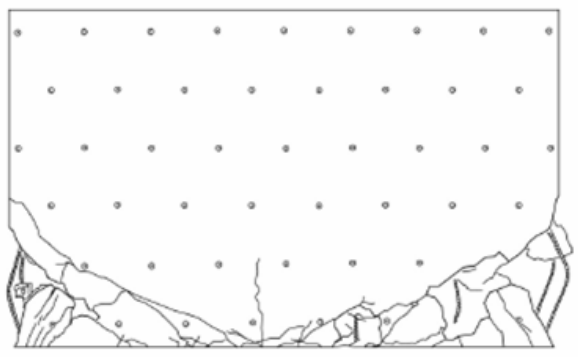

Figure 2.2 Flexural failure of RC walls. (Greifenhagen and Lestuzzi 2005).

2.2.2 Shear failure

This mode of failure occurs usually for shear walls with low aspect ratio or with inadequate shear capacity. Shear failure is brittle in nature which would reduce the energy dissipation capacity of the wall/structure when subjected to a severe ground motion. For this reason, the main aim of all seismic design codes is to avoid such a failure mode by ensuring that the shear capacity of the wall exceeds its flexural capacity. According to Paulay et al. (1982), shear failure of squat RC walls could occur in three modes; diagonal tension, diagonal compression, and sliding shear failure.

2.2.2.1 Diagonal tension and diagonal compression

Due to principal tensile stresses, inclined shear cracks starts to appear, and hence the shear force acting on the wall is resisted by the compression struts formed between the cracks and the tension in the web reinforcement steel. Diagonal tension failure occurs when insufficient horizontal or diagonal reinforcement is used (yielding of shear reinforcement). If the shear reinforcement was sufficient to transfer high shear forces through the shear cracks, diagonal compression failure could occur due to high compression forces in the diagonal compression struts. For this mode of failure and in case of cyclic loading, the web starts to have X-shaped cracks, and then followed by a brittle failure of the concrete web. The concrete compressive strength is the main factor that affects the capacity of the wall that will experience this mode of failure. Figure 2.3(a) shows the diagonal compression shear failure of a RC wall tested by Lopes (2001).

2.2.2.2 Sliding shear failure

Sliding shear failure occurs when the wall has sufficient horizontal reinforcement and relatively small amount of vertical reinforcement in the wall web. In this mode of failure, a continuous horizontal crack originating from flexure will be formed at the base of the wall or at the construction joint (i.e. the weak plane). In this case, the wall section will resist the acting shear forces by the dowel action of the vertical reinforcement and by the friction between the concrete surfaces. For walls with low axial load value, the friction between the concrete layers will not be high, and hence this mode of failure could be critical. Figure 2.3(b) shows the sliding shear failure of a RC wall (Riva et al. 2003).

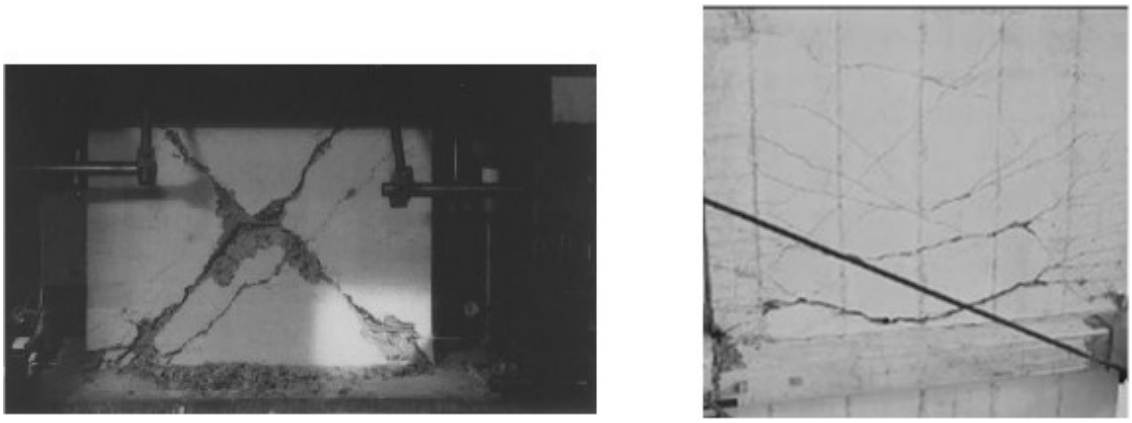

(a) (b)

Figure 2.3 Shear failure of RC walls, (a) Diagonal compression (Lopes 2001), (b) Sliding shear (Riva et al. 2003).

2.2.3 Local buckling of web (Instability of thin wall section)

This mode of failure occurs for slender walls with rectangular sections. To avoid such mode of failure, the design codes require a minimum thickness of the wall as a ratio of the unsupported height of the wall ℓ_u (e.g. ℓ_u /10 in the CSA standard for rectangular ductile walls). The local buckling of web can be also avoided by having boundary elements for the wall, such as columns or flanges at the wall ends.

2.2.4 In-plane splitting failure

In-plane splitting failure was noticed in lightweight RC walls under high compression forces that can result from lateral loads in case of coupled walls or from higher gravity loads (Mosalam et al. 2003). This type of failure occurs suddenly and without any indication. This failure can be prevented by proper confinement of the wall.

2.2.5 Rocking failure

This type of failure occurs when the overturning moment acting on the wall due to lateral loads is greater than the stabilizing moment of the axial load acting on the wall about the foundation corner. This could occur in case of RC precast walls, when the connection between the wall and the foundation is lost. Taghdi et al. (2000) found that RC walls might experience rocking behaviour at a late stage of their testing. They stated that although the rocking behaviour would dissipate the earthquake energy, but still the lateral load resistance of the wall could be insufficient to resist the lateral load demands, and hence seismic retrofit would be necessary.

2.3 DIFFERENT RETROFIT TECHNIQUES OF RC WALLS

Retrofit of an existing RC wall includes either the repair, rehabilitation or strengthening terms. The "*rehabilitation*" and "*strengthening*" terms are used when the performance of the existing wall does not satisfy the existing requirements of the design code and needs to be enhanced. However, the term "*strengthening*" is used when the wall was not subjected to any damage, while the term "*rehabilitation*" is used when the wall has already been damaged and its resistance needs to be restored and improved as well. If the damaged wall's performance was satisfactory before the damage occurred, and it is needed to restore its capacity without any additional resistance, then the term "*repair*" will be representative. There are several factors that control the choice of the retrofitting technique for RC shear walls, some of these factors are:

- The deficiency in the existing wall and its expected mode of failure.
- The goal of intervention (e.g. increased stiffness, strength, ductility, etc).
- Consequences of wall rehabilitation (e.g. increased demand on foundation, etc).
- The allocated budget for retrofit.
- Physical constraints (e.g. architectural requirements, accessibility of the building during the retrofitting process, etc).

Table 2.1 shows different retrofit techniques for RC walls and examples of experimental work conducted by pervious researchers and available in the literature to the authors.

Table 2.1 Different techniques used in retrofit of RC walls.

Retrofit technique		Examples of previous experimental work
Using traditional materials	Concrete replacement	Fiorato et al. (1983), Lefas and Kotsovos (1990), Vecchio et al. (2002), and others.
	Concrete Jacketing	Fiorato et al. (1983), and others.
	Using steel sections	Elnashai and Pinho (1997), Cho et al. (2004), and others.
	Using steel bracings	Taghdi et al. (2000), and others.
	Through-thickness rods	Mosalam et al. (2003), and others.
Using new materials	FRP composites	Lombard et al. (2000), Kanakubo et al. (2000), Paterson and Mitchell (2003), Antoniades et al. (2003), Khalil and Ghobarah (2005), and others.
	Shape Memory Alloys	Effendy et al. (2006), and others.

2.3.1 Concrete replacement

Concrete replacement is the simplest and cheapest technique that can be used to restore strength and ductility of RC walls (Fiorato et al. 1983). In this technique, the damaged concrete is removed, the aggregate of the old concrete is exposed and the surface of the old concrete should be cleaned to remove any loose material and to ensure a strong bond between the old concrete and the new one. If the reinforcing steel bars in the compression zone were slightly buckled after concrete crushing, they should be straightened (Lefas and Kotsovos 1990). The formwork of the web is prepared, the new concrete is mixed and poured from one side of the wall. The top part can be completed using a high-strength epoxy grout to ensure a proper bond with the old concrete (Vecchio et al. 2002). After the removal of formwork, the new concrete should be cured. Therefore, repairing the shear

wall by concrete replacement is causing disturbance to the building function, and hence it is not suitable if the building has to be accessible during repair.

2.3.2 Concrete jacketing

In this technique, the wall dimensions are increased by adding new concrete to the original web. Additional reinforcement could be used to increase the strength and ductility of the wall. The new reinforcement can be vertical and horizontal bars that form the reinforcement mesh or it can be diagonal bars. The new reinforcement should be anchored to the wall foundation. One way of anchoring is by placing the reinforcement in holes that are drilled in the foundation, and then it is grouted with epoxy. The new concrete is casted with the new dimensions and cured after solidification. Fiorato et al. (1983) tested two RC walls, one rehabilitated using diagonal bars after removal of the damaged web concrete in the plastic hinge region and the other one is rehabilitated by increasing the web thickness (jacketing). The tests showed that the strength and deformation capacity of the rehabilitated walls had increased, while their initial stiffness was almost half that of the original walls.

2.3.3 Retrofit using steel material

Steel is the most common material that was used for retrofitting of RC structures. The lower added weight to the structure (compared to concrete jacketing) and the minimum disruption to the building occupants are advantages of using steel retrofitting systems

(Ghobarah and Abou Elfath 2001). On the other hand, steel vulnerability to corrosion, the need for scaffolding, the difficulty of handling the heavy steel plates at the site are problems that arise when retrofitting using steel (Bakis et al. 2002).

Steel sections are attached to the wall to increase the wall strength, stiffness, ductility or a combination of them. The steel plates can be attached vertically or horizontally according to the enhanced property. Elnashai and Pinho (1997) studied the effect of rehabilitation scheme used for retrofitting shear walls using steel plates on the enhancement of a certain property (e.g. wall stiffness, strength or ductility) without altering the other properties. Figure 2.4 shows different rehabilitation schemes of the walls studied by Elnashai and Pinho (1997). They concluded that enhancing the wall stiffness without altering the strength can be achieved by using external steel plates bonded along the wall length near the edges as shown in Figure 2.4(a), the plates can be bonded along the whole height or along the expected plastic hinge height, and a gap should exist between the plates and the foundation or the top slab in order not to affect the wall strength as the critical section will remain as before.

Increasing the wall strength without altering the stiffness can be achieved by using external unbonded steel plates or bars connected with an Interaction Delay Mechanism (IDM) as shown in Figure 2.4(b). The IDM allows the added plates or bars to work only after a certain displacement is exceeded. The plates or bars can be attached to the slabs between the wall height, and then enclosed by a ductile material that provide corrosion and fire resistance to the steel.

Increasing the wall ductility with a minor increase of the stiffness and strength can be achieved by using U-shaped external confining steel plates that are bonded to the wall using epoxy, and bolted using prestressed bolts as shown in Figure 2.4(c). Increasing the wall ductility will increase the energy dissipation capacity of the wall which will enhance the seismic behaviour of the retrofitted wall.

Steel bracings can be also used to enhance the seismic performance of RC shear walls. In that case, the steel bracing can be anchored to the RC wall at small intervals to minimize the buckling length, which will increase the capacity of the bracing member compared to the case of retrofitting the moment resisting frames that is governed mainly by buckling of the compressed bracing member.

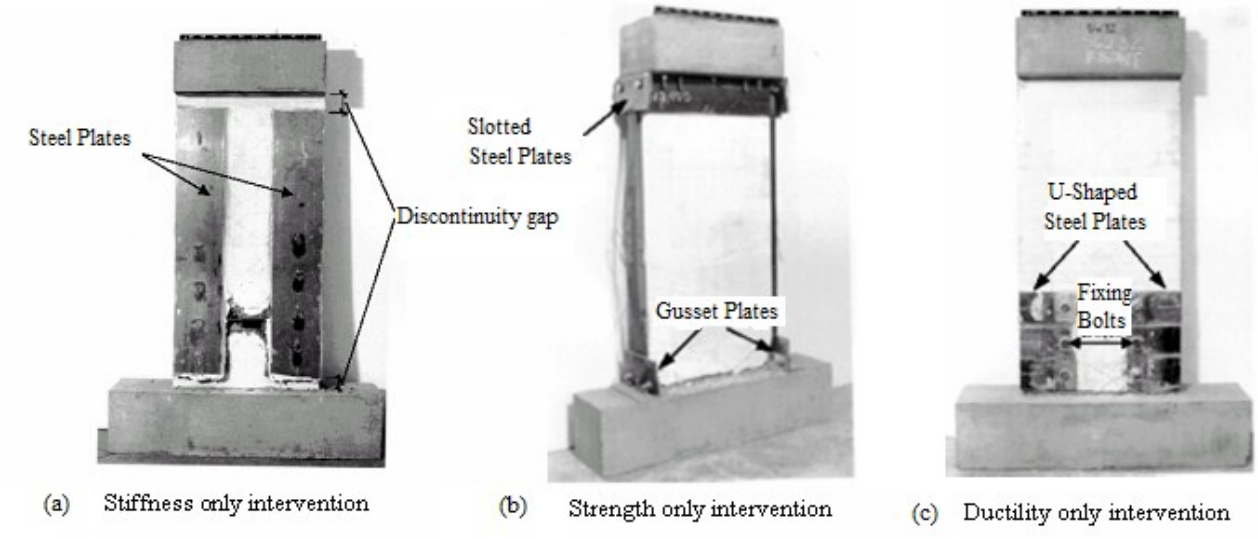

Figure 2.4 Different rehabilitation schemes studied by Elnashai and Pinho (1997).

It is usually recommended to add vertical steel strips at the wall edges when using diagonal bracings, due to the fact that the diagonal forces in bracing members will have a vertical (compression/tension) components that will add higher forces on the wall, in that case it is better to provide vertical strips at the wall ends to resist a part of these forces with the concrete. Taghdi et al. (2000) tested a RC wall that is retrofitted using this technique. The tests showed that the retrofitted wall reached an ultimate lateral load capacity up to 2.8 times its original capacity, and an energy dissipation capacity up to 4 times the original one, which indicates the efficiency of this technique in retrofitting RC walls.

2.3.4 Reduction of flexural strength

This can be a solution to change the wall mode of failure from the brittle shear failure to the ductile flexural failure (ASCE 2006). This can be done by saw-cutting some of the wall vertical rebars near the wall ends. However, the wall still should possess the adequate flexural capacity needed for lateral load resistance.

2.3.5 Use of through-thickness rods for light-weight RC walls

As mentioned before, lightweight RC walls could experience in-plane splitting failure under high axial load especially if embedded steel elements were used in constructing the wall. In this case, confining the wall section is the solution to prevent such a brittle failure mode. Mosalam et al. (2003) used steel rods that can be anchored through the wall thickness to confine the wall as shown in Figure 2.5. The rods can be bonded or

unbonded to concrete. They concluded that this technique was effective in enhancing the performance of the wall and preventing such mode of failure.

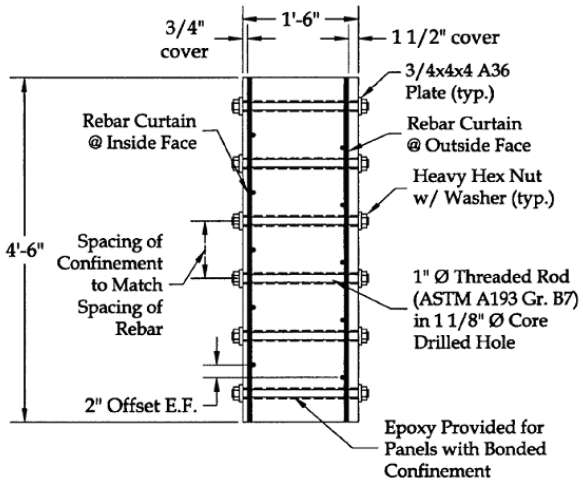

Figure 2.5 RC wall strengthened using through-thickness rods (Mosalam et al. 2003).

2.3.6 Addition of wall boundary elements

Addition of boundary elements can be an effective technique for strengthening RC walls that are deficient in flexure (Cho et al. 2004, ASCE 2006). Reinforced concrete elements or steel sections can be added to act as boundary elements. This technique will not be efficient for walls that would experience shear mode of failure. It is worth noting that, a special attention should be considered to the connection between the existing wall and the new boundary elements.

2.3.7 Retrofit using shape memory alloys

Shape memory alloys (SMA) have recently an increasing attention in civil infrastructure research and seem to have a brilliant future. However, the reported tests on the use of SMA for seismic retrofit of RC walls have been very limited and still more tests are needed. SMA has the ability to undergo large deformations, then it can restore its original

shape when the applied stress is removed (super-elastic effect), or when it is heated (shape memory effect). This will lead to high ductility and energy dissipation capacity without having large permanent deformations in the member (Desroches and Smith 2003). This phenomenon can be very useful in the seismic applications in buildings; such as dampers, bracings, etc. In addition to that, SMA has an excellent resistance against corrosion. Effendy et al. (2006) tested two low-rise RC walls with boundary elements retrofitted using two different types of SMA bracings (Figure 2.6).

Figure 2.6 RC wall strengthened using SMA bars at failure and its hysteretic behaviour (Effendy et al. 2006).

2.3.8 Retrofit using composite materials

Fibre-reinforced polymer (FRP) composite materials have received an increasing attention in the past few decades as a potential material for retrofitting of existing RC structures due to their high strength, light weight, ease of application, and their high resistance to corrosion. FRP laminates, sheets or rods can be used, and the fibres might be prestressed to increase the efficiency of retrofit. The use of FRP composites offers also a faster and easier retrofit alternative, especially when the evacuation of the entire building

during the retrofit is not possible, in that case FRP would provide the required strength and/or ductility without interrupting the use of the building.

2.3.8.1 Increasing the wall shear capacity

Additional shear strength contribution can be obtained by orienting the fibres normal to the axis of the member or to cross potential shear cracks. The wrapping pattern and the number of FRP layers used in the retrofit determine the additional strength and ductility of the wall, and hence the ductility of the structure and its overall response when subjected to a specified seismic hazard level. In that case, FRP wrapping will have a slight effect on the wall flexural strength and stiffness, and hence minimal additional forces will be expected due to retrofit. Also due to the light weight of FRP, negligible weight will be added to the wall foundation.

Paterson and Mitchell (2003) retrofitted RC shear wall using CFRP wraps and through-thickness headed reinforcement. The retrofit scheme aimed to increase the wall shear strength and confinement. The retrofitted wall was able to reach a displacement ductility 57% higher than the control wall, and it was able to dissipate three times the energy absorbed by the original wall. Khalil and Ghobarah (2005) tested two RC wall panels rehabilitated using FRP composites. The rehabilitation aimed to increase the shear capacity and ductility of the walls. The first wall was rehabilitated by wrapping two layers of bi-directional diagonal fibres around the wall, and by applying uni-directional horizontal U-wraps around the wall end columns. FRP anchors were used to anchor the horizontal U-wraps as shown in Figure 2.7(a). The second wall was rehabilitated using the same pattern but four steel through-thickness bolts were fixed at the higher and lower region of the diagonal FRP sheets, and the U-wraps were anchored using nine steel bolts

on each side along the end column height as shown in Figure 2.7(b). It was found that the lateral load capacity has increased by about 40 and 57% for the first and second wall, respectively. The two rehabilitated walls were able to reach displacement ductilities of 3.0 and 4.0 at their maximum strength compared to displacement ductility of less than 1.0 for the control wall. The study concluded also that the use of steel anchors allows almost full utilization of the material, and hence the wall performance was significantly improved compared to the case of FRP anchors.

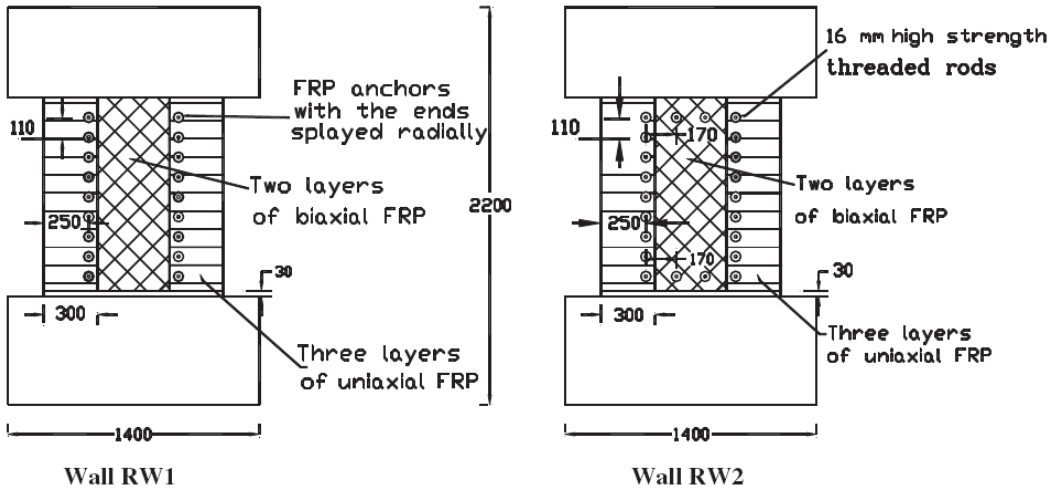

Figure 2.7 The two rehabilitation schemes tested by Khalil and Ghobarah (2005).

2.3.8.2 Increasing the wall flexural capacity

The flexural strength of a RC shear wall can be enhanced by orienting the fibres parallel to the wall axis. FRP sheets are bonded to the wall surface using epoxy and anchored to the wall foundation and to the top slab using steel or FRP anchors. Lombard et al. (2000), Kanakubo et al. (2000), and Antoniades et al. (2005) discussed several ways of anchorage of FRP sheets that can be used for flexural strengthening. Local buckling of the compressed FRP sheets is also an important issue in case of cyclic loading, and it should

be avoided. Near surface mounted FRP reinforcement is another alternative to the externally bonded FRP sheets that can be used for flexural retrofit of existing RC elements (De Lorenzis et al. 2000, and El-Hacha and Rizkalla 2004). In general, increasing the wall flexural capacity will be useful if the original wall would experience flexural mode of failure and additional flexural capacity was required. In that case, the target flexural capacity of the retrofitted wall should not exceed the wall shear capacity, otherwise both flexural and shear capacities should be increased.

2.3.8.3 Increasing the wall flexural and shear capacity

Both flexural and shear capacities can be enhanced together at the same time using horizontal and vertical FRP strips or by using diagonal strips. Lombard et al. (2000) studied retrofitting three RC shear walls using FRP composites when subjected to cyclic lateral excitations. The first wall was repaired to restore the wall original flexural capacity and stiffness. One vertical layer of carbon FRP (CFRP) sheets was applied on each wall face and anchored to the foundation using steel angles. The second wall was strengthened using the same technique to reach higher flexural capacity. The third wall was strengthened to increase the wall flexural and shear capacities by applying one horizontal layer of CFRP sheet that is sandwiched between two vertical layers of CFRP on the two long sides of the wall. The walls were designed to have a ductile flexural failure after retrofit. It was found that FRP-retrofitted walls would have an improved performance provided that a proper anchorage system for the sheets is used. It should be noted that, premature debonding of FRP sheets due to the compressive stresses in FRP vertical strips is a critical issue that should be taken into account especially for the case of cyclic loading.

2.4 MACRO-MODELING OF RC SHEAR WALLS

During the past few decades, enormous efforts have been made to provide numerical tools that are able to simulate the actual behaviour of RC elements including shear walls. The rapid increase in the computational efficiency of computers helped the researchers to develop more sophisticated models that can account for several phenomena of RC shear walls. These phenomena used to be ignored in the analysis due to their complexity. The numerical modeling of RC walls is not only involved in the applications for new construction, but it is also extended to the applications of retrofitting of existing structures.

The two main approaches for modeling of RC elements are micro-modeling and macro modeling. Micro-modeling such as finite element analysis or fiber analysis is based on representing the behaviour of different materials that compose the RC element and the interaction between them. The element is discretized into small elements and principles of equilibrium are applied. This approach is complex and needs high numerical processing efforts, and hence it might not be practical for large structures. Therefore, it is limited to model individual structural components such as a column, a beam or a wall. On the other hand, macro-modeling is based on representing the overall behaviour of the RC element, such as wall deformations, strength, and energy dissipation capacity. The global behaviour of the RC element using a macro-model should be calibrated using a micro-model or an experimental verification to adjust the parameters needed for the model. This approach is simple and does not require high numerical efforts, which makes it suitable to simulate the response of a complete structure. The following subsections summarize the macro-models available in the literature that were used for modeling of RC shear walls.

2.4.1 Two-component beam-column element

The beam-column element was the first element to be used for modeling of RC shear walls and the wall members of coupled shear walls. The two-component element was the first nonlinear beam-column model that was used for structural analysis of a reinforced concrete element. The model developed by Clough et al. (1965) consisted mainly of two parallel components; one was fully elastic and the other was perfectly elasto-plastic as shown in Figure 2.8. The two components were able to represent the material yielding (elasto-plastic behaviour) and the strain hardening (elastic behaviour). The nonlinearity of this model was represented uniformly along the entire member length. The main problem of this model was its inability to represent the element stiffness or strength degradation with cyclic loading. This model was improved by Takizawa (1976) to be able to simulate different hysteretic behaviour of RC elements by using appropriate hysteresis models (general two-component model).

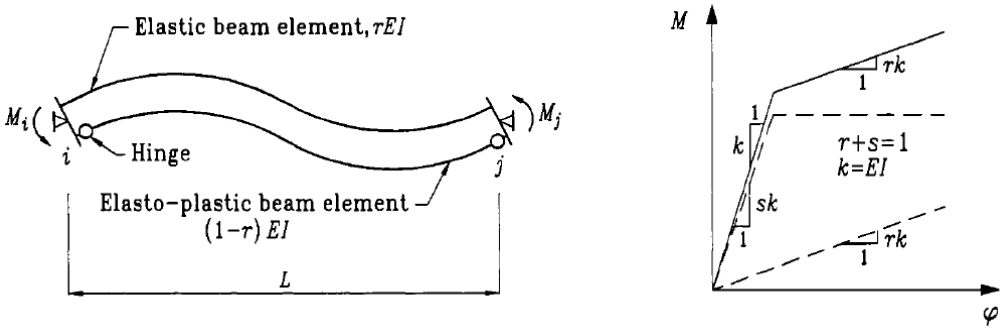

Figure 2.8 Two-component element model (Clough et al. 1965).

2.4.2 One-component beam-column element

This element which was developed by Giberson (1967) consisted of one linear elastic member with two nonlinear rotational springs at the two member ends as shown in Figure 2.9. The member's nonlinear deformations were assumed to be lumped at the zero-length end springs (lumped plasticity). For this model, the deformed shape was assumed to have a double curvature with a fixed point of contra-flexure at the middle of the member, and the plain sections were assumed to remain plain. The one-component model and the general two-component model need an appropriate hysteretic load-deformation (or moment-curvature) relationships to be defined. This requires definition of different properties of the member's plastic hinges such as stiffness, strength, ductility, cyclic behaviour, etc., which may be difficult to be defined unless some assumptions were made. The hysteretic model consists of a primary curve (backbone curve) that control the monotonic loading and some hysteresis rules that control the element loading and unloading behaviour under cyclic loading. The control parameters of the hysteresis rules can be adjusted to simulate the actual cyclic behaviour of the tested wall. Examples of the hysteretic models are the simple bilinear model and Takeda trilinear model (Takeda et al. 1970).

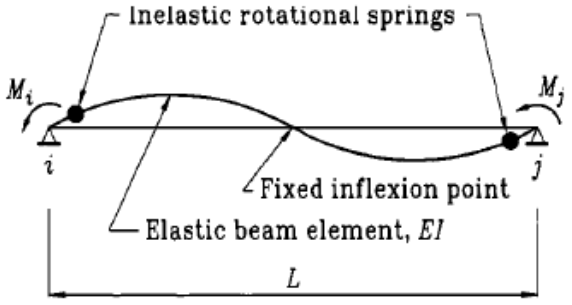

Figure 2.9 One-component element model (Giberson 1967).

2.4.3 Multiple spring model

This model was proposed by Takayanagi and Schnobrich (1976). The multiple spring model consisted of a number of inelastic springs that are connected in series using rigid members as shown in Figure 2.10. The inelastic properties of each spring vary according to the segment properties and the level of axial load on that segment, however the segment properties were assumed to be constant along the segment length. The model was used to represent the behaviour of coupled shear walls, while the coupling beams were modeled using one-component elements. This model was used by Emori and Schnobrich (1981) to model the shear walls of a 10-storey frame-wall building. Linear shear deformations were assumed in the analysis. The models were found to satisfactorily represent the nonlinear behaviour of the studied structure.

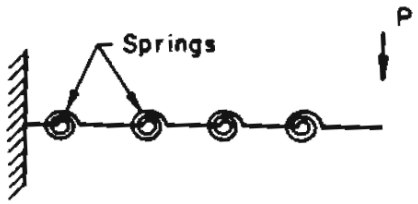

Figure 2.10 Multiple spring model (Takayanagi and Schnobrich 1976).

2.4.4 Multi-axial spring model (MS model)

This model was proposed by Lai et al. (1984) to simulate the axial-flexure interaction of RC columns. The proposed model consisted of an elastic linear member with two multi-axial spring elements (MS elements) of zero dimensions located at the two member ends as shown in Figure 2.11. The MS element proposed by Lai et al. (1984) consisted of 5 concrete and 4 steel springs, each spring was assumed to be uniaxially stressed and its

behaviour was governed by the hysteretic stress-strain characteristics of the simulated material (concrete or steel). The main input for this model was the material (concrete/steel) constitutive laws rather than the load-deformation relationship of the whole member. Multi-linear curves were used to represent the stress-strain or (force-deformation) relationship for concrete and steel springs. The spring deformations were conformed to the plane section assumption. The MS element was simplified by Jiang and Saiidi (1990) to have only 4 composite springs, each spring represented the combined behaviour of concrete and steel materials. The behaviour of the composite springs was defined using unsymmetric load-deformation hysteresis model. Li and Otani (1993) increased the number of springs in the MS element to 16 concrete and 9 steel springs. They differentiate between the core concrete and shell concrete properties to account for the effect of concrete confinement. They reported that the higher number of springs would lead to a higher accuracy, and that the time needed for computation did not increase significantly.

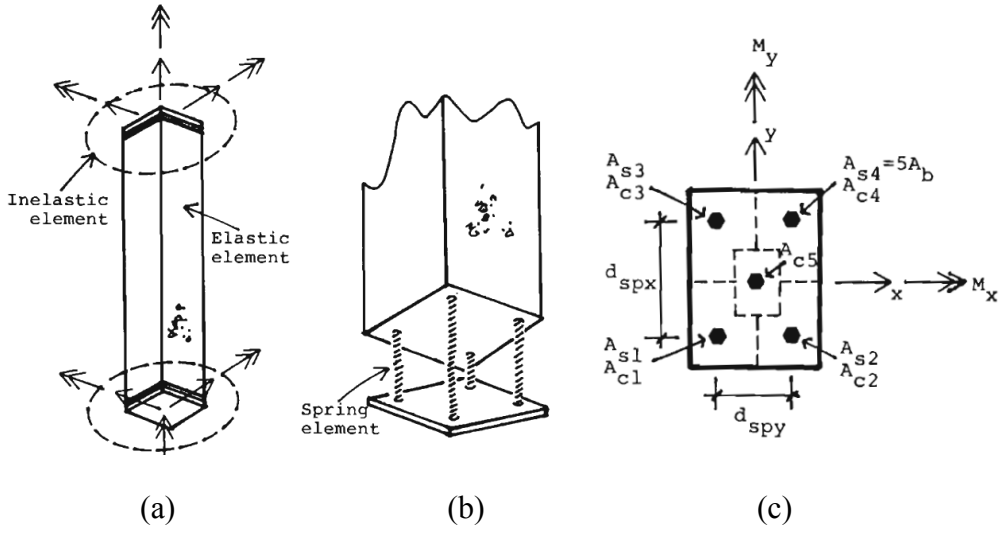

Figure 2.11 Multi-axial spring model by Lai et al. (1984): a) Member model, b) Inelastic element, c) Effective concrete and steel springs.

Subsequently, this model has been extended by increasing the number of springs to be used for the analysis of RC walls. The MS model was used by Galal (2008) to investigate the response of RC walls when subjected to lateral loads. The numerical model was verified using the shake table dynamic tests of CAMUS walls (Combescure 2002).

2.4.5 Combined models

2.4.5.1 Three Vertical Line Element (TVLE) model

This model was first introduced by Kabeyasawa et al. (1982). The model shown in Figure 2.12 consisted of three vertical line elements connected to each other by rigid bars at the top and the bottom wall ends; two edge links with axial springs representing the boundary elements, and the central one-component element with three springs to control the vertical, horizontal, and rotational deformations of the wall. The main drawbacks of this model were the lack of deformation compatibility between the wall and the boundary elements, and the difficulty in defining the properties of the springs. This model was modified later by removing the rotational spring at the central element, and by providing coupling between the axial and flexure behaviour. The modified model was used by Kunnath et al. (1990), Linde and Bachmann (1994) and by Kim and Foutch (2007) to simulate the behaviour of RC shear walls.

Another modification was done by Vulcano and Bertero (1986) to reduce the complexity in defining the hysteretic properties of the model springs. The axial spring of the boundary element was replaced by two axial elements connected in series named as axial-element-in-series model (AESM) shown in Figure 2.13. The upper element is a one-

component element that represents the axial stiffness of the boundary element where the bond between steel and concrete still exists. The lower element is a two-component element (steel and concrete springs) that represents the axial stiffness of the boundary element where the bond is lost. This model should simulate the actual hysteretic response of the materials and their interaction (e.g. concrete cracking, bond deterioration, etc.). Although the model was able to predict the flexural behaviour of the tested wall that was dominated by flexural failure, it was not able to simulate the actual shear deformations of the wall, which indicates that this model is not suitable for walls dominated by shear behaviour. In this model the deformation compatibility between the wall and the boundary element was still not enforced.

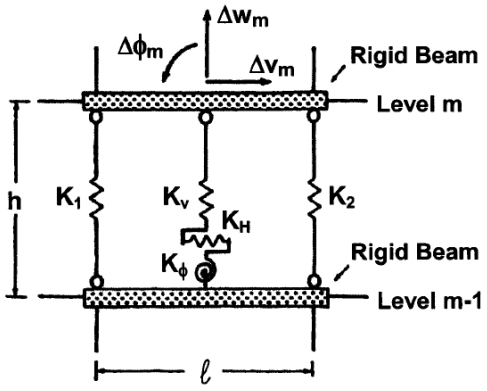

Figure 2.12 Three vertical line element model (Kabeyasawa et al. 1982).

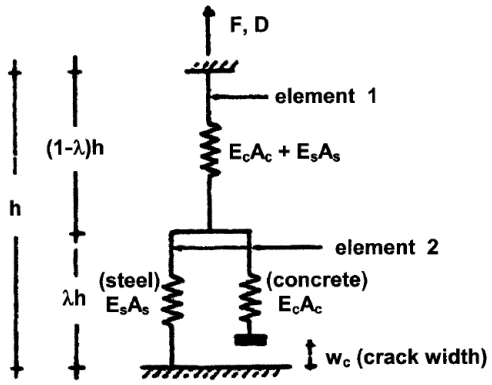

Figure 2.13 Axial-element-in-series model (Vulcano and Bertero 1986).

2.4.5.2. Multiple Vertical Line Element (MVLE) model

This model was first introduced by Vulcano et al. (1988). In this model (Figure 2.14), the wall element was represented by a number of uniaxial elements connected in parallel using infinitely rigid bars located at the top and bottom wall ends; two external elements represents the wall boundary elements, while the other elements simulate the combined

axial-flexure behaviour of the central panel. A horizontal spring was used to represent the inelastic shear behaviour of the wall. The authors modified the axial-element-in-series model (AESM) by having two-component model for element 1, representing the uncracked concrete and steel reinforcement behaviour, instead of the one-component element in the original model as shown in Figure 2.15. The constitutive laws for concrete (cracked and uncracked) and steel elements were defined to describe the hysteretic response of the materials. It was concluded that the model predicted the flexural behaviour of the wall efficiently even when relatively few uniaxial elements were used (4 elements). It is worth noting that, although the proposed model considered both flexural and shear behaviour, but their responses were not coupled. Colotti (1993) modified the MVLE model to include the interaction between axial and shear responses, which led to a more accurate simulation. Simpler constitutive laws and some modifications to the MVLE were introduced by Fischinger et al. (1990) and by Orakcal and Wallace (2006) to improve the model efficiency in predicting the response of RC shear walls without sacrificing the accuracy.

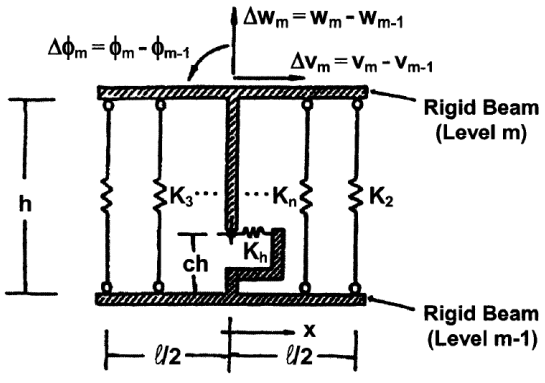

Figure 2.14 Multiple vertical line element model (Vulcano et al. 1988).

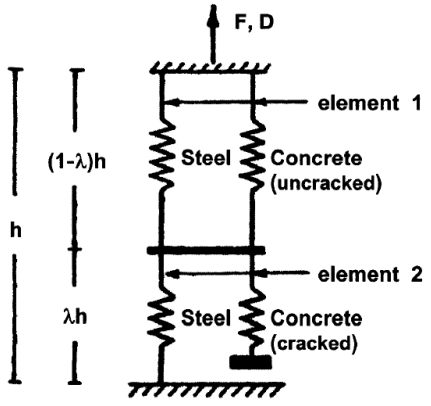

Figure 2.15 Modified axial-element-in-series model (Vulcano et al. 1988).

CHAPTER 3

EXPERIMENTAL PROGRAM
I. SHAKE TABLE TESTS ON FRP-REHABILITATED RC WALLS

3.1 INTRODUCTION

The first phase of the experimental program investigates the seismic behaviour of two 8-storey cantilevered reinforced concrete (RC) shear walls rehabilitated using externally-bonded carbon fibre-reinforced polymer (CFRP) composite sheets when subjected to base excitations from a shake table. The two original reduced-size walls (1:0.429) were tested by Ghorbanirenani et al. (2012) on the shake table of the École Polytechnique de Montréal (EPM) to investigate the effect of higher modes of vibration on the behaviour of multi-storey RC walls. The walls were subjected to several levels of a ground motion excitation that matches the NBCC (2005) design spectrum of Montréal in Québec, Canada. The original walls tested on the shake table, designated as W1 and W2, experienced severe cracking and yielding of the flexural reinforcement at the 6^{th} storey level due to higher demands from the higher mode effects. This part of the wall was not capable of resisting such demands without undergoing excessive plasticity when subjected to the design ground motion (although the design followed the NBCC 2005 and CSA-A23.3, 2004 requirements), and hence it needed to be rehabilitated. After the shake table tests on each of the two original walls W1 and W2, the damaged walls were rehabilitated, designated as W1R and W2R, and re-tested under the same intensity levels of ground motion excitation by the author (El-Sokkary et al. 2012).

The objective of this phase of study is to evaluate the effectiveness of using CFRP composites for retrofitting existing RC shear walls that are susceptible to increased

demands at upper floors; demands that were not accounted for in their initial design and detailing because the effects of higher modes of vibration had not been anticipated.

3.2 ORIGINAL WALL DESIGN AND CONSTRUCTION

3.2.1 Original wall design

The purpose of the shake table tests on the original walls was to investigate the effect of higher modes of vibration on the seismic performance of slender multi-storey RC walls. Two identical RC walls, W1 and W2, were constructed using a prototype 8-storey residential building with a total height of 20.95 m. The building is located in Montréal, Québec and it was scaled by a length factor of 0.429 (Ghorbanirenani et al. 2012). The walls were designed according to NBCC (2005) and CSA-A23.3 (2004) as moderately ductile walls (with a ductility-related force modification factor R_d = 2.0 and an overstrength-related force modification factor R_o = 1.4), and assuming a site class of C. The model wall has a rectangular section with a total height of 9.0 m, a length of 1400 mm, a thickness of 80 mm, and a change in the width at the sixth storey as shown in Figure 3.1. The uniaxial seismic simulator of EPM has a payload capacity of 150 kN and a 3.4 m x 3.4 m plan dimension. Due to the limited vertical capacity of the shake table, it was decided to install the 60 kN seismic weight of each floor beside the shake table in front of each floor level on four multi-level hinged posts as shown in Figure 3.1(a) and (b). Rigid steel beams connect the masses to the wall at each floor to transfer the inertia forces. The axial load carried by the tributary area of the wall was simulated using pre-tensioned tendons that are anchored to the wall base and the wall top. The value of axial load at the wall base was equal to 90.7 kN, while at the 6^{th} storey level it was equal to 64

kN. The as-built walls are shown in Figure 3.1(c), while Figure 3.1(d) shows the wall cross sections and reinforcement details at the base and at the 6th storey levels. More details about the test setup can be found in Ghorbanirenani et al. (2012).

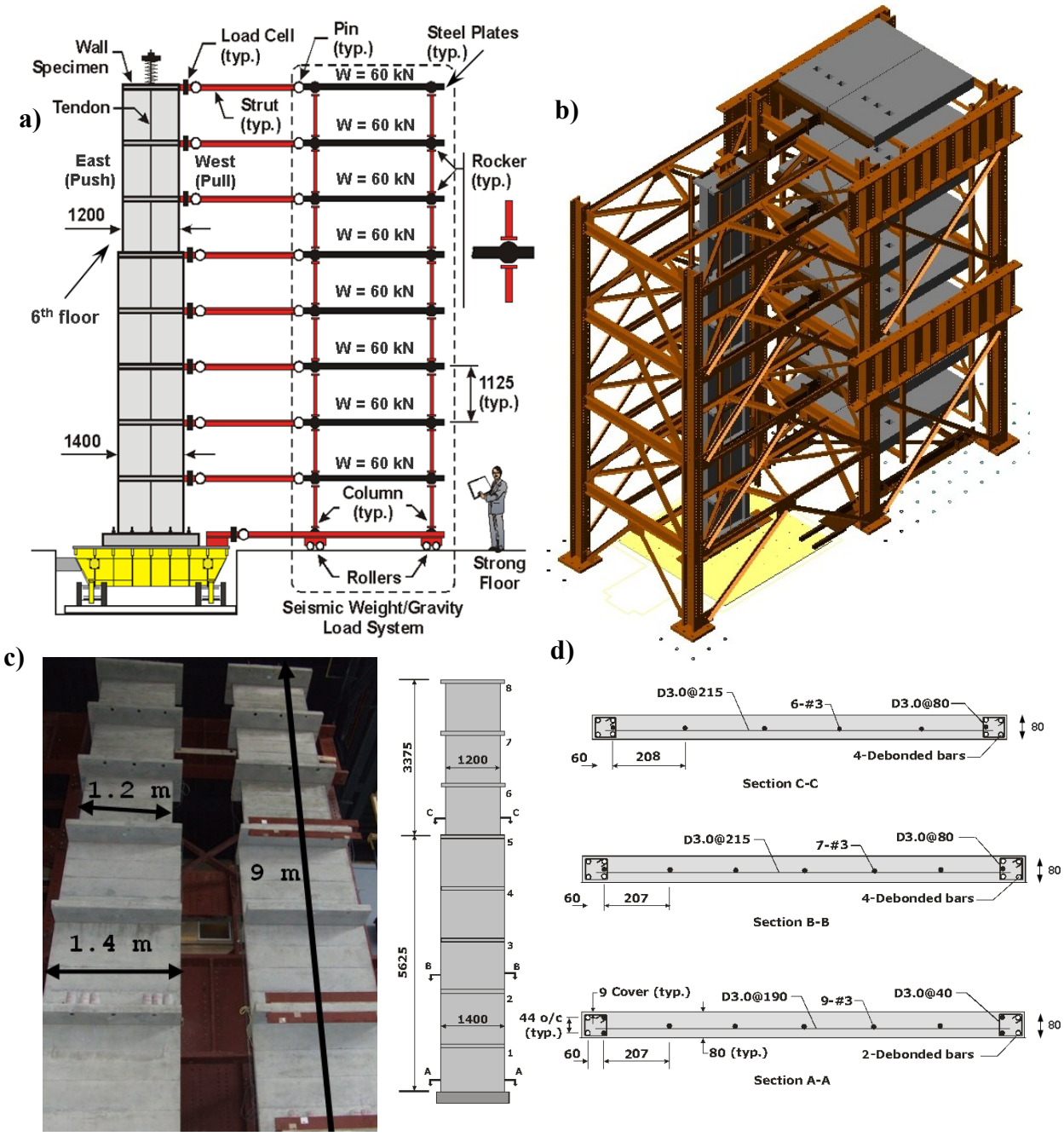

Figure 3.1 a) Test specimen and seismic weight/gravity load system; b) Complete test setup with stabilizing steel frame; c) model wall; and d) Cross section of model wall.

3.2.2 Similitude law requirements

Due to the capacity of the shake table at the EPM, the test specimens had to be scaled. The relations between the model and the prototype can be obtained by the similitude law. For dynamic tests, the most important parameters for modeling are related to geometry, acceleration, and material properties. In this study, the similitude ratio for length S_L of 0.429 was chosen. The $S_L = H_m / H_p$, where H_m and H_p represent the height of the model and the prototype, respectively. The similitude ratio for the modulus of elasticity (S_E) was defined as 1.0. The similitude ratio for mass (S_M) was chosen to be equal to 1.0 so that the entire tributary seismic weight of each floor could be included in the test setup. The artificial mass simulation was used to increase the mass density of material artificially while keeping the modulii of elasticity constant (Moncarz and Krawinkler 1981). The horizontal acceleration was scaled up by a scale factor of 2.65, which resulted in a scale factor of time equal to 0.403. The same gravity acceleration between the model and the prototype was used. The wall dimensions were chosen to ensure that the natural period of the model would fall between 0.5–0.8 seconds. This corresponds to a value of 1.2–2.1 seconds for the prototype. The similitude requirements for the tested walls are shown in Table 3.1.

Table 3.1 Similitude law requirements.

Parameter	**Dimension**	**Scale**
Young's Modulus (E)	$S_E = S_F S_L^{-2}$	1.0
Length (L)	S_L	0.429
Area (A)	S_L^2	0.184
Volume (V)	S_L^3	0.079
Stress (σ)	$S_F S_L^{-2}$	1.0
Strain (ε)	-----	1.0
Displacement (Δ)	S_L	0.429
Rotation (θ)	-----	1.0
Force (F)	$S_F = S_L^2$	0.184
Moment (M)	S_L^3	0.079
Time (T)	S_T	0.403
Frequency (f)	S_T^{-1}	2.48
Acceleration (a)	$S_L S_T^2$	2.65
Mass density (ρ)	S_L^{-3}	12.7
Mass (M)	S_M	1.0

3.3 MATERIAL PROPERTIES

3.3.1 Concrete and steel material

The original walls were constructed using concrete with specified compressive strength, f_c', of 30 MPa for wall W1 and 33 MPa for wall W2. The measured average concrete modulus of elasticity, E_c, was 26,650 MPa and the Poisson's ratio υ was found to be 0.22. The flexure steel yield strength, f_y, was measured to be 455 MPa on average, the flexure steel ultimate strength, f_u = 552 MPa, the shear reinforcement yield strength was 496 MPa, and its ultimate strength was measured to be 601 MPa. D3.0 deformed bars with cross sectional area of 19.6 mm^2 were used for the shear reinforcement and the hoops. The hollow rebars shown in Figure 3.1 are longitudinal steel reinforcement bars that were debonded (no adherence) as their contribution to the wall's flexural resistance was not required in the wall design. However, they are required to provide confinement for the boundary zones as required by CSA-A23.3 (2004) for moderately ductile walls.

3.3.2 Fibre-reinforced polymer (FRP)

Carbon fibre-reinforced polymer (CFRP) composites were used for the rehabilitation of walls W1 and W2. The Tyfo® SCH-11UP composite system (Fyfe 2010) with uni-directional CFRP sheets was used for both retrofitted walls. The resin material Tyfo S epoxy was used as recommended by the manufacturer. Tyfo S epoxy is a two-component epoxy matrix; Part A which is a resin and Part B which is a hardener. Part A is combined with Part B at a ratio of 1.0:0.42 by volume and mixed thoroughly at 400-600 RPM for five minutes until uniformly blended. Table 3.2 shows the mechanical properties of the

Tyfo® SCH-11UP composite system; dry fibre, TyfoS epoxy, and CFRP composite (Fyfe 2010) used in the rehabilitation process.

Table 3.2. Mechanical properties of Tyfo® SCH-11UP composite used in the FRP-rehabilitation (Fyfe 2010).

Parameter	(a) Typical dry fibre	(b) Epoxy material	(c) CFRP composite	
			Test value	Design value
Tensile strength (MPa)	3790	72.4	1062	903
Elongation at break (%)	1.60	5.00	1.05	1.05
Tensile modulus (GPa)	230	3.18	102	86.9
Laminate thickness (mm)	0.175	NA	0.27	

3.4 PROPERTIES OF THE SELECTED GROUND MOTION

The ground motion selected for the original walls and the FRP-rehabilitated ones was a simulated excitation of an M7.0 event located 70 km from Montréal, modified in the frequency domain to match the NBCC 2005 design spectrum of Montréal (Tremblay and Atkinson 2001). The ground motion acceleration was scaled with an intensity scale factor of 2.65 for the similitude requirements. The scaled ground motion has a peak ground acceleration (PGA) of 0.92g, a peak ground velocity (PGV) of 0.42 m/s, and an acceleration/velocity ratio (A/V) of 2.19. The details about the loading protocol for the original walls can be found in Ghorbanirenani et al. (2012). Similar to the original wall test protocol, the FRP-retrofitted walls were subjected to sequential intensities of the same ground motion as follows: 100 and 120% of the design ground motion for the first

rehabilitated wall (W1R); and 100, 120, 150 and 200% of the design ground motion for the second rehabilitated wall (W2R). Prior to each application of the ground motion excitation, an impact test was conducted to examine the dynamic characteristics of the wall. Figure 3.2 shows the acceleration time history for the selected ground motion and its response spectrum that matches the NBCC 2005 design response spectrum.

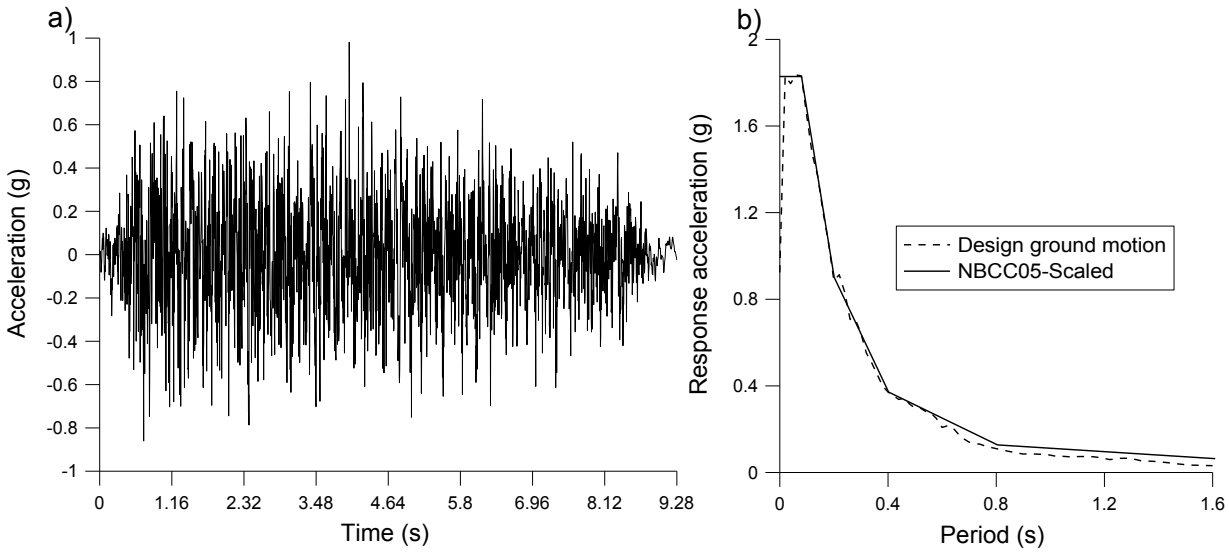

Figure 3.2 Selected ground acceleration: (a) time history; (b) response spectra (Ghorbanirenani et al. 2012).

3.5 BEHAVIOUR OF THE ORIGINAL WALLS

The moderately ductile RC walls W1 and W2 experienced major cracking and yielding of flexure reinforcement at the sixth storey level due to higher demands than those stated in the design code. The wall section at the 6th storey level was subjected to a factored moment demand, M_f, of 137 kN.m and 132 kN.m for wall W1 and W2, respectively, when subjected to 100% of the design ground motion intensity. These values exceeded the factored flexural resistance of the wall section at the 6th storey level,

M_r, which was calculated to be 118 kN.m using section analysis. The rotational demand and strains of the flexure reinforcement at the sixth storey level were even higher than those at the wall base (plastic hinge region) when the walls were subjected to 100% of the design ground motion intensity (Ghorbanirenani et al. 2012). No concrete spalling was observed at any location after the highest ground motion intensity (200% for wall W2). The shear reinforcement did not yield at any location at the 100% ground motion intensity. More details about the original wall behaviour will be explained in the comparisons conducted in Chapter 4.

3.6 THE REHABILITATION STRATEGY

The target of rehabilitation is to enhance the seismic behaviour of the original wall at the two locations that experienced nonlinear response: at the highest demand location at the base of the wall, and at the sixth storey level that experienced a moment demand higher than what it had been designed for. As the causes of damage in the two afore-mentioned locations of the wall are different, the retrofit schemes were not the same. At the sixth storey level, the retrofit strategy was to increase the flexural capacity of the wall section at that level by applying vertical CFRP sheets at the boundary zones of the wall. As a result of increasing the wall's flexural capacity at that level, the retrofit scheme must consider increasing the shear capacity of the panel to respect the capacity design philosophy such that the FRP-retrofitted wall would not fail in shear before reaching its increased flexural capacity. Therefore, in addition to the vertical CFRP sheets at the wall edges, horizontal CFRP wraps were applied to increase the shear capacity of the wall section at the sixth storey. This rehabilitation scheme will thus increase the wall flexural

and shear strengths, and it will provide confinement at the boundary zones of the sixth storey level. As for the plastic hinge location at the base of the wall, only horizontal CFRP wraps were applied to improve the confinement at the boundary zones, thereby increasing the wall's ductility without increasing its flexural strength.

3.6.1 Rehabilitated wall W1R

As the original walls did not experience concrete spalling at any location, no concrete replacement was needed. The wall surface was cleaned and ground in several areas to achieve a smooth surface. The wall corners were chamfered to a radius of 10 mm to avoid stress concentration when wrapping the FRP sheets. Due to the excessive yielding of the flexural reinforcement measured at the sixth-storey of the two original walls resulting from demands greater than those stated in the design codes, the rehabilitation scheme necessitates increasing the wall's flexural capacity at that level. This was achieved by applying a 200 mm wide vertical uni-directional CFRP strip at the wall's extremities on both faces. The width of the vertical CFRP strips were designed such that the factored flexural resistance of the rehabilitated wall section at the 6^{th} storey level becomes greater than the factored moment demand observed in the tests on the original walls (137 kN.m). A design value of 157 kN.m was chosen in order to account for the increase in wall demands due to the increased stiffness arising from the added flexural CFRP reinforcement. The ultimate strain of the FRP vertical sheets was limited to 0.006 as recommended by ISIS Canada (2008) to account for any premature anchorage failure or debonding of the CFRP sheets. A material resistance factor φ_{FRP} of 0.75 was used in the design, as recommended by ISIS Canada (2008) for the rehabilitation of flexural members using CFRP sheets.

The vertical FRP strips were anchored to the top and bottom slabs of the sixth-storey panel using FRP fan anchors as shown in Figure 3.3. The FRP fan anchors were placed in previously drilled holes that were filled with epoxy resin. The drilled holes made an angle of 30^{o} with the wall surface and they went through the wall web and slab for a distance of at least 60 mm as shown in Figure 3.4. The holes were cleaned and washed to remove any dust prior to the installation of FRP anchors to ensure a high bond between the resin and the concrete substrate.

To ensure a ductile performance after increasing the wall's flexural capacity, the shear capacity at the sixth storey was increased by applying one horizontal layer (for each face of the wall) of C-shaped CFRP sheet on top of the vertical FRP strips. The two C-shaped FRP sheets overlapped at the boundary regions of the wall to provide a better confinement of the wall end columns as shown in Figure 3.3. The horizontal CFRP wrapping also helps to reduce the tendency of premature debonding of the vertical CFRP strips under compression during the cyclic loading, identified by Lombard et al. (2000) as an unfavorable response that needs to be avoided.

The horizontal CFRP sheets were anchored along the sides of the wall using previously drilled through-thickness steel anchors of 10 mm diameter spaced vertically at 210 mm intervals. The steel anchors are expected to result in a higher confinement of the wall end columns by providing a lateral support for the FRP wraps at certain intervals, which would enhance the additional confinement provided by the CFRP wraps. The steel anchors were used in lieu of FRP fan anchors (spike type) based on the findings of Khalil and Ghobarah (2005). They reported that steel anchors did not fail in shear as was the

case for FRP anchors, and that with the use of steel anchors, a rehabilitated wall was able to sustain a higher load capacity than one rehabilitated using FRP anchors.

At the base of the wall, no additional flexural strength was needed. Therefore, no vertical FRP strips were used at the base storey. The base panel was wrapped horizontally using the C-shaped CFRP sheets (one at each face) and anchored to the wall using the through-thickness steel anchors, similar to the sixth storey. The horizontal wrapping confines the wall boundary regions, thus increasing the wall ductility and energy dissipation capacity.

For the first rehabilitated wall W1R, the ground motions were applied at two intensity levels: 100% and 120% of the design ground motion intensity. Similar to the tests on the original walls, impact tests were carried out before each application of the ground motion level and at the end of the tests to determine the dynamic characteristics of the tested walls and to estimate the amount of damage.

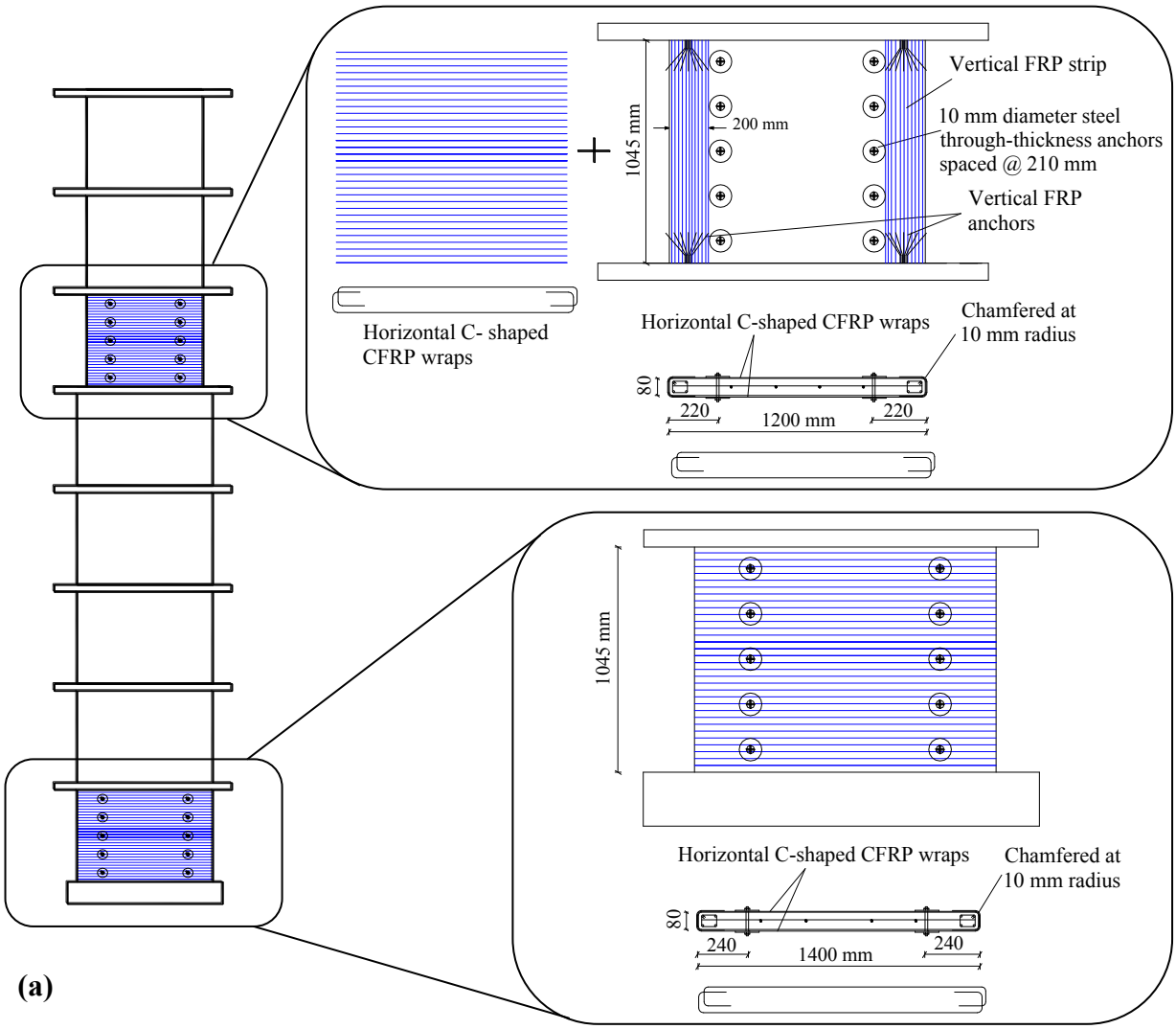

(b)

(c)

Figure 3.3 (a) Rehabilitation scheme of W1R, (b) Base panel rehabilitation, (c) Sixth-storey panel rehabilitation.

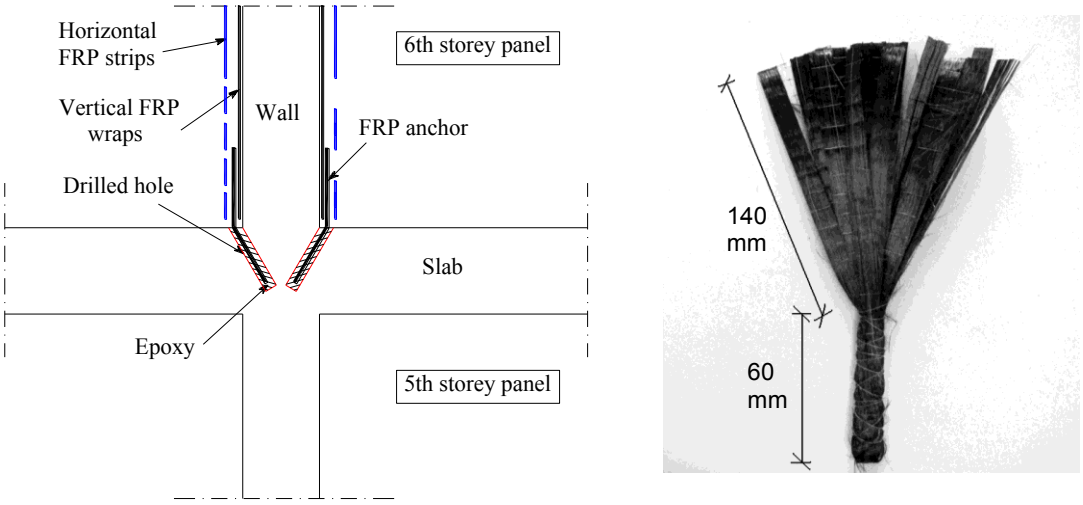

Figure 3.4 Detailing of a CFRP anchor for the first rehabilitated wall, W1R.

3.6.2 Rehabilitated wall W2R

For the second rehabilitated wall, W2R, a rehabilitation scheme similar to that for W1R was used for both the base and the sixth-storey panels. Figure 3.5 shows the rehabilitation scheme of wall W2R. For this wall, it was decided not to use the through-thickness steel anchors. The FRP anchors for W2R were detailed in a different way than W1R, due to the difficulty of drilling the inclined holes through the wall web for W1R. This difficulty was mainly due to the tight spacing of the wall's vertical reinforcement, which was concentrated at the wall boundary columns where the holes for FRP anchors should be drilled. Therefore, it was decided to investigate a different technique for detailing the FRP anchor of W2R. As the amount of reinforcement in the slab is less than the wall web at the wall extremities, it was decided to drill the anchor holes through the slabs. The holes were drilled through the slab thickness with a slight inclination, as shown in Figure 3.6. This approach also allowed a longer embedment length of the FRP anchor

to reduce the probability of an anchor debonding from the concrete substrate. For the rehabilitated wall W2R, the ground motion was applied at four intensity levels 100, 120, 150, and 200% of the design intensity, similar to the original wall test.

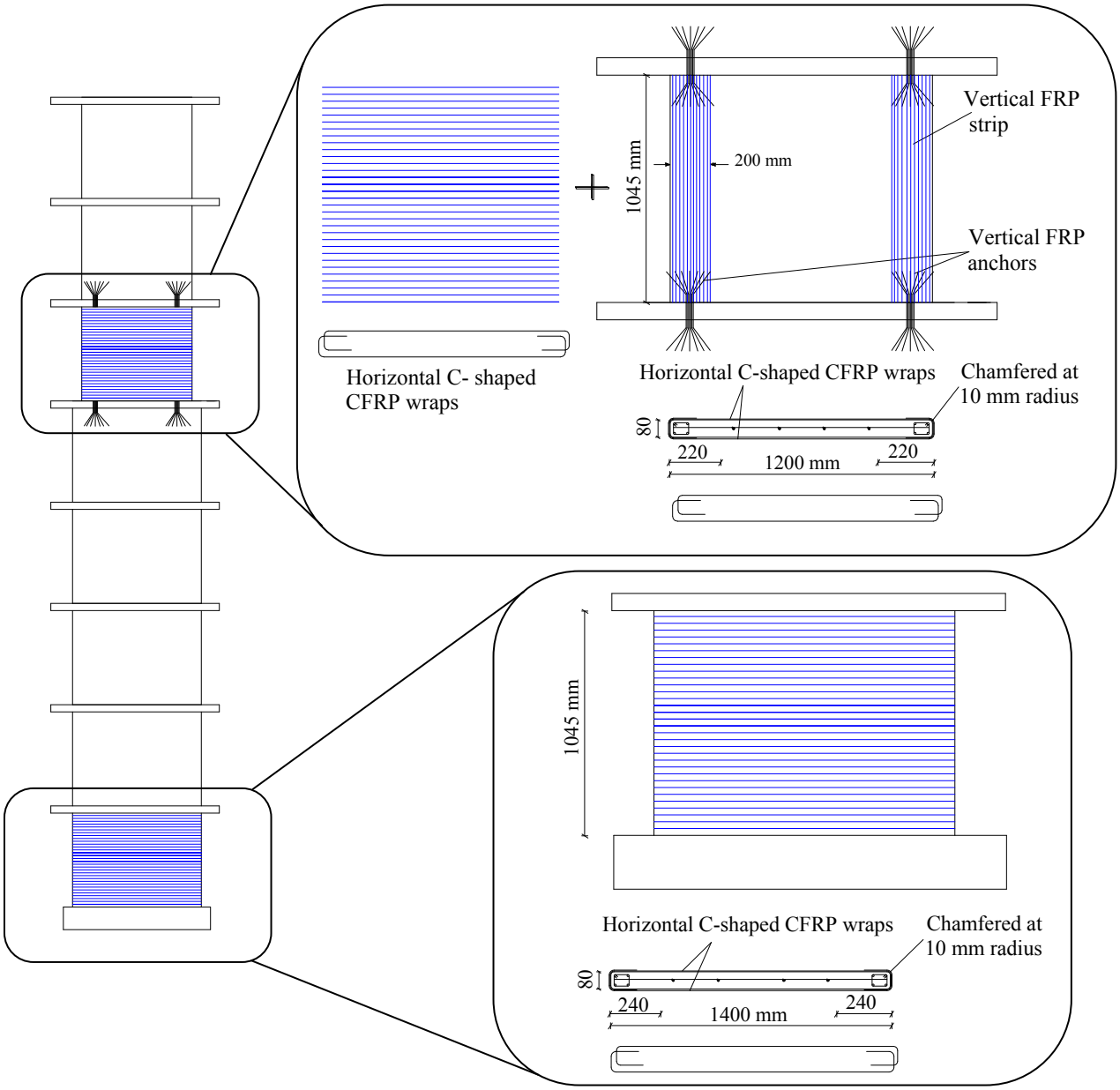

Figure 3.5. Rehabilitation scheme of W2R.

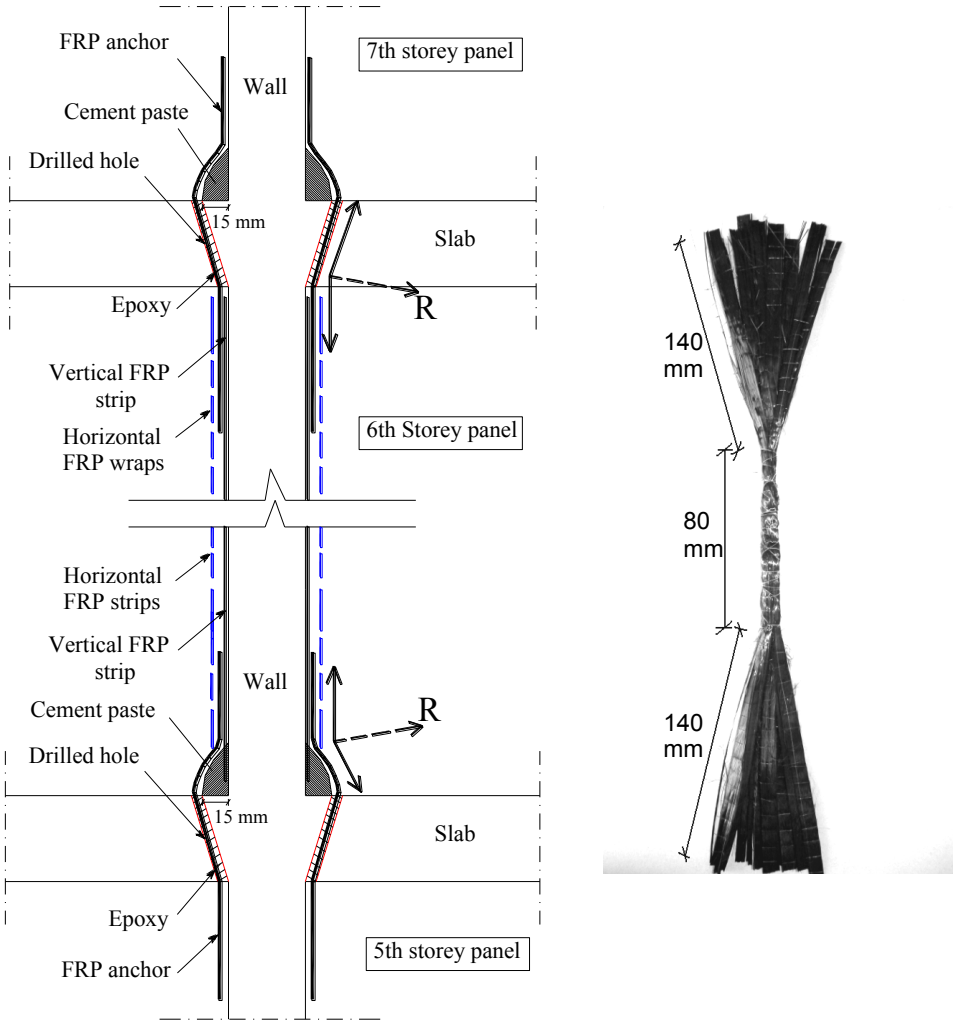

Figure 3.6. Detailing of a CFRP anchor for the second rehabilitated wall, W2R.

3.6.3. Design and fabrication of CFRP anchors

The FRP fan anchors were prepared using the same dry fibres and epoxy resin of the CFRP composite system used in the rehabilitation. The dry fibres weigh 3.1 N/m^2 with a nominal thickness of 0.175 mm/ply. Each FRP anchor used for wall W1R was made from an 80 mm-wide sheet that was cut into 8 strips 10 mm wide and 400 mm long. The strips were folded into two at mid-length and tied at the folded end to form an anchor with embedment length of 60 mm and a fan length of 140 mm as shown in Figure 3.4.

For wall W2R, each FRP anchor was made using a 160 mm-wide sheet that was cut into 16 10 mm-wide strips, each 360 mm long. The strips were tied together at the middle as shown in Figure 3.6 to form an anchor with a double fan 140 mm long with an embedment length of 80 mm (representing the slab thickness). The anchor diameters ranged from 10 to 12 mm. The total amount of fibres in the cross section of the FRP anchors used for walls W1R and W2R was the same, and the anchors were also expected to have the same ultimate capacity. The FRP anchors were designed to have an ultimate capacity equal to 35% of the ultimate strength of the straight fibre composite, to account for the strength reduction due to the bent fibres. The design capacity of the FRP anchor (using ultimate strain of 0.0037 mm/mm) is 16.5 kN. This value was verified using the coupon tests carried out by Ozbakkaloglu and Saatcioglu (2009) in which they tested 81 CFRP anchors under direct pullout. The 16.5 kN anchor design capacity selected was less than the values reported by Ozbakkaloglu and Saatcioglu (2009) for the same fibre strip width and a 53 mm embedment length. Therefore, the capacity of the two FRP anchors used for each vertical CFRP strip was thus equal to 33.0 kN. This value exceeds the nominal tensile strength of the vertical CFRP strips when calculated using their design strain of 0.006 and using the typical test value provided by the manufacturer. These values ensure that vertical CFRP strips would rupture prior to any failure of the CFRP anchors.

3.7 INSTRUMENTATION

Strain gauges attached to the original walls' reinforcement were used; any damaged ones were disconnected from the data acquisition system. Additional strain gauges were applied to the CFRP sheets at different locations and with different orientation. A total of 32 strain gauges with gauge length of 5 mm recorded the strains of the steel reinforcement and the FRP sheets at different locations along the wall height. Their locations at the base and at the 6th storey panels are shown in Figure 3.7. Similar to the original wall tests, floor accelerations were measured using accelerometers attached to each floor, as well as to the shake table.

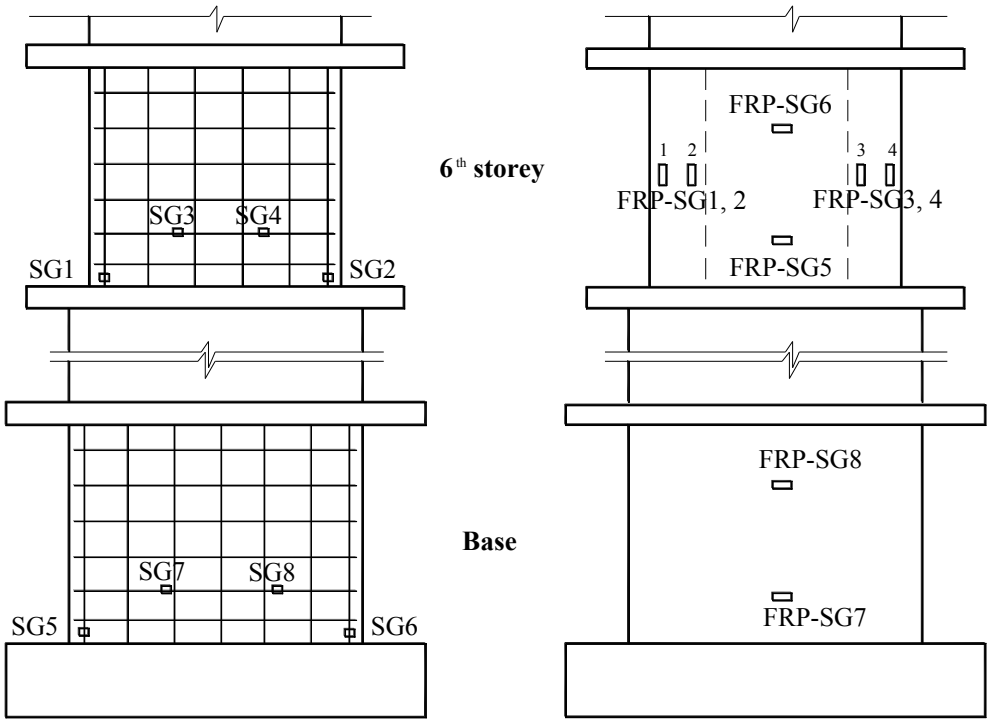

Figure 3.7 Locations of the strain gauges installed on the steel reinforcement and the FRP sheets at the base and 6th storey panels.

The horizontal movement of each floor relative to the shake table movement was measured using horizontal cable-extension position transducers (CEPTs) that are attached to each floor and to a reference wall. The longitudinal and diagonal deformations of the wall base and the sixth-storey panels were measured using vertical and diagonal CEPTs. In addition, three vertical linear variable differential transducers (LVDTs) were attached to the two wall extremities at both levels to measure the wall curvature.

CHAPTER 4

RESULTS OF SHAKE TABLE TESTS

4.1 INTRODUCTION

This chapter presents the experimental results of the shake table tests on the two 8-storey RC shear walls rehabilitated using externally bonded CFRP composite sheets. The reduced-size walls (1:0.429) were tested on the shake table of the École Polytechnique de Montréal and were subjected to several levels of ground motion excitation that match the NBCC 2005 design spectrum of Montréal, Québec, Canada. The damaged original walls were rehabilitated and re-subjected to the same levels of ground motion excitations. During the shake table tests, the loads, displacements, accelerations, and strains were monitored and recorded at a rate of 200 Hz. This chapter presents the test results for each wall specimen and describes their seismic performance before and after rehabilitation. A comparison between the behaviour of the original walls and the FRP-rehabilitated ones is presented.

4.2 RESULTS AND COMPARISONS

4.2.1 Dynamic characteristics

Impact tests were conducted on the wall before and after retrofitting, and prior to each application of the ground motion in order to assess the variation in the dynamic characteristics of the wall. The change in the wall's periods' of vibration is used as an indicator of the global damage (in the case of period elongation), or as an indication of seismic upgrade and stiffening (in the case of period shortening).

Table 4.1 gives the periods of vibration (in seconds) for the first and second tested walls, indicating the first two periods of vibration before and after testing the original walls (W1 and W2), and before and after testing the rehabilitated walls (W1R and W2R). The results in Table 4.1 show the elongation of the first and second periods of vibration for the original walls after the test as a result of their stiffness degradation due to the accumulated incurred damage. After FRP retrofitting, the first and second periods of vibration of the two retrofitted walls decreased (as compared to that of the original damaged walls), which indicates that the FRP rehabilitation scheme increased the wall stiffness. This is attributed to the application of the vertical FRP strips at the sixth storey level which increased the wall stiffness. In addition, we can state that the epoxy resin used for the application of the FRP sheets at the base and the sixth storey panels led to the closure of the wall's surface fine cracks and voids. After the retrofitted walls were subjected to selected ground motion records, the walls' first and second periods of vibration increased again due to the damage occurred.

Table 4.1 Periods of vibration of the original and retrofitted walls before and after application of 100% of the ground motion intensity.

	First Wall		Second Wall	
	T_1 (s)	**T_2 (s)**	**T_1 (s)**	**T_2 (s)**
	Original wall W1		**Original wall W2**	
Before	0.67	0.14	0.65	0.14
After	0.96	0.24	1.31	0.36
	Retrofitted wall W1R		**Retrofitted wall W2R**	
Before	0.76	0.19	0.69	0.17
After	1.09	0.23	1.00	0.28

4.2.2 Storey forces and rotations

Figure 4.1 shows the moment-rotation relationship at the sixth-storey level for the first wall before and after the FRP-rehabilitation (i.e. W1 and W1R) when subjected to 120% of the ground motion intensity. Figures 4.2 and 4.3 show the same relationship for the second wall before and after the FRP-rehabilitation (i.e. W2 and W2R) when subjected to 150% and 200% of the ground motion intensity, respectively. From Figure 4.3, it can be seen that at higher level of the ground motion intensity, the original wall was already damaged and unsymmetric rotational demands were observed. This can be attributed to the large pulse from the shake table that occurred at the beginning of the ground motion record, as shown in Figure 3.2 (at time = 0.7 second), which pulled the wall towards the west side. From the figures, it can be seen that the added vertical FRP strips led to reductions in the maximum storey rotation (θ_{max}) of about 28% for the first wall at 120% intensity, of about 22% for the second wall at 150% intensity and of about

26% for the second wall at 200% intensity, while the walls' moment demands at the sixth-storey level slightly increased. These reductions imply that the rehabilitated walls at the sixth-storey level were able to resist higher force demands with less rotational ductility demands, which shows the effectiveness of the FRP-retrofit scheme used on the sixth storey panel.

Tables 4.2 and 4.3 summarize the rotational demands (θ), the shear force (V) and the overturning moment (M) at the base and for the sixth-storey panels of the original and rehabilitated walls at different ground motion intensities for the first (W1 and W1R) and second (W2 and W2R) walls, respectively. Similar conclusions can be drawn from both these tables when comparing the rotational demands at the sixth-storey level before and after rehabilitation. From the tables, it is clear that the base shear and overturning moment slightly increased after rehabilitation. This increase is due to the additional stiffness at the sixth-storey level obtained from the application of the vertical FRP strips, which led to the reduction of the wall's periods of vibration as shown in Table 4.1. These tables also show that the shear force at the 6^{th} storey level slightly decreased after rehabilitation, whereas the overturning moment at the 6^{th} storey level increased by about 3-10% at different ground motion intensity due to rehabilitation. However, exceptionally, the overturning moment of the first wall at 100% intensity actually decreased by 13% after rehabilitation.

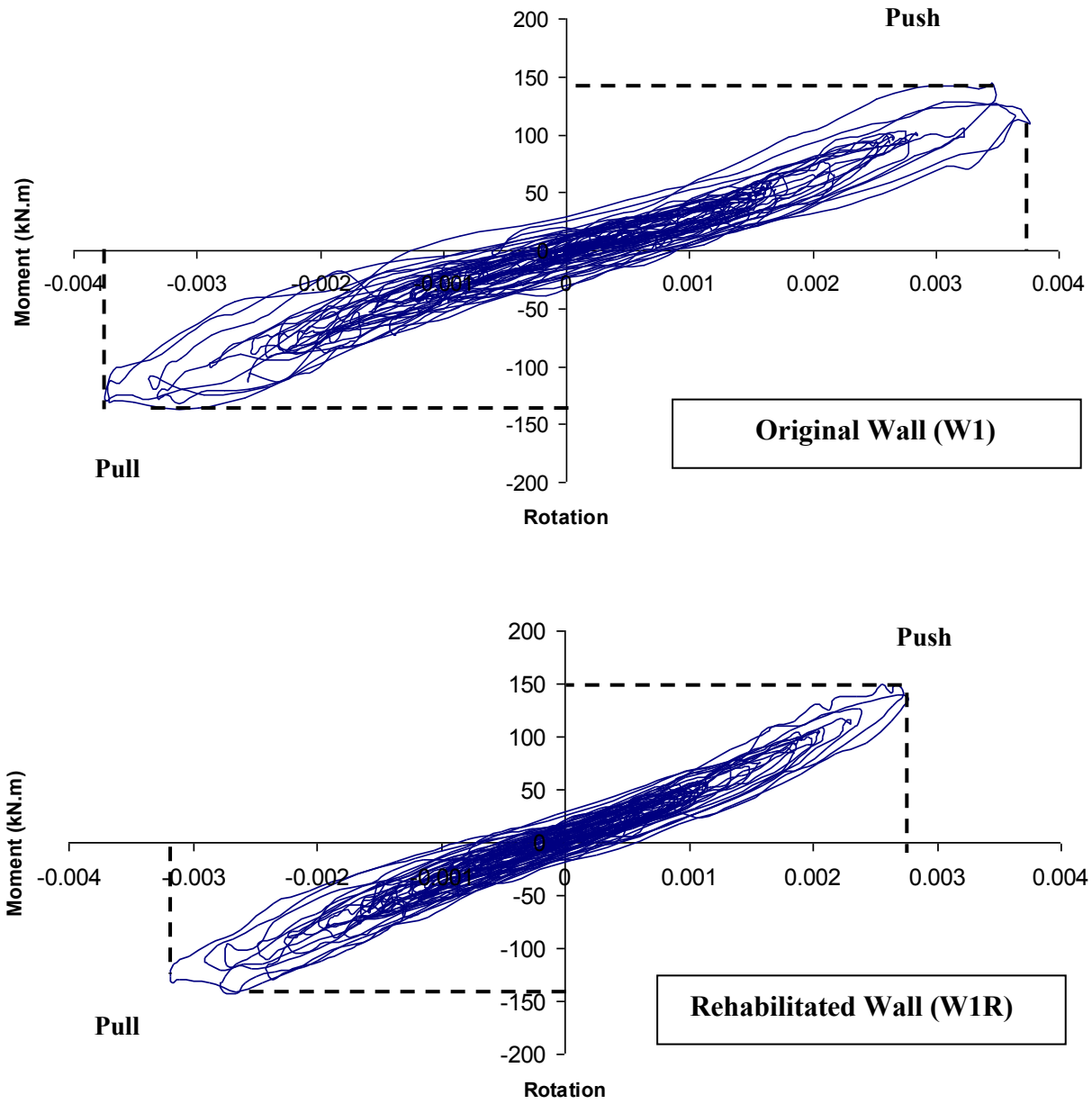

Figure 4.1. Moment-rotation relationship at the sixth-storey level for the first original and rehabilitated wall (W1 and W1R) when subjected to 120% of the ground motion intensity.

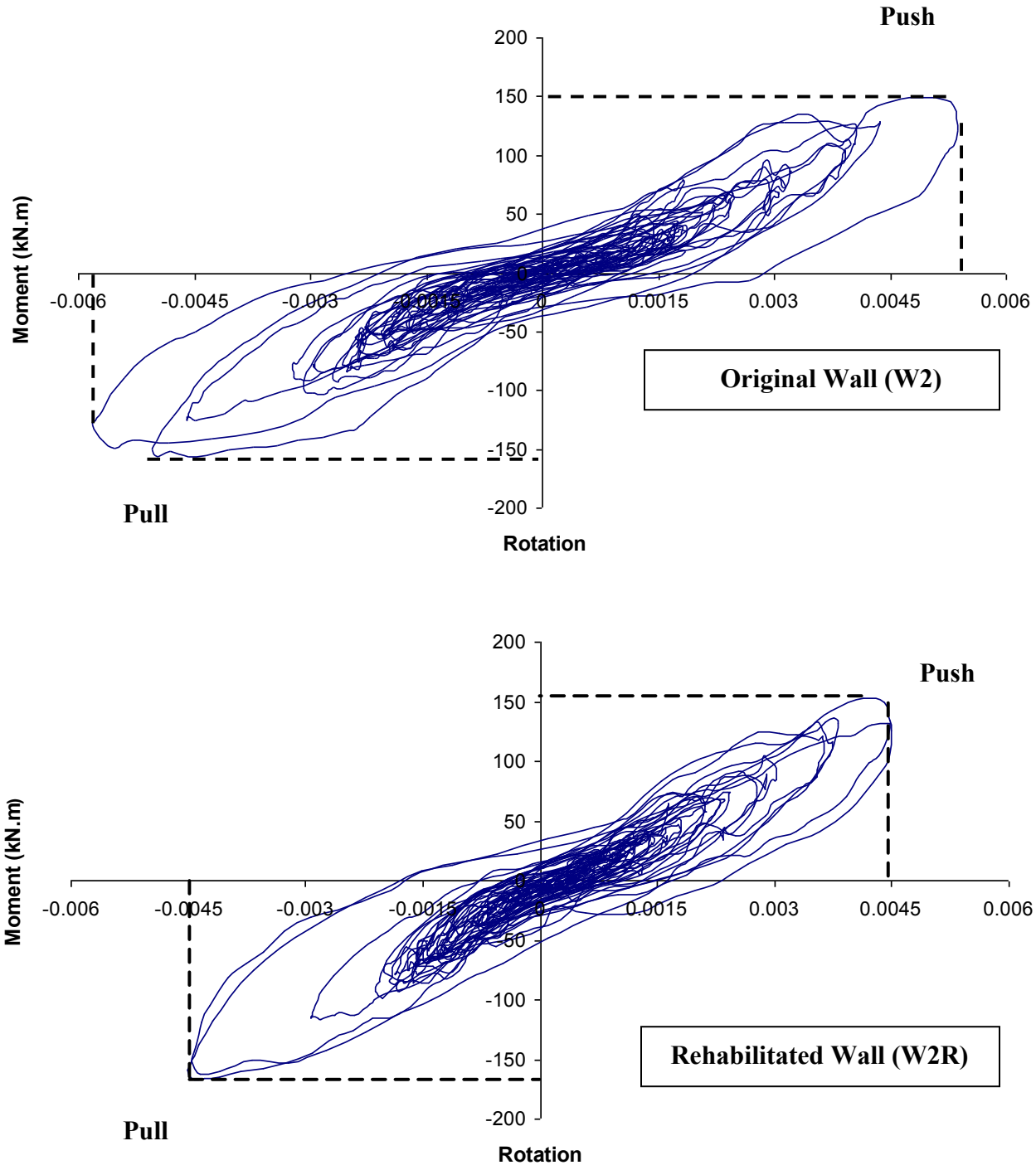

Figure 4.2 Moment-rotation relationship at the sixth-storey level for the second original and rehabilitated wall (W2 and W2R) when subjected to 150% of the ground motion intensity.

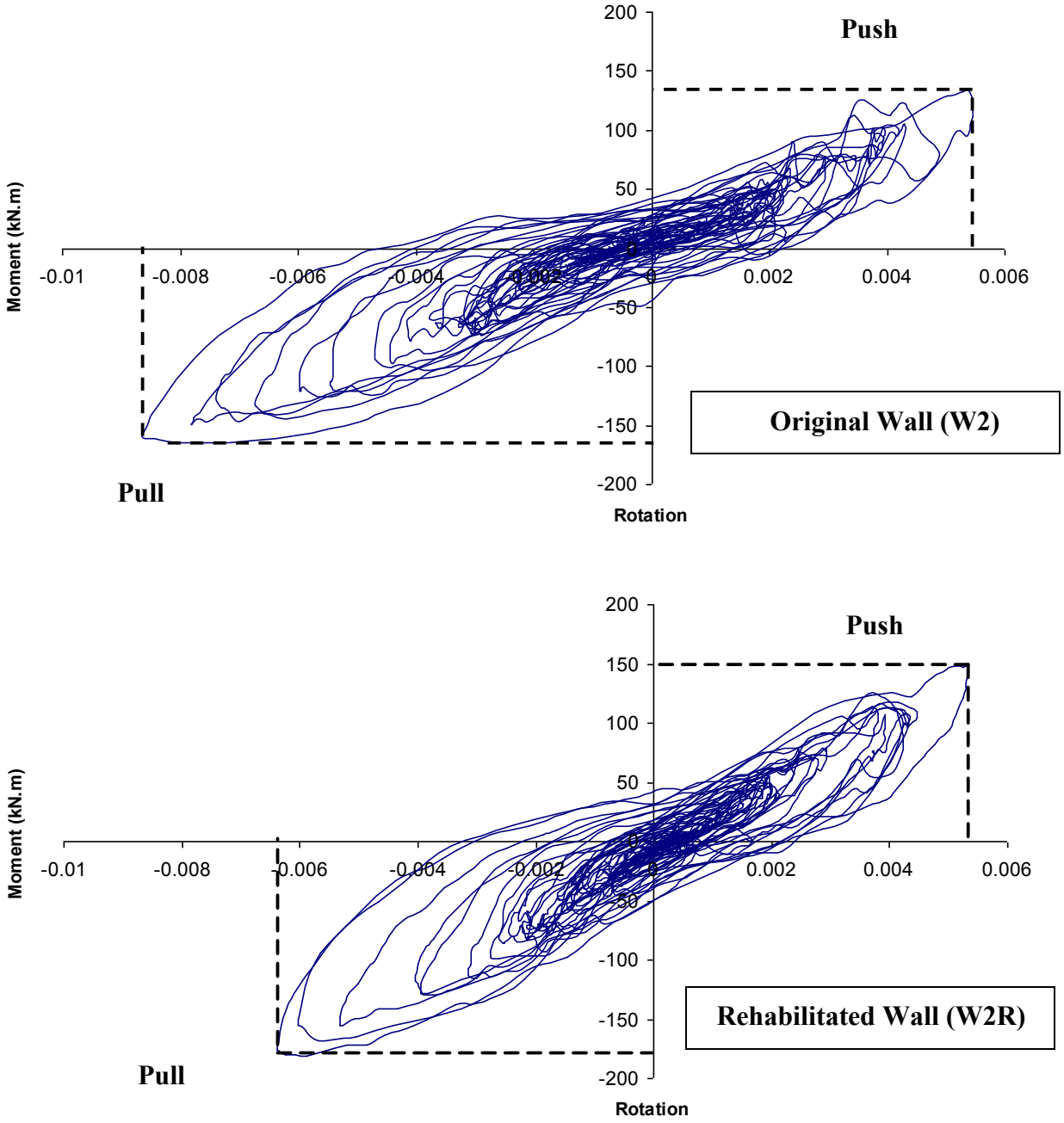

Figure 4.3 Moment-rotation relationship at the sixth-storey level for the second original and rehabilitated wall (W2 and W2R) when subjected to 200% of the ground motion intensity.

Table 4.2 Test results of the first original and rehabilitated wall W1 and W1R.

	Level	100% intensity		120% intensity	
		W1	**W1R**	**W1**	**W1R**
θ § (10^{-3} rad)	6th	2.84	2.30	3.77	3.17
	Base	2.43	1.89	2.58	2.62
V † (kN)	6th	40.2	39.3	46.2	43
	Base	118	131	139	156
M ‡ (kN.m)	6th	137	118	144	150
	Base	241	259	261	274

§ rotational demand
† storey shear force
‡ storey overturning moment

Table 4.3 Test results of the second original and rehabilitated wall W2 and W2R.

	Level	120% intensity		150% intensity		200% intensity	
		W2	**W2R**	**W2**	**W2R**	**W2**	**W2R**
θ § (10^{-3} rad)	6th	2.78	3.17	5.82	4.51	8.61	6.39
	Base	2.54	2.60	3.59	3.35	3.72	3.83
V † (kN)	6th	45	41.5	46	40	65	53
	Base	140	161.9	172	172	183	202
M ‡ (kN.m)	6th	141	145	157	167	165	181
	Base	225	237	243	253	253	255

§ rotational demand
† storey shear force
‡ storey overturning moment

4.2.3 Storey displacements

Figures 4.4 and 4.5 show the maximum inter-storey drift ratio (I.D.) along the wall height before and after rehabilitation for the first and second walls, respectively. The figures show the effectiveness of the FRP-rehabilitation scheme at the 6th storey panel in reducing the maximum I.D. ratio for the retrofitted walls at that level. This effect is more noticeable for the second wall when subjected to higher intensities of the ground motion (150 and 200%), as indicated in Figure 4.5. That figure also shows that the FRP-retrofit of the 6th storey panel of the second wall reduced the maximum I.D. ratio for the upper floor. As no flexural strength was added to the base panel, no reduction of the maximum I.D. ratio occurred at the lower storeys. On the contrary, the maximum I.D. ratio increased at the lower storeys due to the higher moment demands observed after rehabilitation and the accumulated damage incurred after the repeated application of the ground motion at several intensities.

Figure 4.6 shows the roof drift ratio time history of the original and rehabilitated walls when subjected to 120% of the ground motion intensity. This figure reveals that there was no significant effect of the FRP-rehabilitation scheme on the maximum roof drift ratio. It is worth noting that the situation would have been different if the FRP-rehabilitation scheme had considered increasing the wall flexural strength at the base panel.

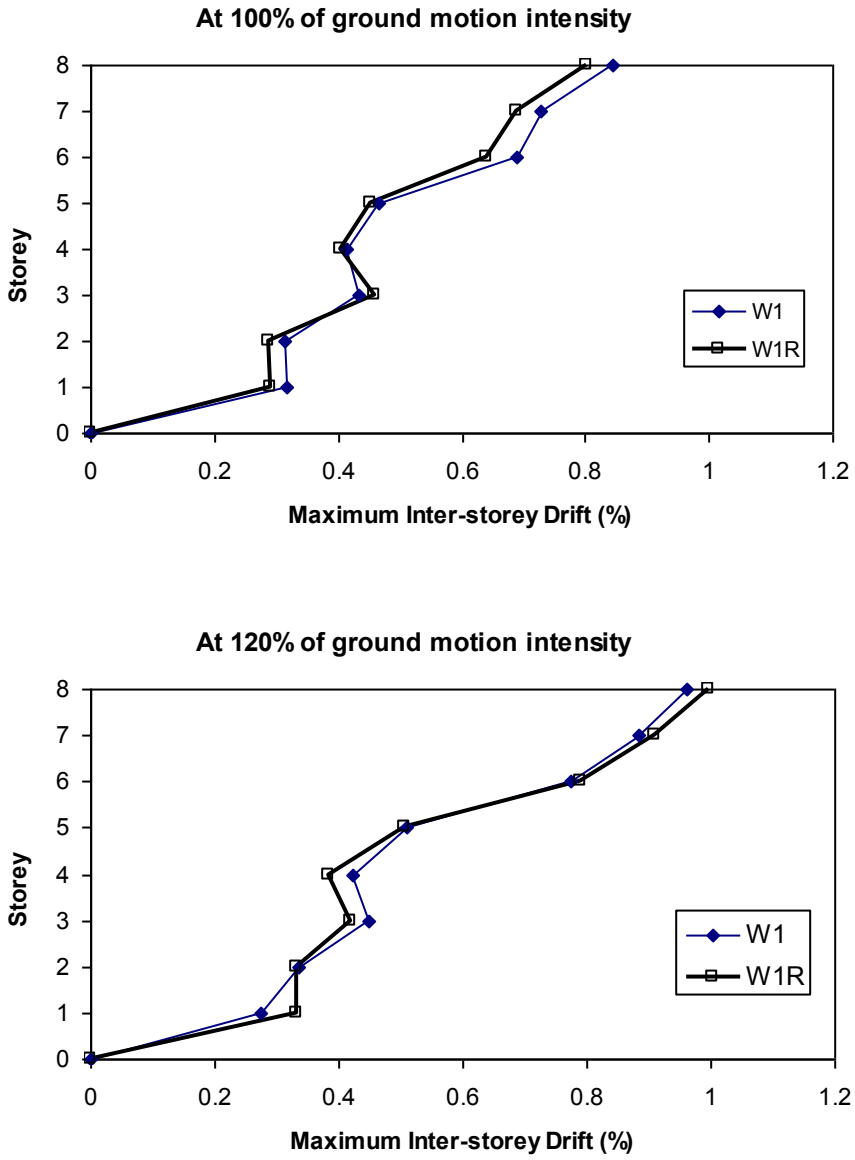

Figure 4.4 Maximum inter-storey drift of the first original and rehabilitated wall (W1 and W1R).

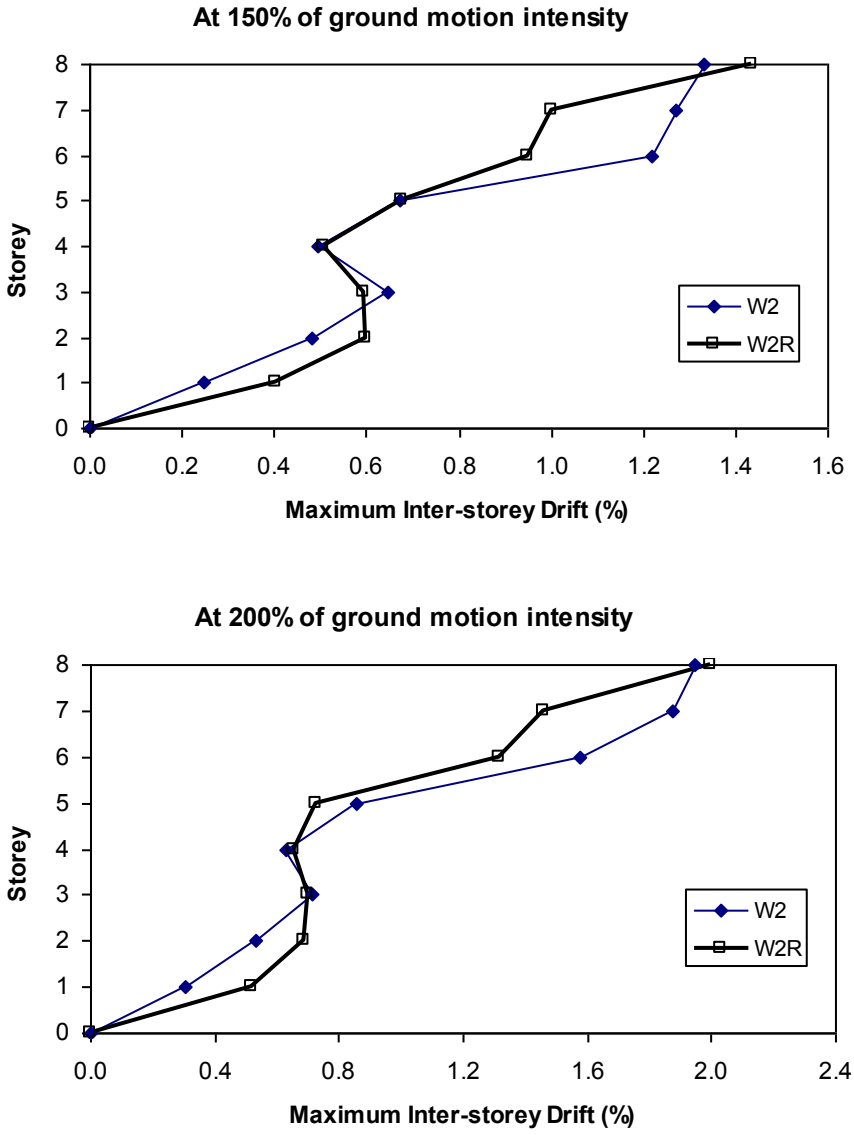

Figure 4.5 Maximum inter-storey drift of the second original and rehabilitated wall (W2 and W2R).

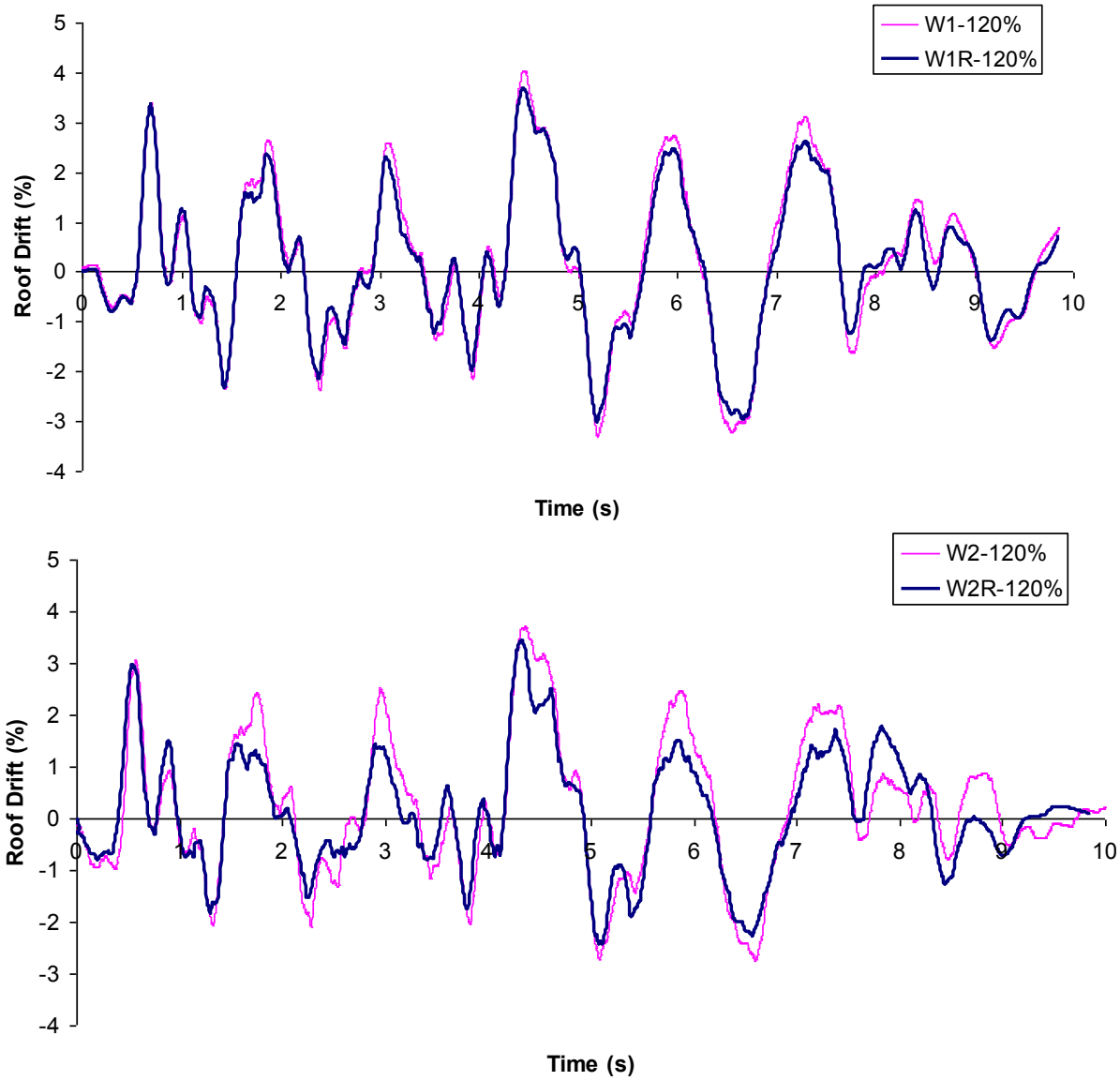

Figure 4.6 Roof drift ratio time history of the original and rehabilitated walls when subjected to 120% of the ground motion intensity.

4.2.4 Strains of steel reinforcement and FRP sheets

Tables 4.4 and 4.5 present the longitudinal and transverse steel reinforcement strain values as well as the vertical and horizontal FRP sheet strains for the first and second walls, respectively. The shown values are for the original (W1 and W2) and the FRP-rehabilitated walls (W1R and W2R) when subjected to two different ground motion intensities. For the first original wall, W1, most of the strain gauges attached to the steel reinforcement were still functioning after testing, which allowed their use in the tests on the FRP-rehabilitated wall, W1R. No yielding of the shear reinforcement occurred at the wall base or at the sixth-storey level.

For the longitudinal steel reinforcement strains, Table 4.4 indicates that a significant reduction of longitudinal reinforcement strains at the sixth storey level occurred, mainly because of the application of the vertical FRP strips at that level which led to the reduction of the wall rotational demands, as mentioned in the previous section. On the other hand, the strain values of the longitudinal steel reinforcement at the wall base did not decrease, since no vertical FRP sheets were applied at the base during rehabilitation. The vertical FRP strips reached a strain of 2000 μ strain (almost 33% of the FRP material's design capacity) at 120% of the ground motion intensity. No FRP anchorage failure or debonding was detected. Similar conclusions can be observed from Figures 4.7 and 4.8, which show the strain time histories for the longitudinal steel reinforcement and the vertical FRP strip at the 6^{th} storey level on the east side of the first wall before and after rehabilitation when subjected to 100% of the ground motion intensity. Figures 4.9 and 4.10 show the same time histories for the strains on the west side of the first wall when subjected to 120% of the ground motion intensity.

Table 4.4 Strains of steel reinforcement and FRP sheets for the first wall (micro-strain).

		100% intensity		120% intensity	
		W1	**W1R**	**W1**	**W1R**
Base panel	**Longitudinal steel reinforcement**	2,350	2,380	2,360	2,440
	Transverse steel reinforcement	870	430	1,016	490
	Horizontal FRP sheets	NA	50	NA	50
Sixth storey panel	**Longitudinal steel reinforcement**	10,920	3,630	9,800	3,250
	Vertical FRP sheets	NA	1,580	NA	2,000

Table 4.5 Strains of steel reinforcement and FRP sheets for the second wall (micro-strain).

		120% intensity		200% intensity	
		W2	**W2R**	**W2**	**W2R**
Base panel	**Longitudinal steel reinforcement**	2,500	2,700	11,370	--
	Transverse steel reinforcement	1,440	1,040	2,500	1,130
	Horizontal FRP sheets	NA	106	NA	165
Sixth storey panel	**Longitudinal steel reinforcement**	15,100	--	--	--
	Vertical FRP sheets	NA	1,320	NA	1,900

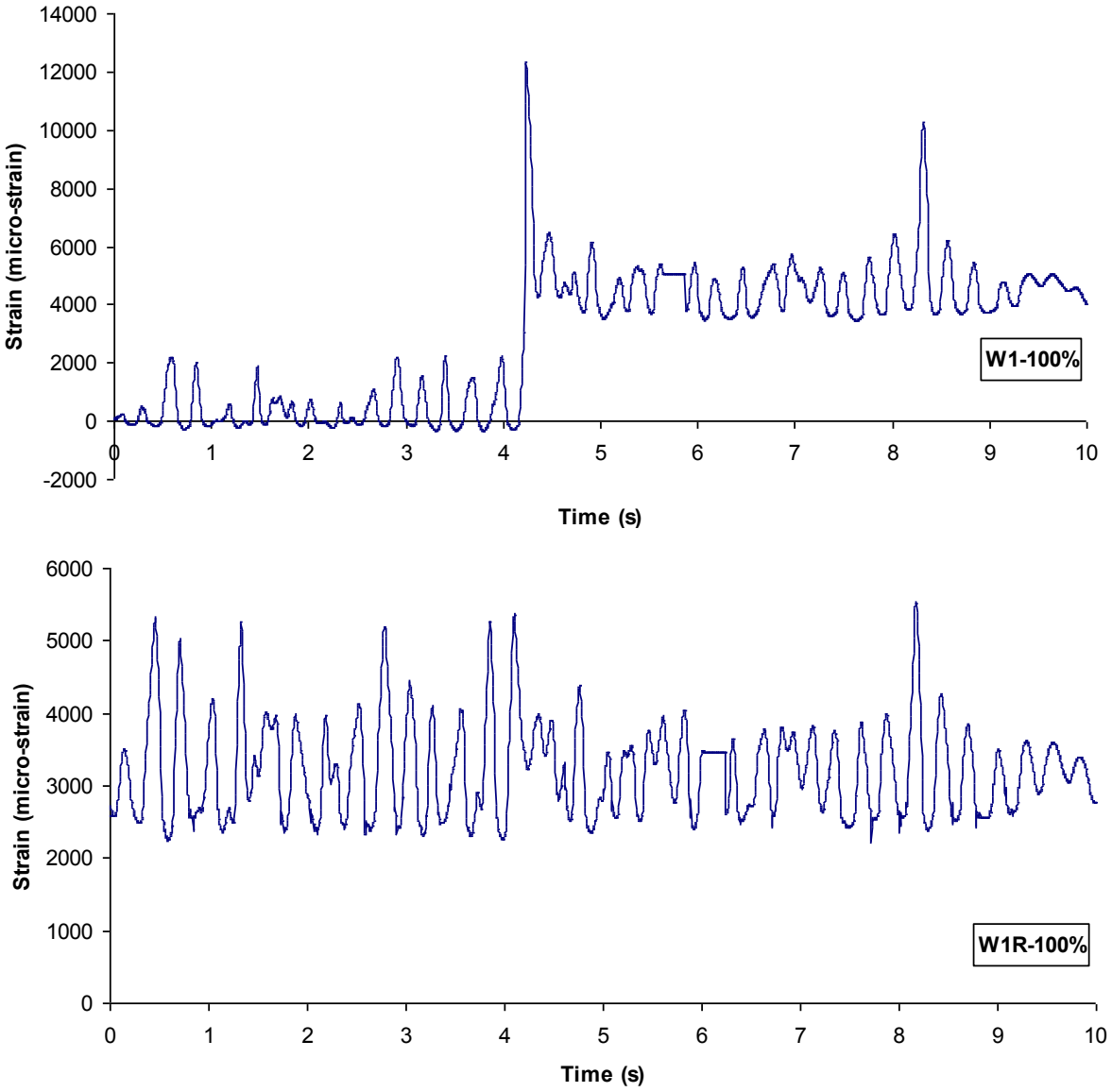

Figure 4.7 Strain gauge SG1 time history for the first wall before and after rehabilitation when subjected to 100% of the ground motion intensity.

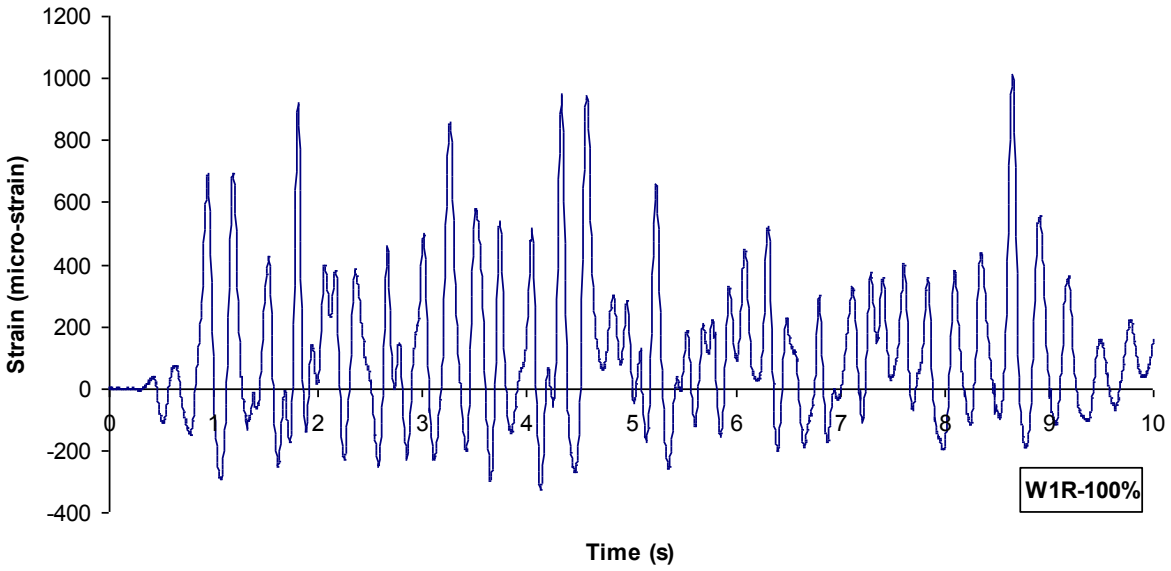

Figure 4.8 Strain gauge FRP-SG1 time history for the first rehabilitated wall W1R when subjected to 100% of the ground motion intensity.

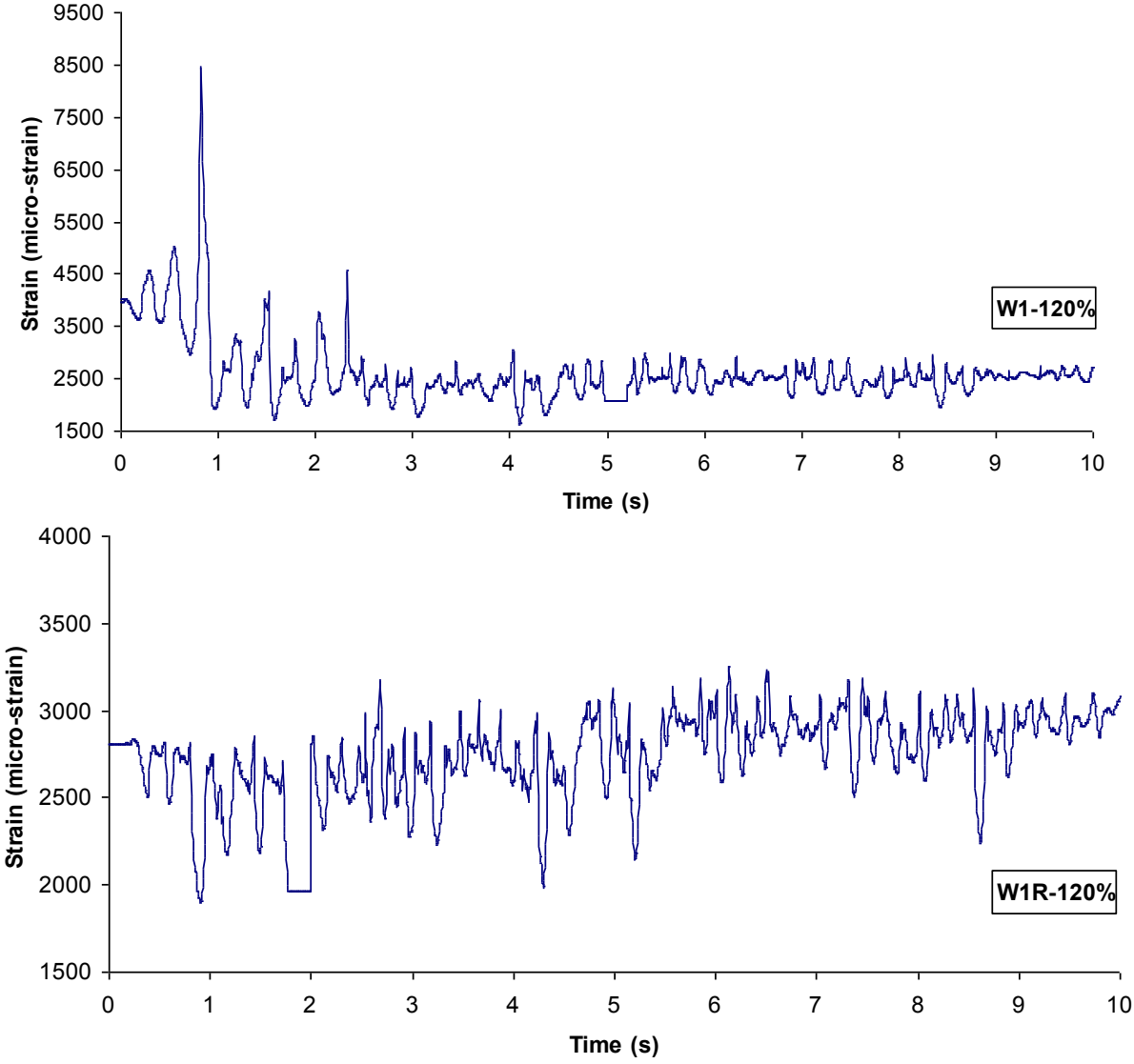

Figure 4.9 Strain gauge SG2 time history for the first wall before and after rehabilitation when subjected to 120% of the ground motion intensity.

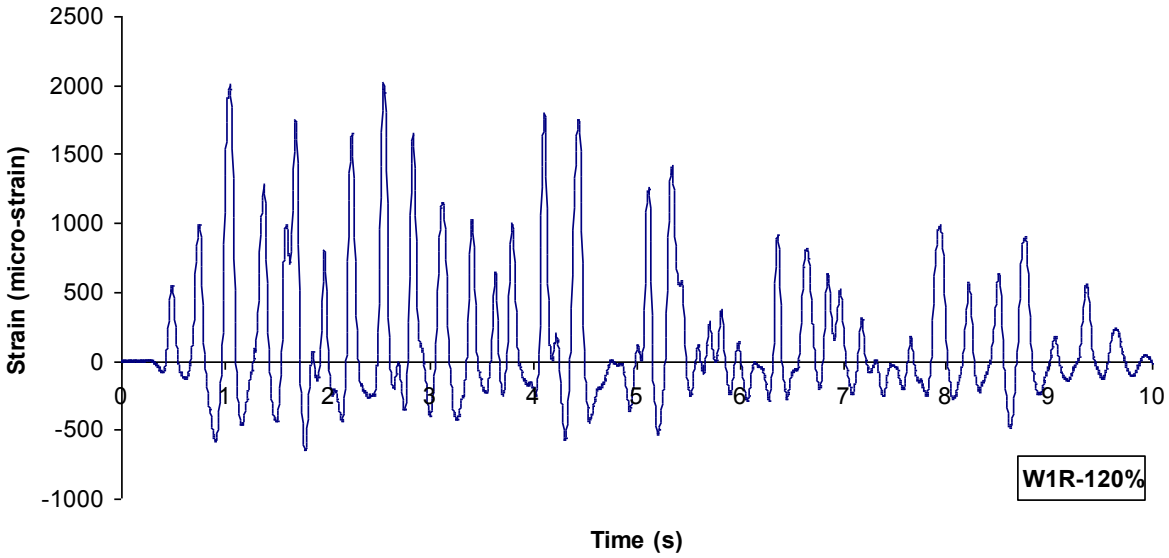

Figure 4.10 Strain gauge FRP-SG4 time history for the first rehabilitated wall W1R when subjected to 120% of the ground motion intensity.

From Tables 4.2 and 4.4, and considering the 120% of the ground motion intensity, it can be seen that the strain of the longitudinal reinforcement at the 6th storey panel of the original wall, W1, reached a value of 9800 μ strain when the wall's factored moment demand, M_f, was equal to 144 kN.m. This factored moment demand exceeded the wall's factored flexural resistance, M_r, at the 6th storey level which was calculated to be 118 kN.m. Performing section analysis of the original wall, the strains of the longitudinal reinforcement would be 3300 μ strain at $M_f = M_r = 118$ kN.m. The main design target of the FRP-rehabilitation scheme is to increase the factored moment resistance of the 6th storey panel without increasing the strains of its flexure steel reinforcement. For W1R, the FRP rehabilitation was able to reduce the strains in the longitudinal steel reinforcement (at a higher moment demand of $M_f = 150$ kN.m) to 3250 μ strain when subjected to 120% of the design ground motion intensity, which is less than

the strain value corresponding to the factored moment resistance of wall W1 (3300 μ strain). This shows the efficiency of the FRP-rehabilitation scheme in achieving the main design target even at 120% of the design ground motion intensity.

Table 4.4 also shows that the horizontal CFRP sheets applied at the wall base (where the high shear force demands were observed) were able to reduce the strains in the transverse steel reinforcement at that location. On the other hand, the strains of the transverse reinforcement at the sixth storey level were insignificant. It is worth noting that the strains of the horizontal CFRP sheets did not reach very high values, as the wall behaviour was mainly governed by its flexure. Nevertheless, the horizontal FRP sheets are still needed in case the retrofitted wall's flexural capacity exceeds its original shear capacity, in addition to their main function of confining the wall's boundary elements and hence increasing the wall ductility at the base.

For the second original wall, W2, the capacity of most of the strain gauges installed on the flexure reinforcement at the wall base and at the sixth storey level was exceeded due to the excessive yielding that occurred when the original wall was subjected to 200% of the design ground motion intensity, as indicated in Table 4.5. The shear reinforcement at the wall base yielded (ε_s = 2500 μ strain) when the wall was subjected to 200% of the design ground motion intensity, while at the sixth storey level, the shear reinforcement strains were insignificant. The strains in the horizontal FRP sheets were not significant at the base panel, however, they were able to reduce the strain of the transverse steel reinforcement at that level by almost 55%. Similar conclusions can be conducted from Figure 4.11, which shows the time history for transverse steel

reinforcement strain at the base panel of the second wall before and after rehabilitation when subjected to 200% of the ground motion intensity.

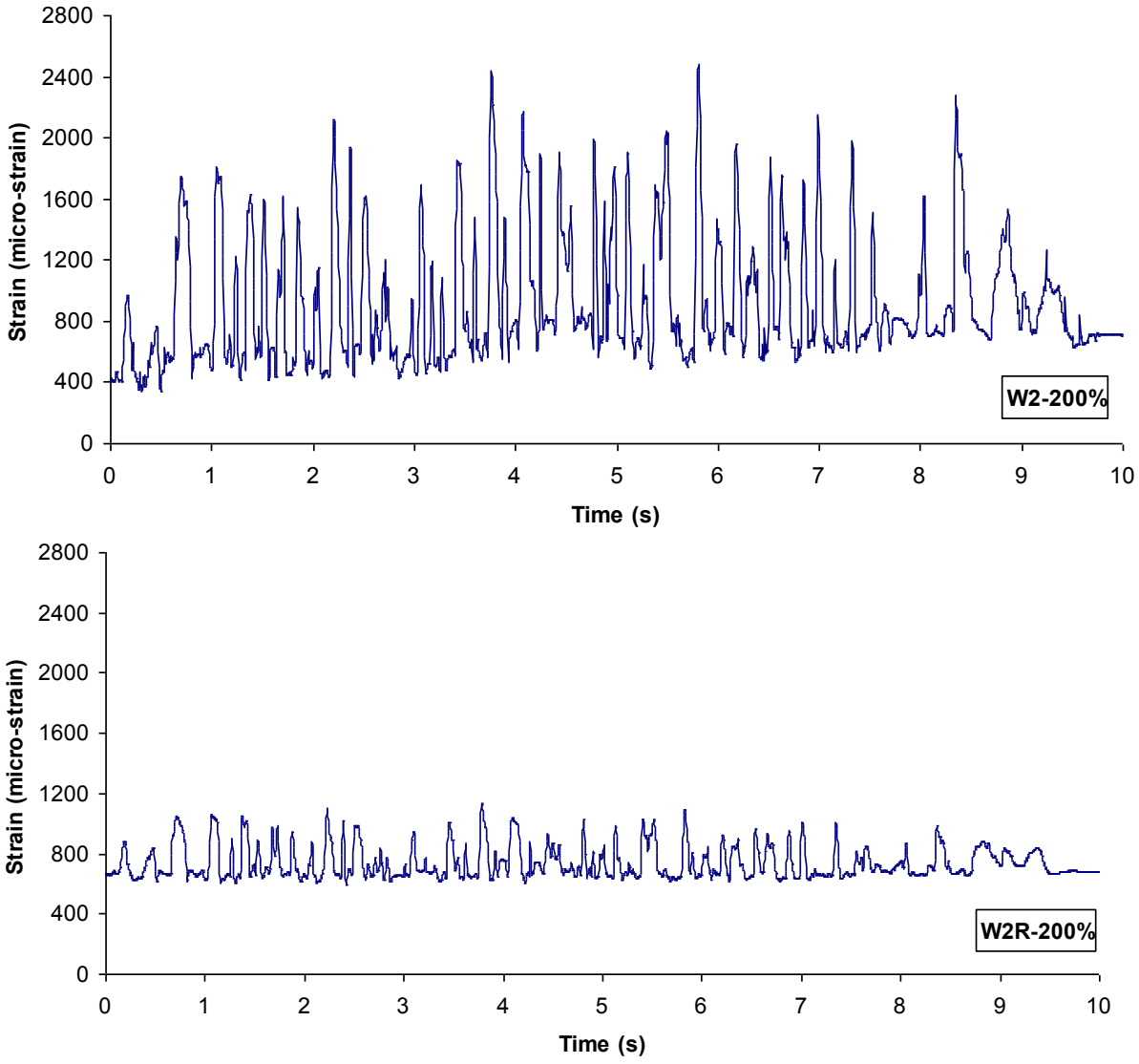

Figure 4.11 Strain gauge SG7 time history for the second wall before and after rehabilitation when subjected to 200% of the ground motion intensity.

4.3 IMPORTANCE OF ANCHORAGE DETAILING

Figures 3.4 and 3.6 show the two different FRP anchorage detailings used for the rehabilitated walls, W1R and W2R, respectively. For the second rehabilitated wall (W2R), it was expected that the CFRP vertical strips would reach higher strains when the wall was subjected to 200% of the ground motion intensity than the strains attained by W1R at 120% intensity. From Tables 4.4 and 4.5, the vertical CFRP strips for W2R (at 200% of ground motion intensity) reached strain values that were even less than those of W1R (at 120%). In addition, by comparing the moment-rotation curves for W2 and W2R in Figure 4.3, it is clear that the CFRP sheets reduced the wall rotation only for the pull cycles (where the wall rotation reduced from 0.0086 to 0.0065). During the push cycles, almost no change was observed in the wall rotation after rehabilitation. This indicates that the vertical FRP strips were not anchored properly to the slabs on the wall's west side. On the other hand, Figure 4.1 shows that the vertical CFRP strips applied to the sixth storey panel of the first wall, W1R, were able to reduce the wall rotation in both the push and pull directions. This indicates the importance of anchorage detailing in the efficiency of FRP flexure rehabilitation.

During the tests on the second rehabilitated wall (W2R), the horizontal CFRP wraps around the 6^{th} storey panel were not able to prevent the FRP anchor at the bottom slab from stretching outwards from the wall while being tensioned (Figure 3.6). Consequently, part of the CFRP anchor strain was lost during this undesired elongation, resulting in small strains in the vertical CFRP strips. The CFRP anchor connected to the top slab was efficient as the resultant force in the FRP anchor (R) was acting against the concrete slab,

not against the horizontal CFRP wraps, as shown in Figure 3.6. Interestingly, the CFRP anchor on the east side of wall W2R was partially efficient when subjected to 200% of the ground motion intensity. This phenomenon was observed because the wall experienced a higher rotational demand during the pull cycles, which tended to elongate the CFRP strips on the east side of the wall more than the ones on the west side, as can be seen in Figures 4.2 and 4.3. This elongation exceeded the lost elongation in the CFRP anchors that was previously mentioned (outwards stretch), which resulted in the ability of the CFRP strips to reduce the wall rotation for W2R during the pull cycles as seen in Figure 4.3. Therefore, it is recommended to install the FRP anchors as they were installed for wall W1R, despite the difficulty of drilling the holes through the wall web thickness. If the other detail has to be used, the designer has to ensure that the FRP anchor is detailed such that it only elongates in the direction parallel to its axis without any undesired outwards deformations that would waste part of the anchor's longitudinal strains (i.e. stretch without developing resisting forces).

4.4 EFFECT OF FRP-REHABILITATION ON THE BEHAVIOUR OF UNREHABILITATED PANELS

Tables 4.2 and 4.3 showed that the walls' shear force and bending moment demands changed after rehabilitation due to the vertical CFRP strips applied to the sixth storey panel. Figure 4.12 shows the maximum bending moment demands for the first and second walls before and after rehabilitation when subjected to different intensities of the design ground motion. Figure 4.13 show the maximum shear force demand before and after the FRP-rehabilitation of the first and second walls. From Figure 4.12, it can be seen that the bending moment demands for some storeys increased by 3-8% after rehabilitation at the 150% intensity, and by 6-13% for the 200% intensity. From Figure 4.13, it can be seen that the shear force demands at the base panel increased by 12% after rehabilitation at the 120% intensity, and by 10% at the 200% intensity. This increase in the demands would lead to an increase in the reinforcement strains of unrehabilitated panels after rehabilitation. In this case, due to the flexure rehabilitation of one panel of the wall, other panels may need to be rehabilitated if that rehabilitation leads to a significant increase in their demands and strains. This situation can be predicted using a numerical micro- or macro-model in which the additional stiffness due to FRP retrofit can be simulated. A numerical macro-model to simulate the cyclic behaviour of FRP-retrofitted RC wall panels is proposed in Chapter 7. This macro-model can be used to examine the behaviour of multi-storey RC walls in a complete building when they are retrofitted using CFRP sheets.

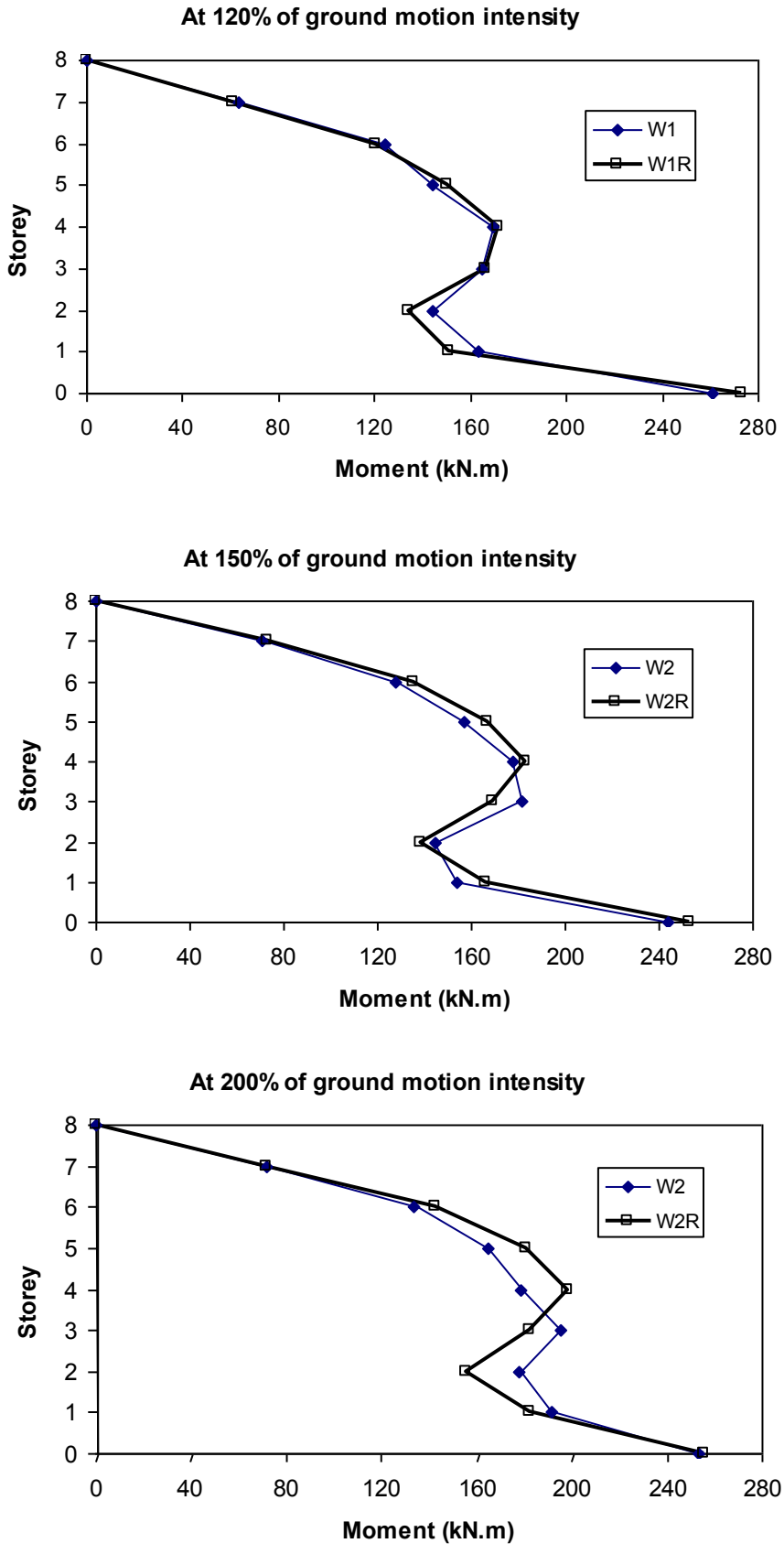

Figure 4.12 Effect of FRP-rehabilitation on the wall bending moment demands.

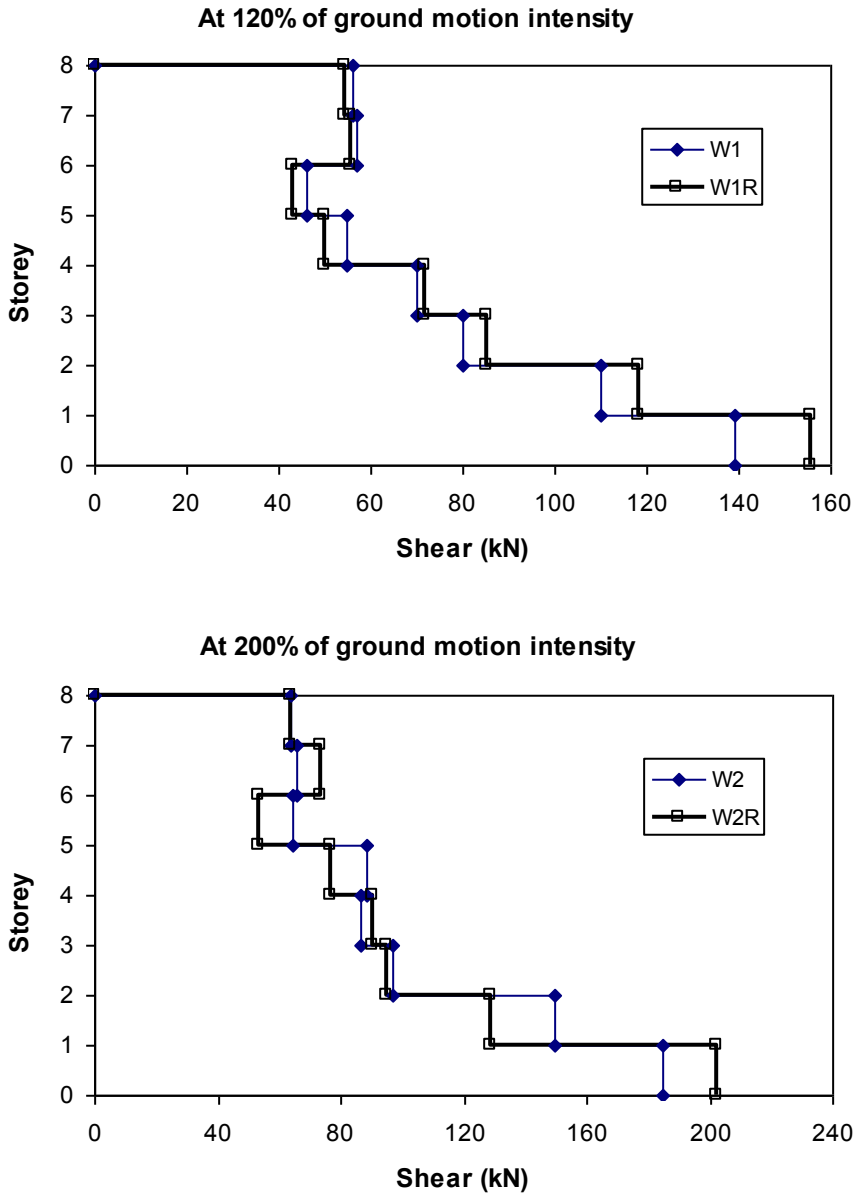

Figure 4.13 Effect of FRP-rehabilitation on the wall shear demands.

CHAPTER 5

EXPERIMENTAL PROGRAM
II. CYCLIC TESTS ON FRP-RETROFITTED RC WALL PANELS

5.1 INTRODUCTION

As explained earlier in Chapter 4 as part of the shake table tests, the two 8-storey RC shear walls were rehabilitated at their base and at the 6th storey levels using externally-bonded CFRP composites and were then tested under simulated ground motion excitation. The rehabilitation scheme was to increase the flexural and shear capacities of the walls at the 6th storey panel because of the observed increase in demand at that level, whereas the added CFRP wraps at the base panel was to increase the ductility capacity at the wall base.

One of the observations in the shake table tests was that the FRP was not fully utilized, since the capacity of the rehabilitated walls could not be reached due to the limited capacity of the shake table. Therefore, it was decided to conduct cyclic tests on a number of RC wall panels that represented the 6th storey panel of the 8-storey shear wall. The specimens will represent the control wall and the FRP-retrofitted walls using two different retrofitting schemes. The goal of the retrofit schemes is to increase the flexural and shear capacities of the RC shear wall panels, similar to the rehabilitation scheme that was applied at the 6th storey panel of the 8-storey walls. This chapter describes the wall design and construction, the material properties, test specimens, test setup, instrumentation, loading, and retrofit schemes.

5.2 WALL DESIGN AND CONSTRUCTION

5.2.1 Modeling of the sixth-storey panel

The shake table tests of the 8-storey walls showed that the base and the 6th storey panels experienced excessive yielding and cracking, while minor inelasticity was observed for the other storeys. Therefore, instead of testing the whole 8-storey wall, only the base panel or the 6th storey panel needs to be modeled and tested. The remaining storeys can be assumed to behave in an elastic manner. Figure 5.1 shows a schematic diagram for the part of the 8-storey wall to be tested under cyclic loading. The base storey panel or the 6th storey panel can be tested separately, and the effect of the remaining part of the shear wall will be taken into account, as shown in the figure. The top moment, ΔM, and the axial compressive force acting on the wall, P, will be applied, in addition to the shear force, F. The 6th storey panel will be modeled in this phase of the experimental program, as it was the panel that required additional flexural and shear strength.

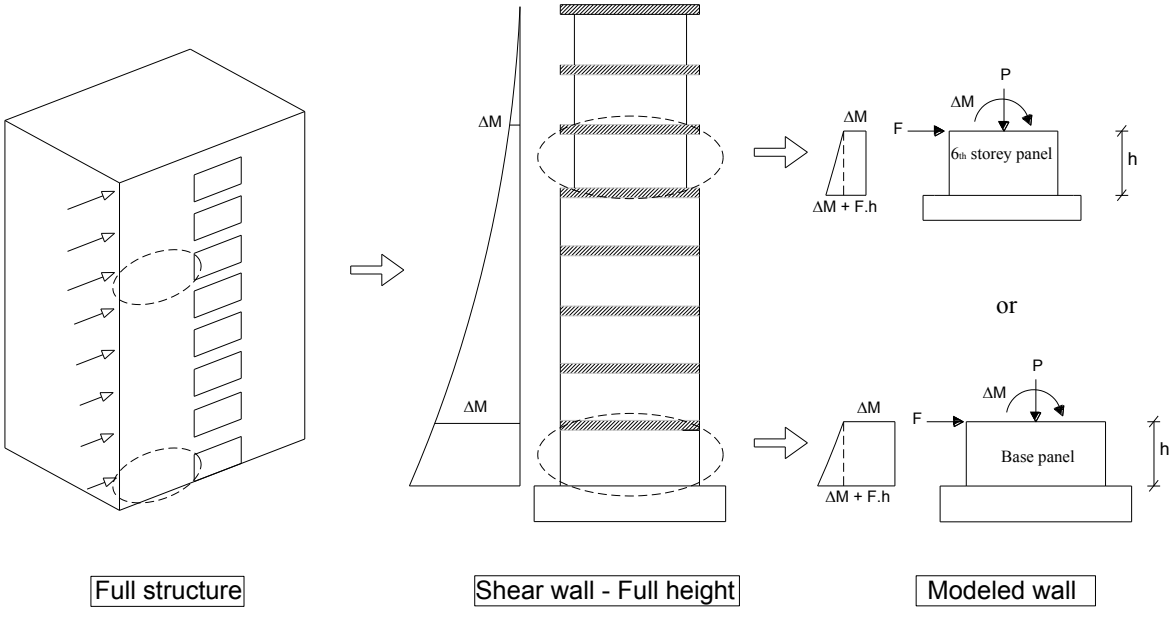

Figure 5.1 Representation of the plastic hinge regions of the 8-storey wall.

5.2.2 Similitude law requirements

According to Sabnis et al. (1983), there are two types of models: elastic models and strength models. Elastic models represent behaviour in the elastic range, and strength models represent the behaviour of the prototype up to failure. Strength models are classified in three different categories:

a) True models, where all the variables (first- and second-order) are modeled according to similitude law requirements. First-order variables are those variables that may have a significant influence on the physical parameters that are being studied. The other variables are considered as second-order variables;
b) Adequate models, where some of the second-order variables can not be modeled according to the similitude law requirements; and
c) Distorted models, where some of the first-order variables cannot be modeled according to the similitude law requirements.

For cyclic loading, the flexural strength and ductility of the control and retrofitted walls can be determined so the efficiency of the retrofit schemes can be judged. In this part of the experimental program, the mass of the wall is negligible compared to the mass of the structure which is the main source of inertia forces during an earthquake. In addition, the load will be applied statically during the tests. Therefore, the mass of the wall can be considered as a second-order variable and can be overlooked. The similitude law requirements used for the shake table tests shown in Table 3.1 were used in the cyclic tests. However, time was excluded, and only two dimensions were included; force F and length L.

5.2.3 Design of the test wall panels

Three wall panels were constructed and tested. The test walls represent the 6th storey panel of the 8-storey wall that experienced major inelasticity at that level due to demands that were higher than those stated in the design code. The walls were designed according to the NBCC (2005) and CSA-A23.3 (2004) as moderately ductile walls with ductility-related reduction factor, R_d, of 2.0 and overstrength-related reduction factor, R_o, of 1.4. The 6th storey level was designed according to the calculated seismic demands at that level and it was not detailed to act as a plastic hinge region. In order to provide confinement of the wall boundary elements as required by the CSA-A23.3 (2004) for moderately ductile walls, four unbonded steel bars were provided at the boundary elements and rectangular hoops were spaced at 80 mm intervals. The steel bars were unbonded using greased sleeves to avoid any contribution to the flexural resistance of the wall panel. The shear reinforcement bars were hooked at their ends to ensure they develop their full strength. The wall dimensions and reinforcement are shown in Figure 5.2.

As shown in Figure 5.2, a rigid reinforced concrete top block was poured monolithically with the wall and the bottom footing. The top rigid block ensures the uniform transfer of axial load, bending moment and shear force to the wall section.

5.2.4 Construction of the test wall panels at Concordia's Structures Lab

Wooden forms were assembled separately for the top block, the test wall, and the bottom footing. The reinforcement cages for the top and bottom blocks were prepared separately and then they were placed into their forms. Spacers were used to achieve the concrete

cover for the reinforcement. The flexure reinforcement of the wall was connected to the top and bottom cages, and then the wooden forms of the three parts were assembled together in the horizontal position as shown in Figure 5.3. To eliminate the effect of having lap splices in the current study, the wall flexure reinforcement was extended in the top and bottom blocks and bent to 90 degrees to ensure a sufficient anchorage length as shown in Figure 5.2. Prior to assembling the steel cage, a number of strain gauges were installed on the flexure and shear reinforcement bars. The wooden forms were braced using wooden posts to avoid any unacceptable deformations before the wall reached its full strength. A ready-mix concrete was delivered to Concordia's Structures laboratory. The concrete was poured with the wall lying horizontally, and it was mechanically vibrated to remove any air voids. The concrete was cured using wet burlaps covered by plastic sheets to provide a moist environment during the first week.

In order to transfer the loads from the test specimens to the strong floor of the Structures lab, it was decided to construct a rigid RC footing that can fit in the future different specimen dimensions and different test setups. The rigid footing was constructed with threaded holes that allow the specimen to be anchored to the rigid footing. Figure 5.4 shows the wooden form and the steel reinforcement of the rigid footing prior to the pouring of concrete. The rigid footing will act as a new strong floor with several anchor holes and will allow for future testing of different types of specimens without the need to build a massive footing for each new specimen.

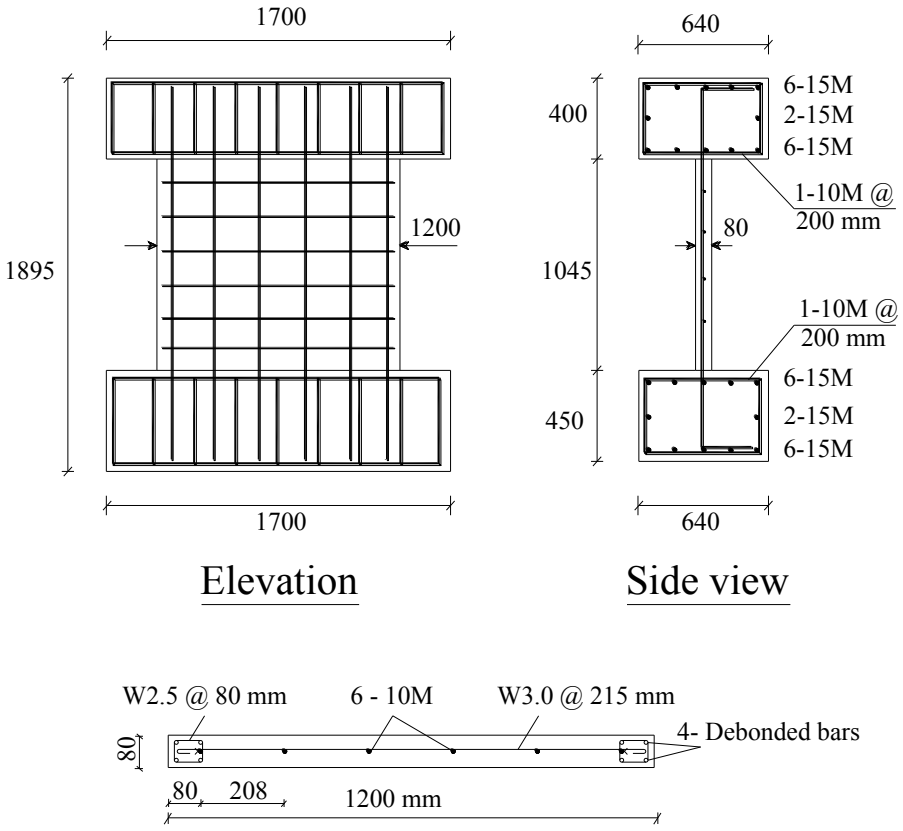

Figure 5.2 The wall panel specimen and its reinforcement.

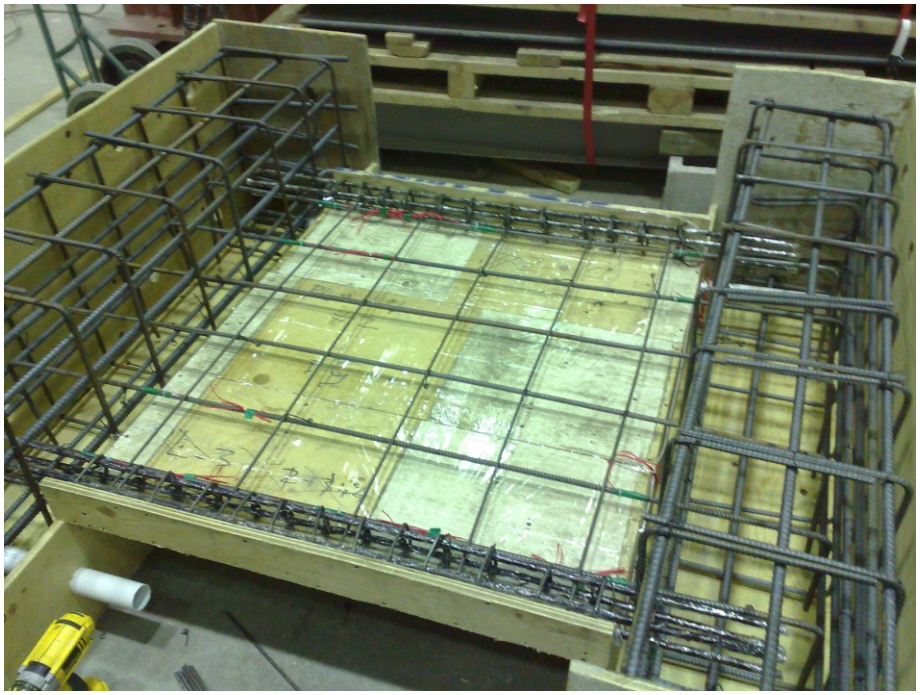

Figure 5.3 The wooden form and the steel cages.

Figure 5.4 The rigid footing prior to the pouring of concrete.

5.3 MATERIAL PROPERTIES

5.3.1 Concrete

Three wall specimens were cast at Concordia's Structures Laboratory using a ready mix concrete. Two specimens were cast at the same time (the retrofitted walls RW1 and RW2) and the third one was cast separately on another day (the control wall CW). The concrete slump for the control wall was 75 mm, while the slump of the retrofitted walls was 70 mm. These values provided adequate workability during the concrete casting. For each cast, three cylinders were tested after 28 days and the other three were tested on the day of testing. The concrete cylinder compression tests at 28 days and on the test day are shown in Table 5.1.

Table 5.1 Results of concrete cylinder tests.

Date	Control wall	Retrofitted walls
28 day strength (MPa)	43	34
Test day strength (MPa)	45	37

5.3.2 Steel reinforcement

Grade 400, 10M deformed steel bars were used as the main flexural reinforcement and 4.5 mm diameter plain bars were used for the shear reinforcement as well as for the hoops. The yield and ultimate tensile strength were determined using coupon tests. The results of the coupon tests are summarized in Table 5.2.

Table 5.2 Mechanical properties of steel reinforcement.

Bar designation	Nominal bar diameter (mm)	Yield strength (MPa)	Ultimate strength (MPa)
10M	11.3	450	550
W2.5	4.5	620	740

5.3.3 Fibre-reinforced polymer (FRP)

Carbon fibre-reinforced polymer (CFRP) composites were used for the retrofit of the wall panels. The Tyfo® SCH-11UP composite system (Fyfe 2010) with uni-directional CFRP sheets was used for both retrofitted walls, similar to the one used for the rehabilitation of the 8-storey walls tested under the simulated ground motion excitation. The mechanical properties of the Tyfo® SCH-11UP composite system: dry fibre, Tyfo S epoxy, and CFRP composite are the same as those used in the retrofit of the 8-storey shear wall tested on the EPM's shake table, presented in Table 3.2.

5.3.4 FRP anchors

FRP anchors used in the retrofit were prepared at the Structures' laboratory. The anchors were cut and fabricated from the dry fibres used in the Tyfo SCH-11UP composite system. A total of 16 anchors were used for each of the retrofitted wall specimens. Tyfo S epoxy was used to bond the fibres to the concrete substrate. The properties of the Tyfo® SCH-11UP composite system were presented in Table 3.2.

5.4 TEST SETUP

The test setup consists of three MTS hydraulic actuators which are mounted against a steel reaction frame as shown in Figures 5.5 and 5.6. The adjustable main bridge of the reaction frame was elevated to the proper height calculated to fit the two vertical actuators, the rigid steel loading beam, the wall specimen, and the rigid RC footing. The adjustable secondary bridge was also assembled at the proper height at the level of the rigid steel loading beam. Each MTS hydraulic actuator has a capacity of 1000 kN in compression and 750 kN in tension with a 400 mm stroke (± 200 mm). At both ends of the hydraulic actuator mounts, swivel hinges allow rotation in both the vertical and horizontal planes. Two actuators were placed vertically to enable the application of axial load and bending moment on the wall's top block, while a horizontal actuator was used to apply the shear force and moment acting on the wall. A rigid steel loading I-beam was used to uniformly transfer the actuator forces to the wall top block. The rigid steel I-beam was connected to the actuators using welded steel plates and threaded steel rods. The rigid steel I-beam was connected to the specimen top block using 8 threaded steel rods as shown in Figure 5.6. The specimen bottom block was connected to the rigid RC footing using 8 threaded rods. In order to ensure a full bearing of the threaded rods on the top and bottom blocks, concrete grout was poured to fill the gap between the rods and the block holes. This will also ensure that no relative movement will occur between the rigid steel beam and the specimen or between the specimen and the rigid RC footing. Two steel double angle braces connected the rigid I-beam to the laboratory wall as shown in Figure 5.7. The steel braces were designed to guide the steel loading beam and allow a smooth in-plane movement of the wall panel. The steel braces would eliminate

any out-of-plane movement that could arise from misalignment of the horizontal force or due to possible unsymmetrical damage of the wall at the failure phase.

The three actuators were controlled using a Flex Test™ GT digital controller with a supervisor computer connected to the digital controller. The software used for controlling the actuators was Model 793.1 Multipurpose Testware™ (MTS 2011). An external data acquisition system connected to another computer was used for collecting the instrumentation readings. Force tuning of the three actuators was performed on a dummy specimen prior to the first test, as recommended by the manufacturer to ensure accurate control of the actuators in force mode.

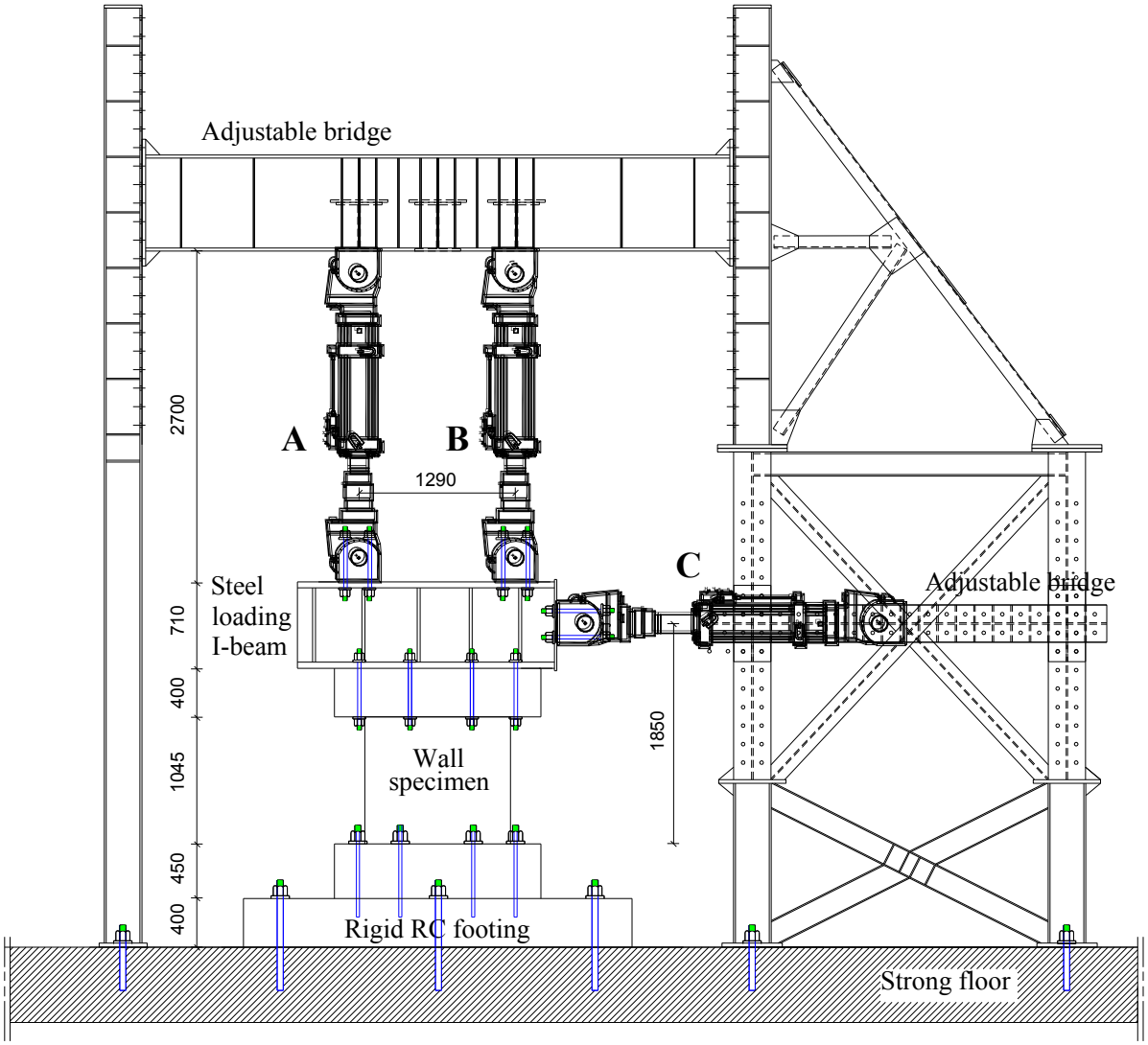

Figure 5.5 Schematic of the test setup at Concordia's Structures Laboratory (dimensions in mm).

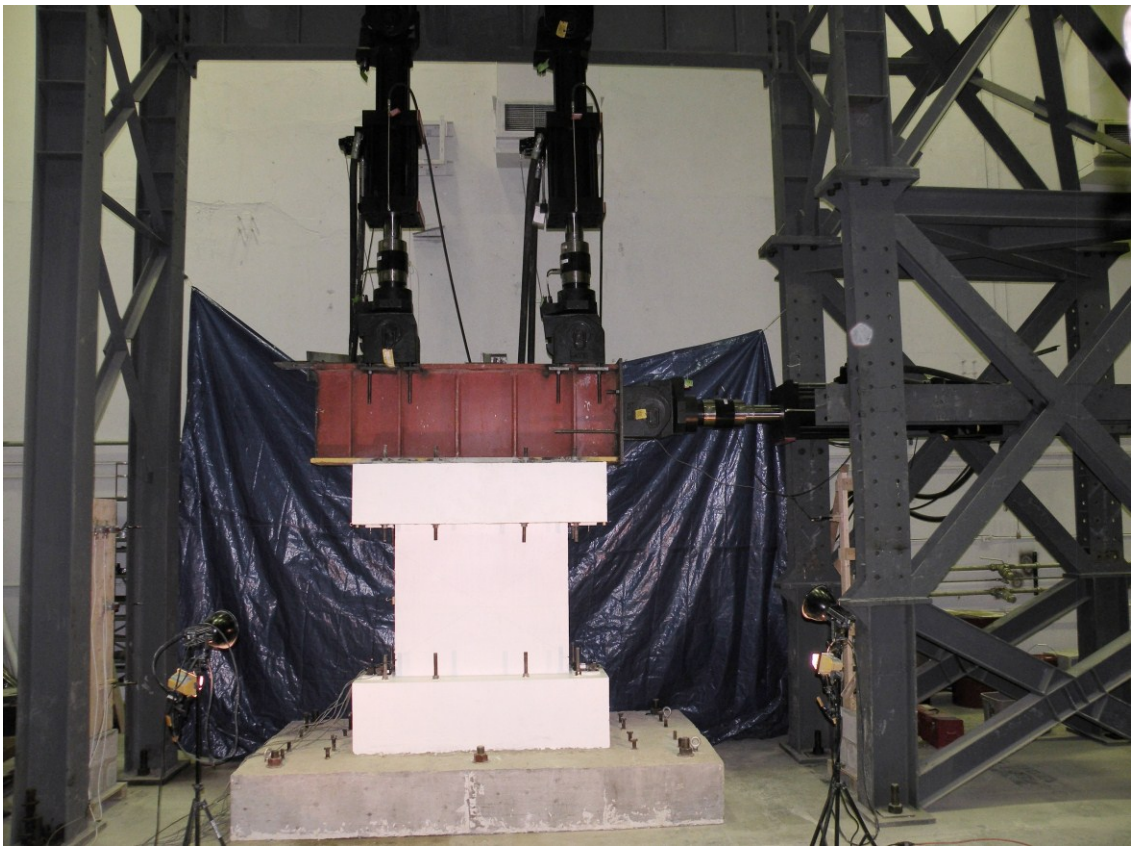

Figure 5.6 Test setup of the three wall panels.

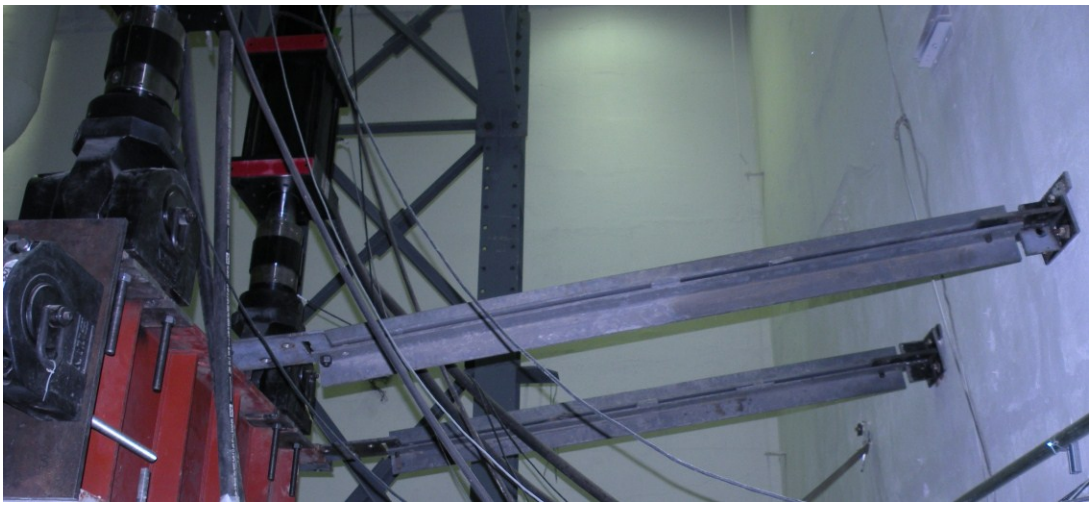

Figure 5.7 The steel braces to restrain the out-of-plane movement of the wall.

5.5 LOADING

Static cyclic loading procedures were applied to study the behaviour of the control wall panel and the FRP-retrofitted ones under lateral seismic forces. The two vertical actuators were used to apply an axial compression force and a moment, whereas the horizontal actuator was used to apply a horizontal shear force (that resulted in an additional moment at the base of the wall panel).

5.5.1 Moment-to-shear ratio

The moment-to-shear ratio (M/VL) used in the cyclic tests was selected to match the value obtained from the shake table tests on the 8-storey walls at the sixth storey level. The M/VL ratio at the wall base was selected to be 2.75 and therefore, the ratio at the top was equal to 1.88. The selected M/VL ratio classifies the wall as a flexural wall, according to Elnashai et al. (1990). The actuators were controlled to keep the moment value at the wall base equal to 3.3 m times the wall shear force, in addition to the constant axial force of 66 kN at the wall base. This was achieved by controlling the vertical actuators in force control mode based on the feedback from the load cell in the horizontal actuator. The forces in the two vertical actuators F_A and F_B (Figure 5.5) are related to the horizontal actuator force F_C by means of the following equations:

$$F_A = 24 + 1.115\ F_C \text{ (kN)} \quad (5\text{-}1)$$

$$F_B = 24 - 1.115\ F_C \text{ (kN)} \quad (5\text{-}2)$$

where the positive sign convention is compression. The equations are valid whether the horizontal actuator is controlled in a force or in displacement mode. The constant axial

load of 48 kN applied using both vertical actuators (24 kN per actuator) as well as the weight of the rigid steel I-beam and the specimen represent the axial load applied on the 8-storey wall at the 6th storey level during the shake table tests (described in Chapter 3).

5.5.2 Loading protocol

During the test, the vertical compression load of 24 kN was first applied using each of the vertical actuators and with the horizontal actuator force held at zero. The horizontal actuator control mode depends on the state of the specimen, while the vertical actuators are always controlled in force mode. The horizontal actuator is controlled in a force mode until the yield load is reached. The control mode is then switched to displacement control after the wall flexure reinforcement yielding. The yield load was determined using the readings of the strain gauges installed on the wall flexural reinforcement and using the load cell reading. The horizontal force was applied at a slow rate of 20 kN/min. A special cycle at 20 kN was applied to the control wall to detect the cracking load. A load cycle at the yield load, and several cycles after the flexural reinforcement yielding at different displacement ductilities were applied. A displacement ductility level is defined as the ratio of the top horizontal displacement of the wall panel to the wall displacement when first yielding of the extreme flexural reinforcement occurred. Each cycle was repeated twice in order to determine the strength and stiffness degradation due to the repetition of loading cycles. After each cycle, the cracks were identified and the specimen was inspected.

5.6 INSTRUMENTATION

The wall specimens were heavily instrumented to measure the applied forces, strains, and displacements. The applied forces were measured using the load cells included in the actuators. Fourteen strain gauges were installed on the steel reinforcement of each specimen and another 14 strain gauges were installed on the FRP sheets for each of the retrofitted specimens. The locations of the strain gauges installed on the steel reinforcement are shown in Figure 5.8. The steel rebars were prepared prior to the strain gauge installation. The bar ribs were removed and the bar surface was smoothened and cleaned at the gauge location. Each strain gauge was glued to a ground and smoothed surface on the steel rebar, and then covered with a protective rubber layer to protect the strain gauge during the concrete casting. For the strain gauges applied on the FRP sheets, the surface of the sheets was covered with a thin layer of epoxy at the locations where the strains were to be measured, and the gauge was glued to the smooth hardened epoxy. The locations of strain gauges installed on FRP sheets will be described in the following sections for each of the retrofitted wall specimens.

The wall displacements were measured using eight cable-extension position transducers (CEPTs) that were attached to the specimen and to two rigid reference walls as shown in Figure 5.8. The top lateral displacement of the wall, the wall mid-height displacement, the bottom end block movement, the wall top rotation, and the wall shear deformation were all measured. The full stroke of the CEPTs varied from 25 mm to 300 mm depending on the expected deformation at each location, and hence, they have different levels of accuracy.

The wall top rotation, θ, was obtained using the readings of the vertical position transducers P1 and P4 (accuracy of ±0.125 mm) according to the formula:

$$\theta = (P1 - P4) / a \tag{5-3}$$

The wall shear deformation, Δ_s, was obtained using the readings of the diagonal position transducers P2 and P3 (accuracy of ±0.32 mm) according to the formula given by Beyer et al. (2011):

$$\Delta_s = \frac{1}{4b}[(c + P_2)^2 - (c + P_3)^2] - (\alpha - 0.5)\,\theta\,h \tag{5-4}$$

where α is a parameter proposed by Hiraishi (1984) that accounts for the variation of curvature over the height of the panel, and *h* is the panel height. The value of α is equal to 0.5 for constant curvature (pure bending), and equal to 2/3 for triangular curvature distribution. In this study, the value of α was assumed to be 0.6, which is reasonable for the studied case due to the additional moment applied using the two vertical actuators that resulted in a wall's top moment equal to 0.67 of the moment at the base of the wall.

The lateral displacement at the top of the wall was measured using the position transducer P5 for small deformations (accuracy of ±0.05 mm) and using P6 at larger deformations (accuracy of ±0.3 mm). The lateral displacement at the mid-height was measured using P7 (accuracy of ±0.3 mm). The bottom end block movement was obtained using the reading at P8 (accuracy of ±0.05 mm) to get the wall's lateral net displacement. The instruments were calibrated to obtain the proportionality constant between displacement and voltage before and after each test.

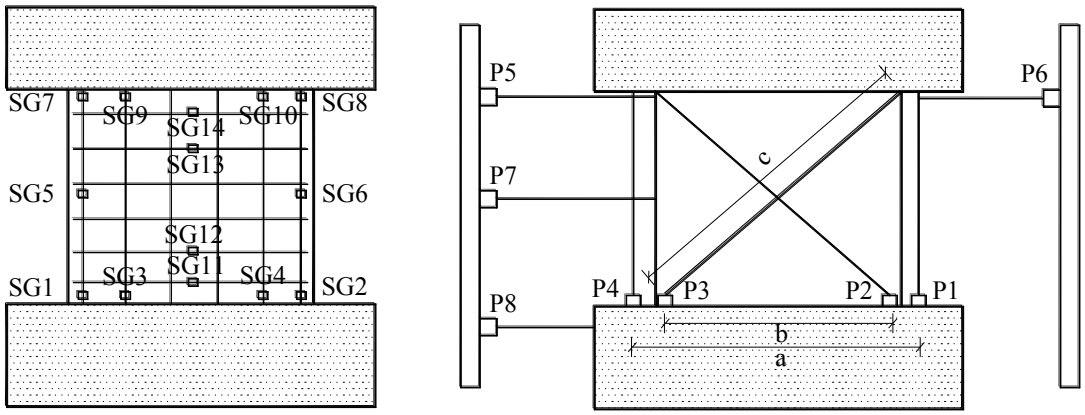

Figure 5.8 Strain gauge locations and displacement transducer positions.

5.7 CONTROL WALL

One control wall panel CW was tested under static cyclic loading up to failure. The control wall panel represents the 6th storey panel of the 8-storey wall tested under axial, top moment, and lateral load excitation. The flexural capacity of the control wall was calculated using the strain compatibility procedures and using the concrete and steel properties obtained from the cylinder and coupon tests. The concrete ultimate compressive strain was assumed to be 0.0035, and the concrete ultimate tensile strength f_r was taken 4.0 MPa. The axial load value at the base of the wall was 66 kN. The wall capacity was calculated taking the strain hardening of steel reinforcement into account. The contribution of compression steel reinforcement to the wall flexural capacity was considered in the calculations. The control wall was calculated to have a cracking load of 23 kN, yield load of 39 kN, factored flexural resistance of 47.3 kN and nominal flexural resistance at failure of 60.8 kN. The wall nominal shear resistance was calculated to be 151 kN.

5.8 RETROFITTED WALLS

Two specimens, RW1 and RW2, identical to the control wall specimen, were strengthened using CFRP sheets and tested under static cyclic loading. Two different retrofit schemes were considered in the cyclic tests. The main target of both retrofit schemes was to enhance the seismic performance of the tested wall panels by increasing the flexural capacity of the wall section so that it could resist the higher demands at the top floors of multistory shear walls arising from higher mode effects (El-Sokkary et al. 2012). From the shake table tests, it was found that the factored moment at the 6^{th} storey level of the tested wall M_f was almost 17% greater than the design factored resistance M_r when subjected to the design ground motion. Therefore, the retrofit design strategy requires that the factored resistance of the retrofitted walls would be at least 1.17 times that of the control wall. A value of 1.25 was selected in the design of retrofitted walls RW1 and RW2. As a result of increasing the wall's flexural capacity, the retrofit schemes must consider increasing the shear capacity of the wall panel to continue following the capacity design philosophy, where the FRP-retrofitted wall would not fail in shear before reaching its increased flexural capacity.

5.8.1 First retrofitted wall RW1

The first retrofit scheme of RW1 was similar to the one used in the shake table tests described in Chapter 3. The retrofit strategy aimed to increase the flexural capacity of a wall section by applying vertical CFRP sheets at the boundary zones of the wall. This was achieved by applying a 200 mm wide vertical uni-directional CFRP strip at the wall extremities on both faces, as shown in Figure 5.9. The chosen width was designed so that

the factored resistance of the retrofitted wall would be 1.25 times the factored resistance of the control wall. In the design of the vertical CFRP sheets, the ultimate strain of the FRP composite was limited to 0.006 as recommended by ISIS Canada (2008) to account for any premature anchorage failure or debonding of the CFRP sheets. A material resistance factor φ_{FRP} of 0.75 was used in the design, as recommended by ISIS Canada (2008) for the rehabilitation of flexural members using CFRP sheets. The retrofitted wall was calculated to have a yield load of 48.5 kN, factored resistance of 59 kN, and nominal resistance at failure of 69.2 kN. The expected failure mode of the retrofitted wall used in the estimation of the wall's ultimate load was failure of the CFRP vertical sheet system after reaching the design strain.

The vertical FRP strips were anchored to the top and bottom blocks using FRP fan anchors as shown in Figure 5.9. The FRP anchors were placed in pre-drilled holes that were filled with epoxy resin. The drilled holes made an angle of 20^o with the wall surface towards the core of the wall from both sides, and they went through the top and bottom block for a distance at least 120 mm as shown in Figure 5.10. Two anchors were used for each strip on each wall face at the top and at the bottom (total of 16 anchors). Horizontal CFRP sheets were applied on top of the vertical CFRP strips to increase the wall shear capacity. Two C-shaped CFRP sheets overlapped at the boundary regions of the wall to provide a better confinement of the wall end columns, as shown in Figure 5.9. The horizontal CFRP wraps also reduce the premature debonding tendency of the vertical CFRP strips under compression during the cyclic loading. Fourteen strain gauges were

installed on the CFRP sheets in the same direction of the fibres at the locations shown in Figure 5.11. The first FRP-retrofitted wall RW1 before testing is shown in Figure 5.12.

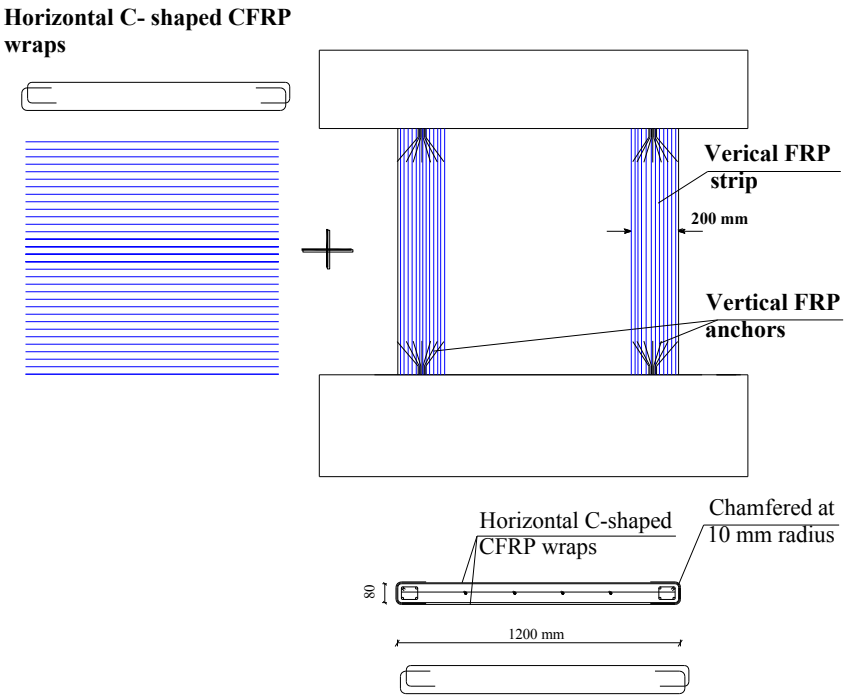

Figure 5.9 Schematic of the first FRP retrofit scheme for RW1.

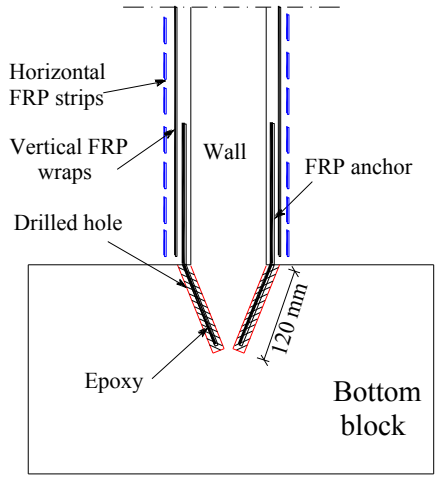

Figure 5.10 Schematic of the wall side view showing the details of FRP retrofit for RW1.

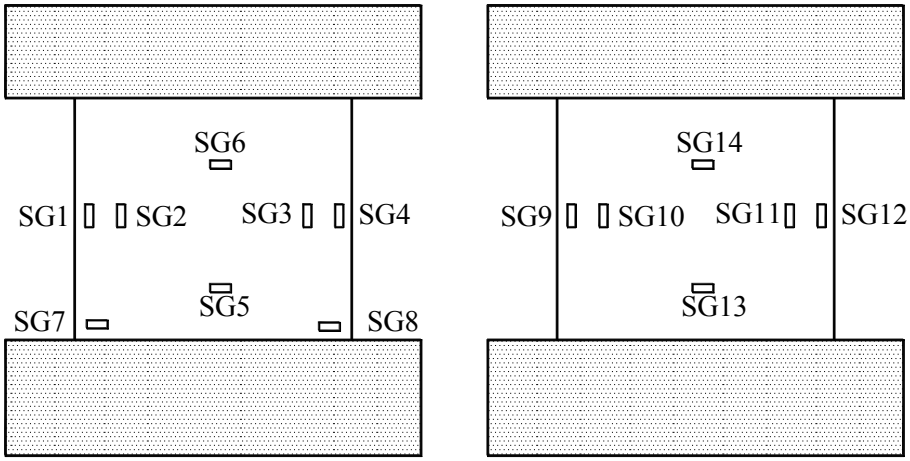

Figure 5.11 Locations of the strain gauges installed on FRP sheets of wall panel RW1.

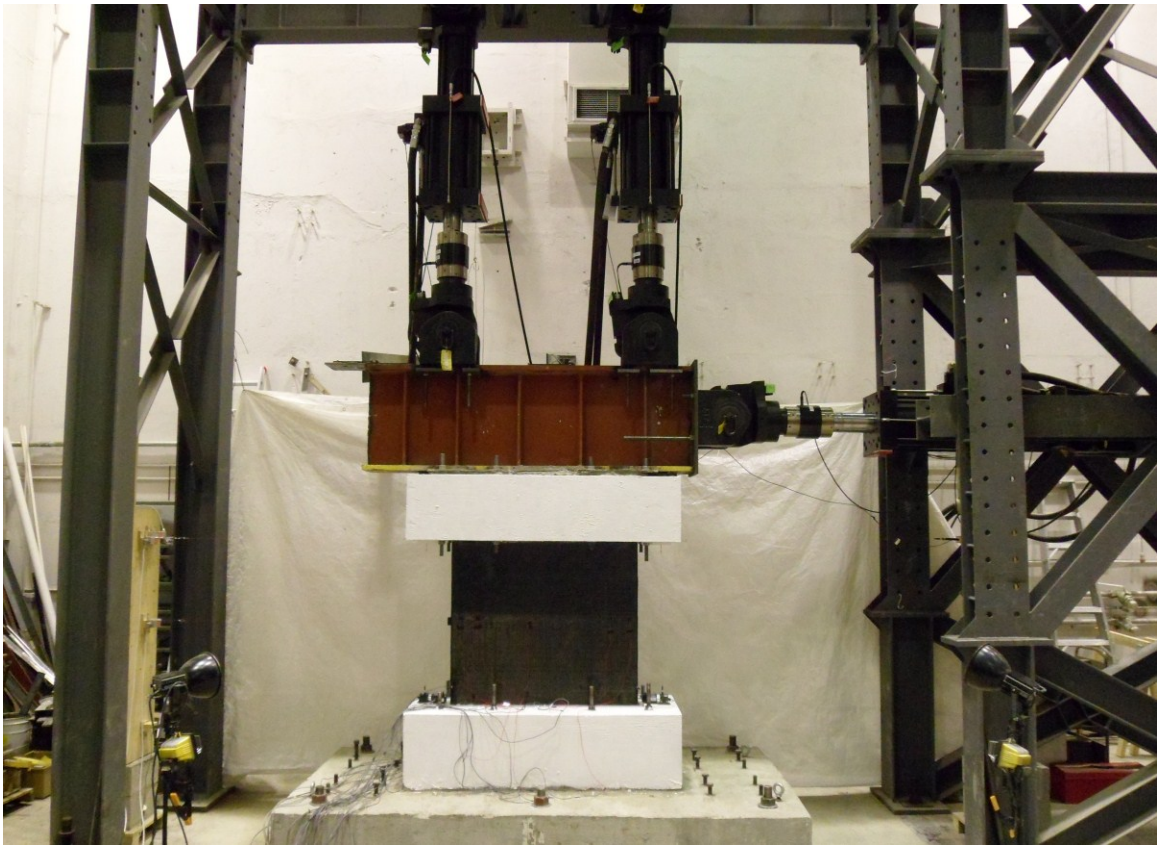

Figure 5.12 FRP-retrofitted wall RW1.

5.8.2 Second retrofitted wall RW2

In this retrofit scheme, the flexural and shear capacities of the wall were increased, similar to the first retrofitted wall RW1, but using a different layout of the fibres. Instead of using vertical and horizontal CFRP sheets to enhance the flexural and shear behaviour of the wall, respectively, diagonal CFRP strips were applied on each face of the wall panel. The 45º diagonal strip results in an inclined force that will be resolved into vertical and horizontal components. These components increase the flexural and shear capacity of the wall section, as shown in Figure 5.13. The vertical component of the force will be transferred to the top and bottom blocks using FRP anchors similar to the first retrofit scheme. The anchors were placed vertically to transfer the vertical component of the force created in the CFRP diagonal sheets. The horizontal component will be resisted by applying two 200 mm wide horizontal C-shaped wraps near the wall's top and bottom blocks as shown in the figure. The width of the diagonal strip was selected to be 280 mm. This will result in an effective cross sectional area of the inclined fibres (when resolved in the vertical direction) close to that of the 200 mm wide vertical strip used in the first retrofit scheme. This layout of the CFRP sheets will make the wall cracks visible and hence the retrofitted wall can be monitored after retrofit, which was not the case for the first retrofit scheme where the whole wall surface was covered by the sheets. This retrofit scheme also uses less FRP composite material, which will greatly reduce the cost of retrofit in the case of larger-scale walls. The strain gauges installed on the CFRP sheets are shown in Figure 5.14. The FRP-retrofitted wall RW2 prior to testing is shown in Figure 5.15.

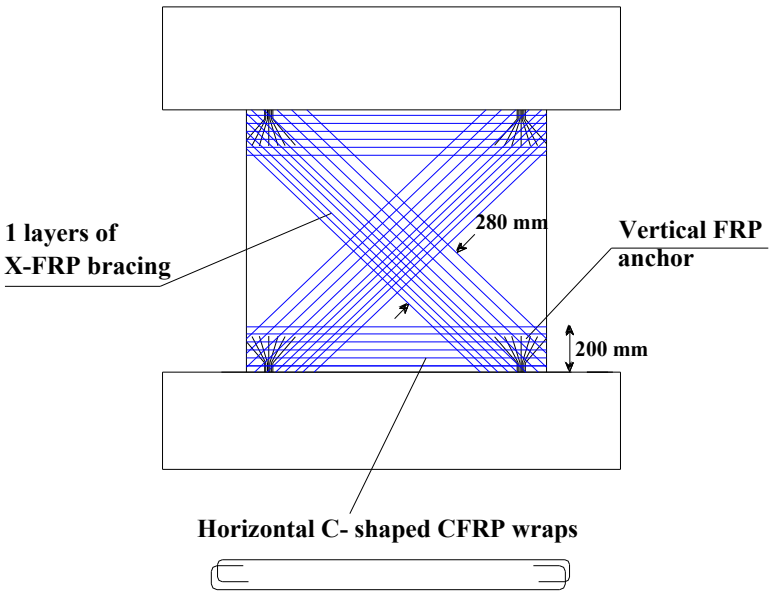

Figure 5.13 Schematic of the FRP retrofit scheme of wall panel RW2.

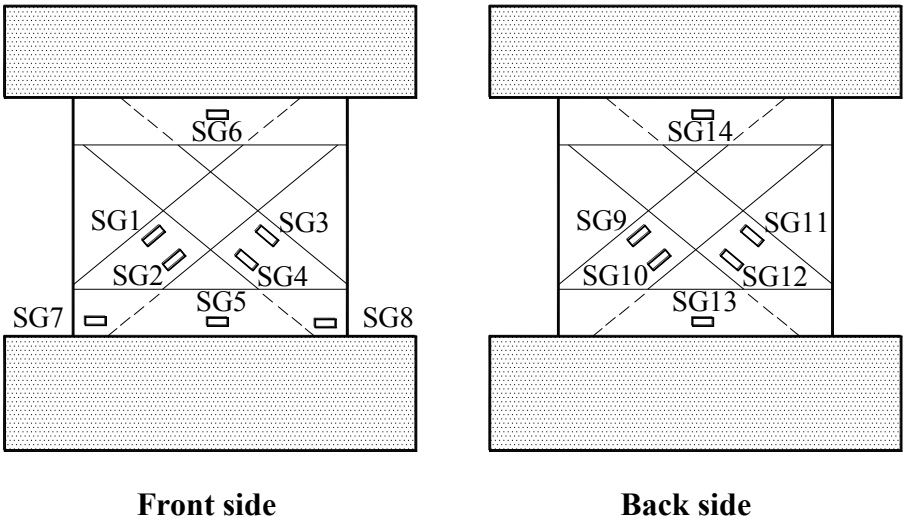

Figure 5.14 Locations of strain gauges applied on FRP sheets of wall panel RW2.

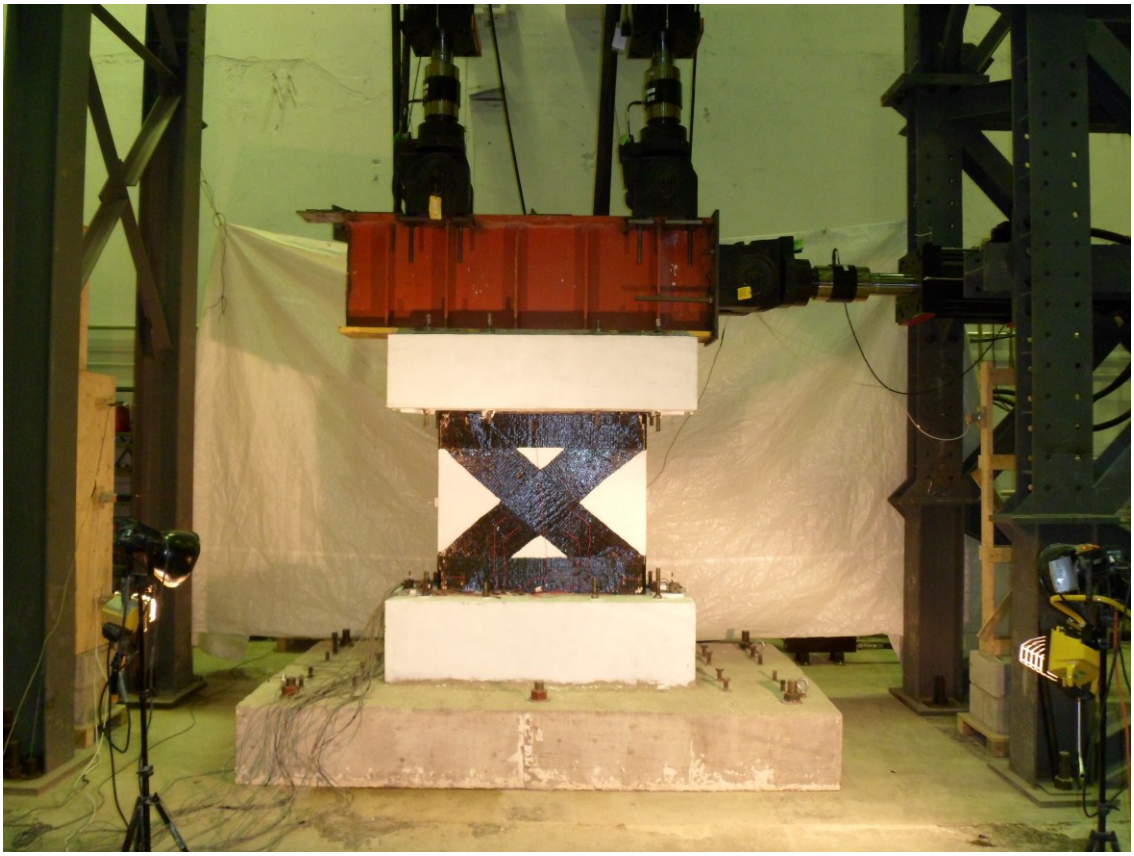

Figure 5.15 FRP-retrofitted wall RW2.

5.8.3 Application of CFRP sheets

The wall surface was cleaned and ground in several areas to achieve a smooth surface. The wall corners were chamfered to a radius of 10 mm to avoid stress concentration when wrapping the FRP sheets. The wall surface was covered by a primer coat prior to the application of CFRP sheets. The CFRP sheets were cut to the design dimensions and the FRP anchors were prepared. The two parts of the Tyfo S epoxy were mixed and the wall was painted with an initial coat of Tyfo S epoxy. Next, each layer of CFRP sheets was soaked with the epoxy prior to the application. A steel roller was used to remove any excessive adhesive and any air bubbles trapped between the CFRP layers.

5.8.4 Design and installation of CFRP anchors

The FRP fan anchors used in the retrofit were prepared from the dry fibres used in the Tyfo SCH-11UP composite system. Tyfo S epoxy was used with the FRP fan anchors, similar to its use with the sheets. Each FRP anchor was made of 12 strips, each 12 mm wide and 680 mm long. The strips were folded into two at mid-length and tied at the folded end to form an anchor with an embedment length of 120 mm and a fan length of 220 mm, as shown in Figure 5.16 (a). The anchor diameters ranged from 12 to 14 mm. The anchors were designed to have an ultimate strength equal to 40% of the ultimate strength of the straight fibre composite to account for the strength reduction due to the bent fibres. The ultimate anchor capacity (using an ultimate strain of 0.0042 mm/mm) was 33.3 kN. This value matches the coupon tests conducted by Ozbakkaloglu and Saatcioglu (2009), where they tested 81 CFRP anchors under direct pullout. Therefore, the capacity of the two FRP anchors used for each vertical or diagonal CFRP strip is equal to 66.6 kN. This value is 15% greater than the ultimate tensile strength of the vertical or diagonal CFRP strips using the typical test value provided by the manufacturer, or 57.8 kN for the strip width selected here. This would ensure the rupture of the vertical or diagonal CFRP strips before the fracture of the FRP fan anchors. The embedment length of 120 mm exceeded the embedment length used by Ozbakkaloglu and Saatcioglu (2009), which was 100 mm to ensure that no bond failure would occur between the CFRP anchor and the concrete substrate.

The holes were drilled in the bottom and top blocks, inclined towards the core of the wall from both its faces, at an angle of 20^{o} with the wall surface. The drilled holes had a

diameter of 20 mm and a depth of 120 mm. The holes were cleaned using compressed air to remove any dust prior to installation of the FRP anchor. The FRP anchor was soaked in the Tyfo S epoxy and inserted in the drilled hole. The hole was then filled with epoxy using a syringe. The FRP fans were soaked with epoxy and spread out as shown in Figure 5.16 (b). It should be noted that for practical applications in existing RC shear walls, the steel rebars could induce a real concern while drilling the holes for the anchors. Therefore, the location of the steel rebars must be accurately predicted to avoid hitting them during the drilling process.

(a) **(b)**

Figure 5.16 FRP fan anchors used in retrofit of RW1 and RW2.

CHAPTER 6

RESULTS OF CYCLIC TESTS

6.1 INTRODUCTION

In this chapter, the experimental results of the quasi-static cyclic loading tests on the RC wall panels are presented. A control wall, CW, panel and two FRP-retrofitted wall panels, RW1 and RW2, were tested while subjected to constant axial load, P, varying moment, M, and shear force, V, at the top of the wall panel as described in Chapter 5. The test setup and the relation between the acting forces P, M, and V were designed such that the moment-to-shear ratio, M/VL, for the tested panels was equal to 2.75. This value matches the moment-to-shear ratio at the sixth storey level of the 8-storey RC walls tested on the shake table at EPM. The 8-storey wall represents a typical moderately-ductile RC wall in a building located in Montreal, designed according to NBCC 2005. During the cyclic tests, the loads, displacements and strains were monitored and recorded each half-second using two data acquisition systems. The walls were monitored and inspected closely to identify the developed cracks and their propagation till failure. This chapter describes the seismic performance of each wall panel specimen and presents their experimental data. A comparison between the behaviour of the control wall panel and the FRP-retrofitted panels was carried out and is presented in detail.

6.2 CONTROL WALL (CW)

One control wall panel was tested as-built without strengthening. The CW panel was tested by applying lateral load push and pull cycles at the top of the wall in a force-control mode in three stages: at 20 kN, 30 kN, and at the load corresponding to yielding

of flexure reinforcement. After the yielding of the wall flexure reinforcement, the control mode was switched from force control to displacement control. The force control mode was used in the pre-yielding stage, as wall displacements are very small and difficult to control in this linear phase, and we need to carefully seek the yielding displacement without overshooting, which would be much more difficult using a displacement control mode. The first crack was observed near the wall's base at 20 kN during the pull cycle, as shown in Figure 6.1. Another horizontal crack near the wall's mid-height was observed at a 30 kN load during the pull cycle. Both cracks propagated at the yield load, as indicated. The yield load was determined when the strain value of the extreme flexure reinforcement bar reached the yield strain of 0.00225. The yield load occurred at 40.5 kN, with a lateral displacement of 1.4 mm corresponding to a lateral drift ratio of 0.134%. After reaching the yielding load, the wall was subjected to increasing cyclic displacements that correspond to displacement ductility levels, μ_Δ, of 1.5, 2, 3, 4, 5, etc., up to failure. The displacement ductility, μ_Δ, is defined as the ratio of the displacement level, Δ, divided by the displacement at yield, Δ_y. Each cycle started in the push direction and was assigned a positive notation of the lateral force and displacement. Each cycle after the yield load was repeated twice in order to determine the strength and stiffness degradation due to the loading repetitions.

6.2.1 Lateral Displacements of CW

The wall's lateral displacement was measured at the top of the wall as well as at the wall mid-height. The relationship between the applied lateral load and the wall's top displacement is shown in Figure 6.2. From the figure, it can be seen that after the yielding

load, the wall showed a gain in its strength upon increasing the lateral displacement. This is mainly due to the strain hardening of the flexural steel reinforcement up to a lateral displacement of 4.2 mm (μ_Δ = 3.0) and drift ratio of 0.40%. After the wall yielding, more horizontal fine cracks were observed, and they began to propagate (Figure 6.1). These cracks did not widen, whereas it was observed that only the base crack became wider with the increased wall displacement. As can be seen from Figure 6.2, the wall did not show an increase in its lateral strength beyond the load cycle at a displacement of 4.2 mm (μ_Δ = 3.0). The ultimate strength measured for the control wall at that displacement level was +61 kN in the push direction, and -57 kN in the pull direction. The repetition of each loading cycle resulted in strength deterioration and stiffness degradation of about 6% due to the crack opening and closure mechanism in the respective second cycles. Concrete crushing was observed at the toe of the wall on the compression side at a lateral displacement of 11.2 mm, which corresponds to μ_Δ = 8.0 and drift ratio of 1.08%. The control specimen was able to sustain a lateral displacement of 14 mm, which corresponds to μ_Δ = 10.0 and drift ratio of 1.34%, with no strength deterioration. At the repeated cycle of the 14 mm load cycle in the push direction, the extreme flexure reinforcement bar ruptured and the lateral load dropped to +37 kN; i.e., the wall reached its failure limit at this level. At the repeated cycle of the 15.4 mm (μ_Δ = 11.0) load cycle in the pull direction, the other extreme flexure reinforcement bar ruptured and the load dropped to -32.5 kN. The test was stopped after completing the 15.4 mm loading cycle as the wall had reached almost 65% of its capacity in both the push and pull directions. The maximum lateral drift that the control wall reached before failure was 1.34% at 14 mm lateral displacement, which corresponds to a displacement ductility of μ_Δ = 10.0. Figure 6.3 shows the relationship between lateral displacement measured at the wall mid-height and

the applied lateral load. The wall mid-height displacement was measured to be, on average, 50% of the corresponding top displacement; however the relationship is very similar in shape to the wall's top displacement plot. The failure mechanism of the control wall was rupture of the extreme flexure reinforcement bars accompanied by concrete crushing of the wall toes, as shown in Figure 6.4.

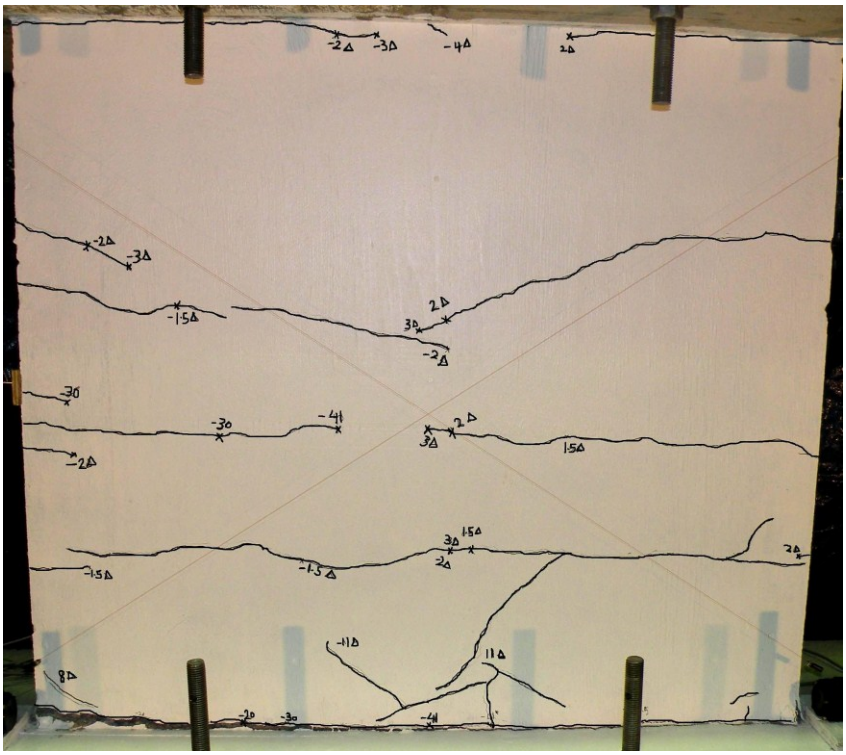

Figure 6.1 Crack pattern of the CW at failure.

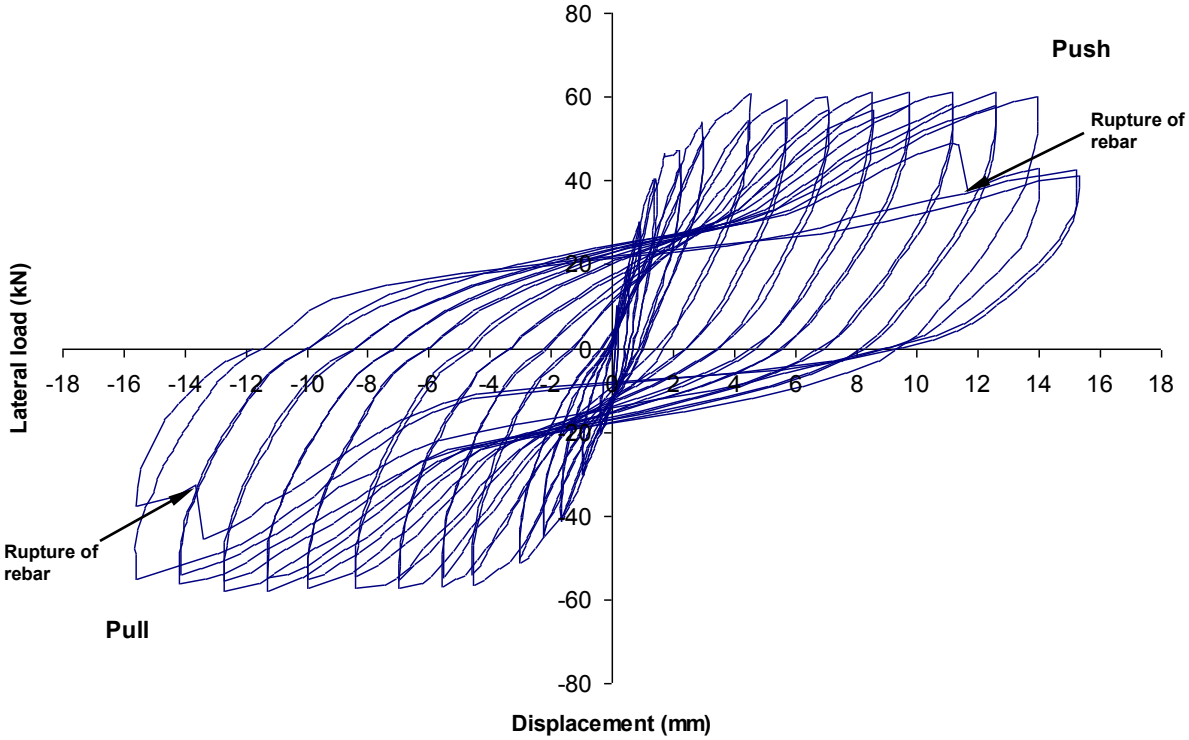

Figure 6.2 Lateral load-top displacement relationship of the CW.

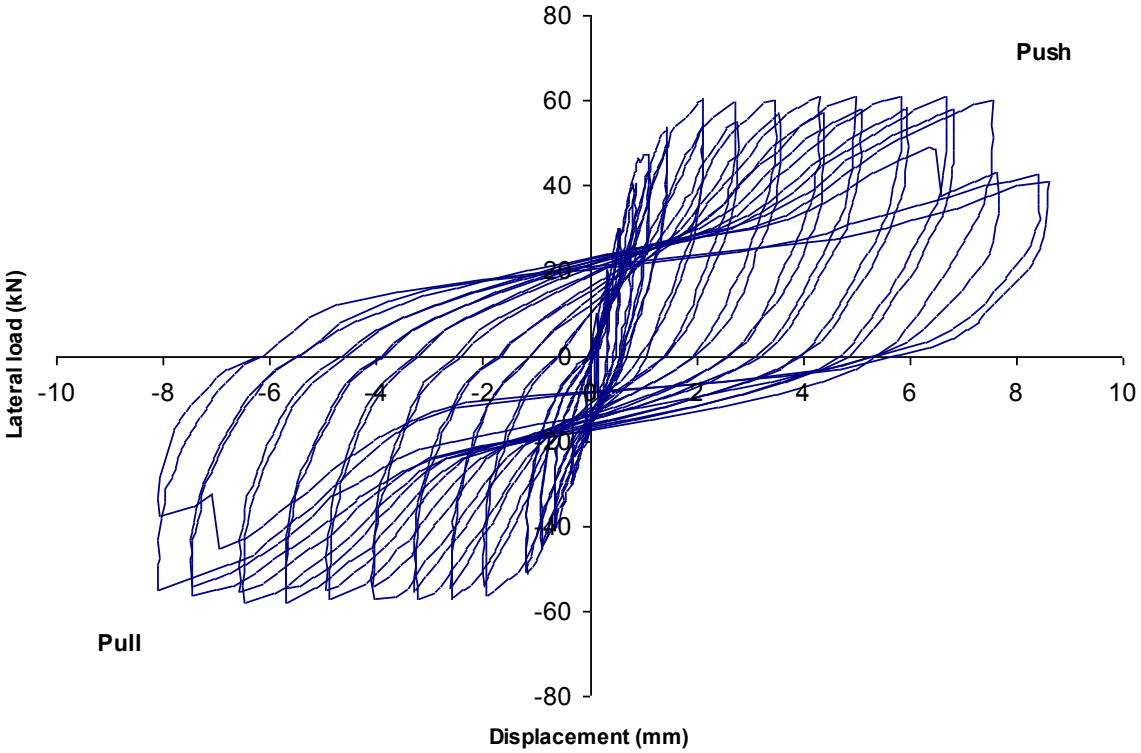

Figure 6.3 Lateral load-mid-height displacement relationship of the CW.

Figure 6.4 Concrete toe crushing of the CW.

6.2.2 Top Rotations of CW

The wall's top rotation, θ, was calculated using two high accuracy displacement transducers, P1 and P4, shown in Figure 5.8. The two transducers were fixed to the foundation block and attached to the wall's top block. The wall's top rotation was calculated from the readings of P1 and P4 using Equation 5-3, where the distance between the transducers, *a*, was measured to be 1500 mm for the control wall CW. Figure 6.5 shows the variation of the wall rotation with the applied lateral load. The wall rotation at the yield load was measured to be 0.0013 rad. This figure shows that the maximum rotation of the wall before failure was 0.0114 rad in the push direction and -0.0133 in the pull direction. The wall rotational ductility, μ_θ, is defined as the ratio of the wall rotation at certain load level to the wall rotation at the yield load. Hence, the wall was able to

achieve a rotational ductility at failure, μ_θ, of 8.70 in the push direction and 10.2 in the pull direction.

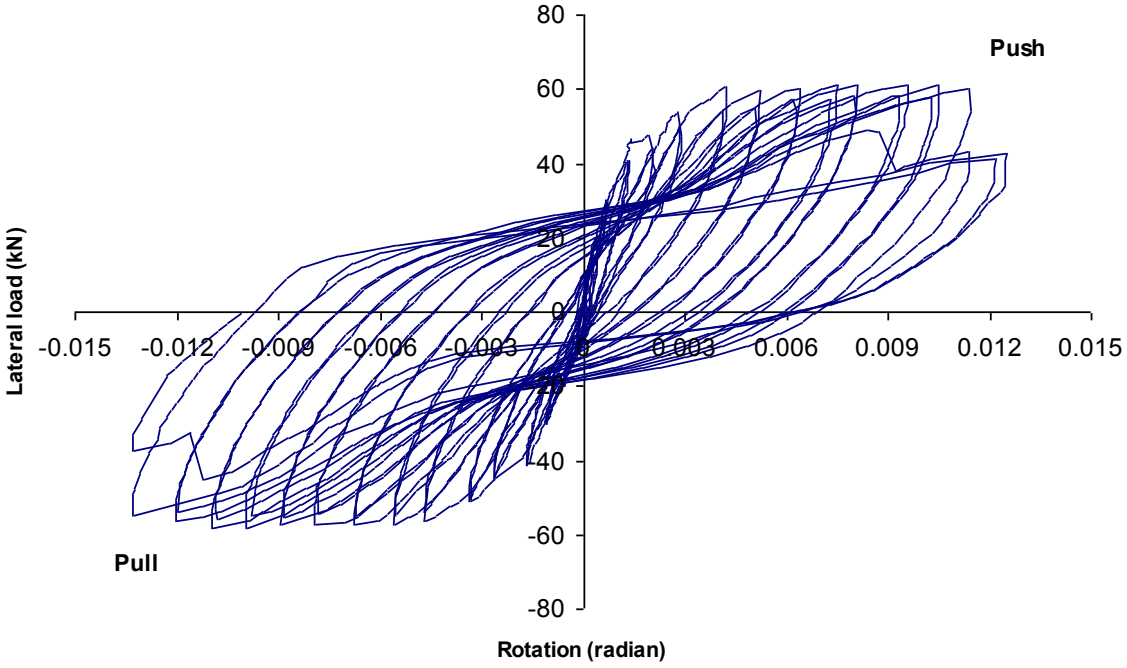

Figure 6.5 Lateral load-top rotation relationship for the CW.

6.2.3 Shear Deformation of CW

The shear deformation, Δ_s, was calculated using the readings of the diagonal position transducers P2 and P3, indicated in Figure 5.8, using Equation 5-4. The distances b and c in the figure were measured to be 1380 and 1640 mm, respectively. Figure 6.6 shows the wall shear displacement plotted against the applied lateral load. The wall shear displacement at failure was measured to be 3.9 mm at a lateral load of +61 kN in the push direction, and -5.8 mm at a lateral load of –57 kN in the pull direction.

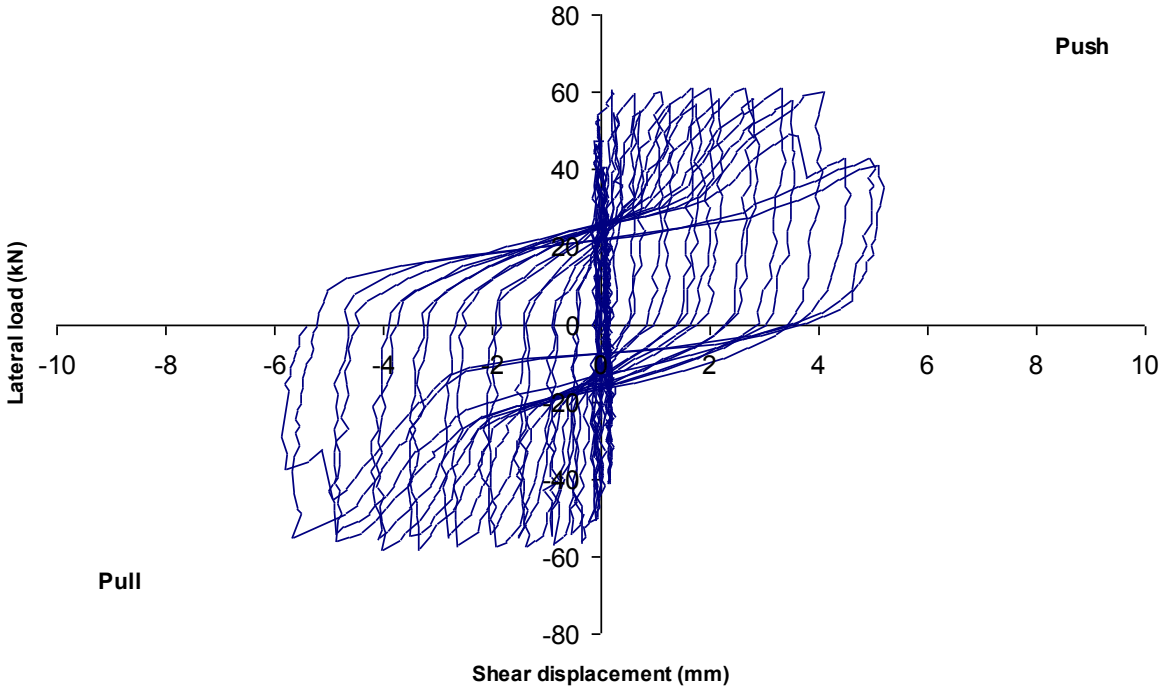

Figure 6.6 Lateral load-shear displacement relationship of the CW.

6.2.4 Strains in steel reinforcement of CW

The maximum strains along the flexure rebars' lengths were recorded by the strain gauges, SG1 and SG2, installed on the outermost flexure reinforcement bars at the wall base as shown in Figure 5.8. The readings of SG1 and SG2, confirmed by the change in stiffness of the lateral load-deformation relationship, were used to determine the yield load of the specimen. The measured strains from SG1 and SG2 plotted versus the applied lateral load are shown in Figures 6.7 and 6.8, respectively. The strain values for these two gauges increased rapidly when the wall reached lateral displacement of 2.8 mm ($\mu_\Delta = 2.0$) and the operational range of the gauges were exceeded (15000 micro-strain). For strain gauges SG3 and SG4, the operational ranges were exceeded at a lateral displacement of

4.2 mm (μ_Δ = 3.0). Figure 6.9 shows the reading of SG7 (located at the top of the wall) versus the applied lateral load. This figure shows that the wall flexure reinforcement yielded at the top at a lateral load of 55 kN. The maximum strain reached at the top was almost 1.1 times the yield strain. This indicates that most of the wall nonlinearity occurred at the wall base, as was observed during the test.

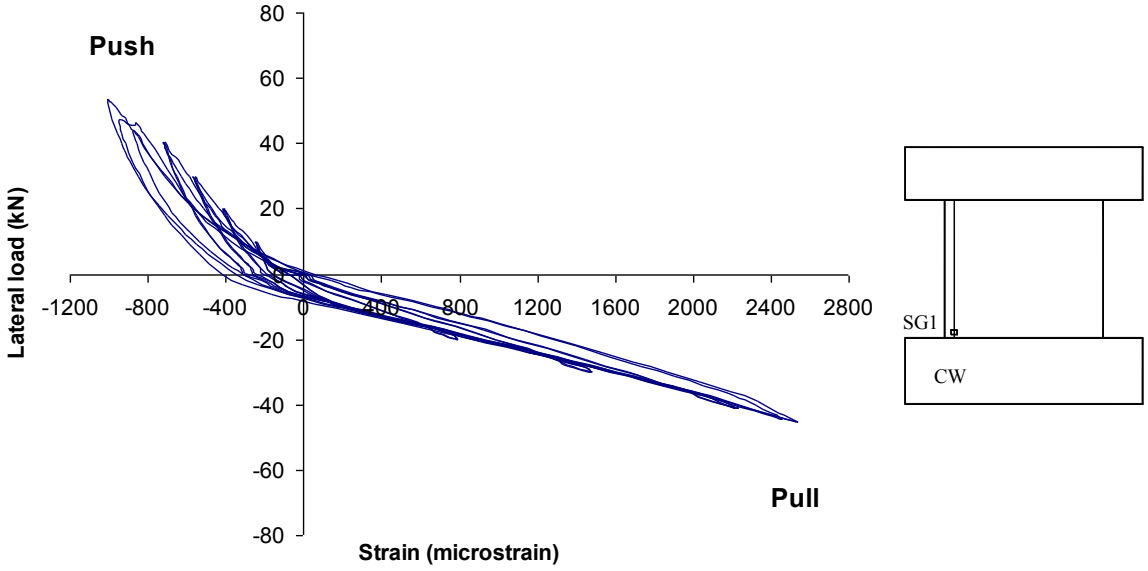

Figure 6.7 Strain gauge SG1 readings for control wall CW.

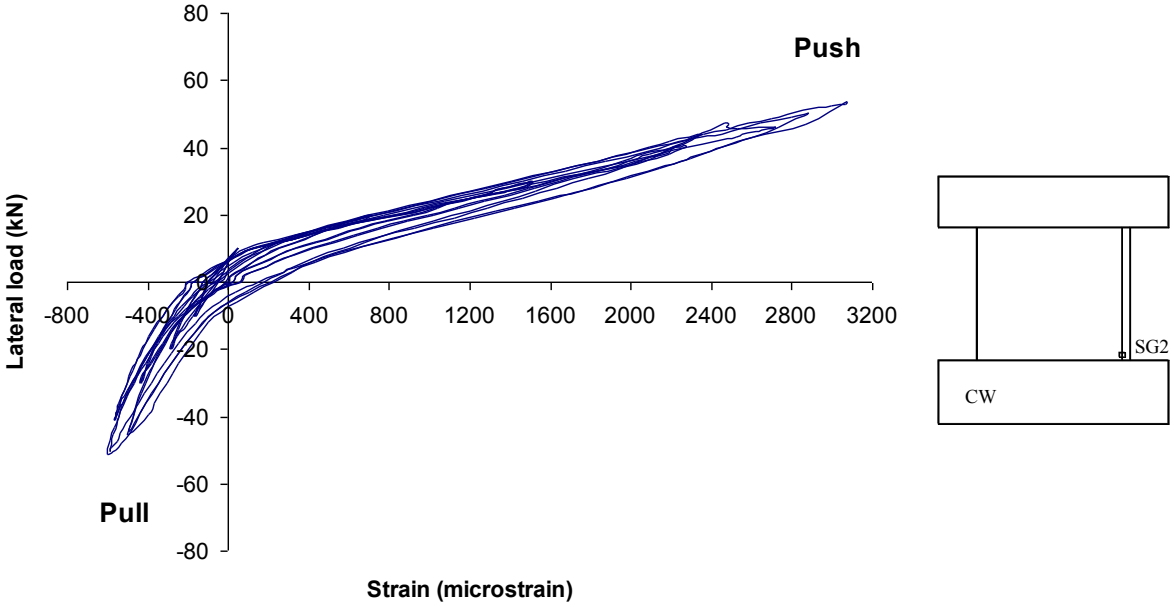

Figure 6.8 Strain gauge SG2 readings for control wall CW.

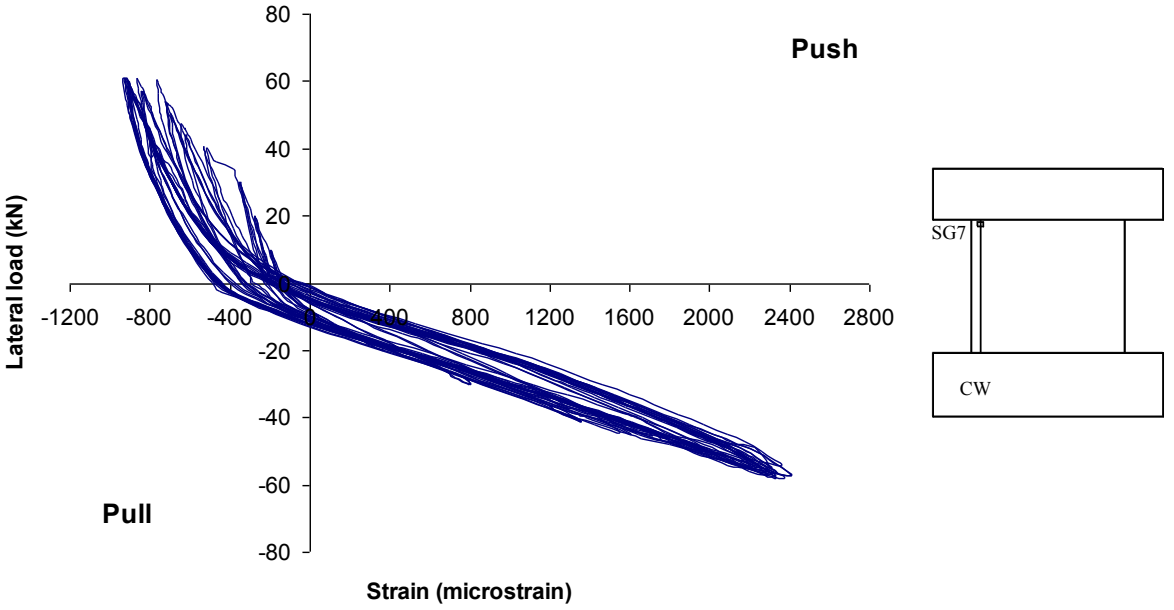

Figure 6.9 Strain gauge SG7 readings for control wall CW.

The strains in the horizontal reinforcement bars were not significant, as can be observed in Figure 6.10. The maximum strain reached in the shear reinforcement was measured to be 550 micro-strain, which is almost 18% of the shear reinforcement yield strain (3100 micro-strain). This is attributed to the fact that the wall's concrete contribution to the nominal shear capacity, V_c, calculated according to CSA-A23.3 (2004), was 92.7 kN -- almost 50% greater than the shear force that corresponds to the wall's flexural capacity.

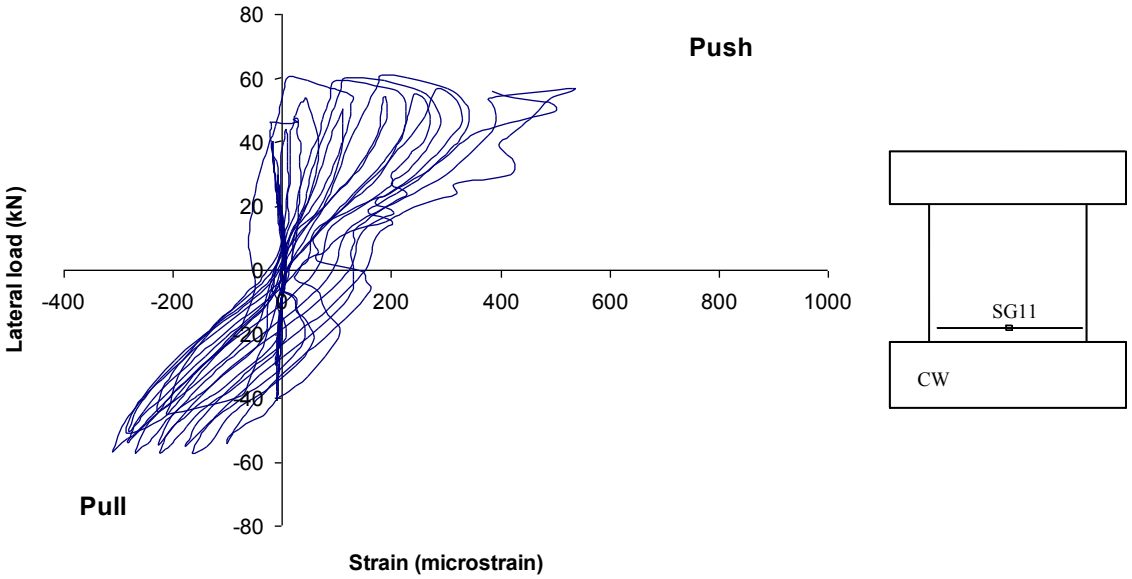

Figure 6.10 Strain gauge SG11 for control wall CW.

6.3 RETROFITTED WALL RW1

This untested wall specimen was strengthened by applying vertical CFRP strips at the wall extremities (boundary element zones) that are anchored to the wall's top and bottom blocks (representing top and bottom slabs); in addition to two overlapping horizontal C-shaped CFRP wraps. The FRP-retrofitted wall was tested by applying lateral loads at the top of the wall of 20 and 40 kN in force control mode to check the proper functioning of the instrumentation. The load was then increased in a force control mode until the load that corresponded to the yielding of flexure reinforcement was reached. The strain gauges SG5 and SG6 installed on the flexure reinforcement at the wall mid-height (shown in Figure 5.8) were used to monitor the strains in order to identify the yield load of the retrofitted wall. These gauges were used because the strain gauges installed on the flexure reinforcement bars near the wall base, SG1 and SG2, read lower values than the mid-height gauges due to the presence of FRP anchors at their level. The yield load was determined to be 59 kN, occurring at a lateral displacement of 1.5 mm which corresponds to a lateral drift ratio of 0.144 %. After reaching the yield point, the wall was tested in displacement control mode up to failure. The wall was subjected to cyclic displacements with increasing displacement ductility levels, μ_{Δ}, of 1.33, 1.67, 2.0, 2.5, 3.0, 3.5, 4.0, 4.5, 5.0, 5.5, 6.0, 6.5, 7.0, 8.0, 9.0 and 10.0. Each cycle was repeated twice until a displacement ductility of 5.5 was reached, afterwards, each cycle was applied only once until the test was stopped.

6.3.1 Lateral Displacements of RW1

The relationship between the applied lateral load and the wall's top displacement is shown in Figure 6.11. From the figure, it can be seen that after the yield load, the wall started to gain strength with a relatively high stiffness (as compared to the control wall CW) upon increasing the cyclic lateral displacement. This type of gain is due to the contribution of the vertically anchored FRP strips. The retrofitted wall RW1 was able to reach a lateral load of +109 kN in the push direction and -103 kN in the pull direction at a lateral displacement of 6.75 mm, corresponding to $\mu_\Delta = 4.5$ and lateral drift of 0.65%. For this wall, it was not possible to track the formation of cracks in the concrete underneath because the wall was completely covered by FRP sheets, except for a small portion near the wall top block at the foundation block. At the maximum lateral load level (109 kN), cracks at the wall base were not visible due to the presence of FRP anchors that were stitching the cracks at this level. However, cracking of the wall footing near the FRP anchors started to propagate at this high level of force as shown in Figure 6.12, which marked the beginning of a local footing failure due to pull out of the FRP anchors. The repetition of each load cycle resulted in a strength deterioration and stiffness degradation of about 4 to 5%. This value is less than the 6% value of the control wall CW.

At a lateral displacement of 7.5 mm ($\mu_\Delta = 5.0$), the wall strength started to degrade in both the push and pull directions, and the local cracks in the wall's bottom block started to widen. Displacements corresponding to 20% strength degradation ($\Delta_{0.8u}$) are usually taken as an acceptable ultimate performance level (Priestley et al. 1996, Priestley et al. 2007). At a displacement ductility of 5.5, the wall strength degraded to 78% of the

wall ultimate strength in the push direction and 75% in the pull direction, which can be identified as the wall's failure displacement ductility level at a drift ratio of 0.79%. The wall was considered to reach its failure capacity at this level, but the test was continued as the wall was able to sustain higher displacement. However, the loading cycle was only applied once after that level. At a lateral displacement of 9.0 mm ($\mu_\Delta = 6.0$), the strength of the retrofitted wall RW1 almost reached that of the control wall in the pull direction. At a lateral displacement of 10.5 mm ($\mu_\Delta = 7.0$), the wall behaviour was similar to the control wall behaviour, and a complete pull out of the FRP anchors occurred. The test was stopped when the wall reached a lateral displacement of 19.5 mm due to the severe damage of the wall footing. No rupture or debonding of FRP anchors or FRP sheets was observed. The failure mode of the retrofitted wall RW1 was pull out of the FRP anchors at the wall base accompanied by a local concrete cone failure of the wall footing, as illustrated in Figure 6.13. Figure 6.14 shows the wall's lateral displacement measured at its mid-height plotted against the applied lateral load. Similar to the control wall CW, the wall mid-height displacement of the retrofitted wall RW1 was measured to be, on average, 50% of the corresponding top displacement.

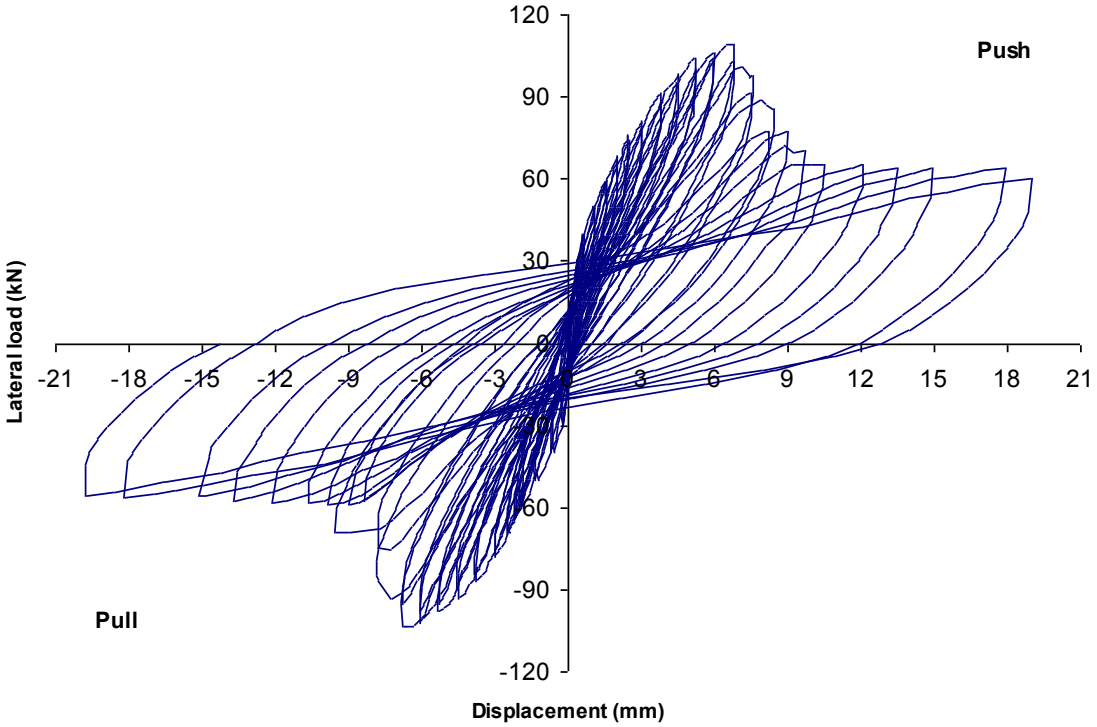

Figure 6.11 Lateral load-top displacement relationship of the retrofitted wall RW1.

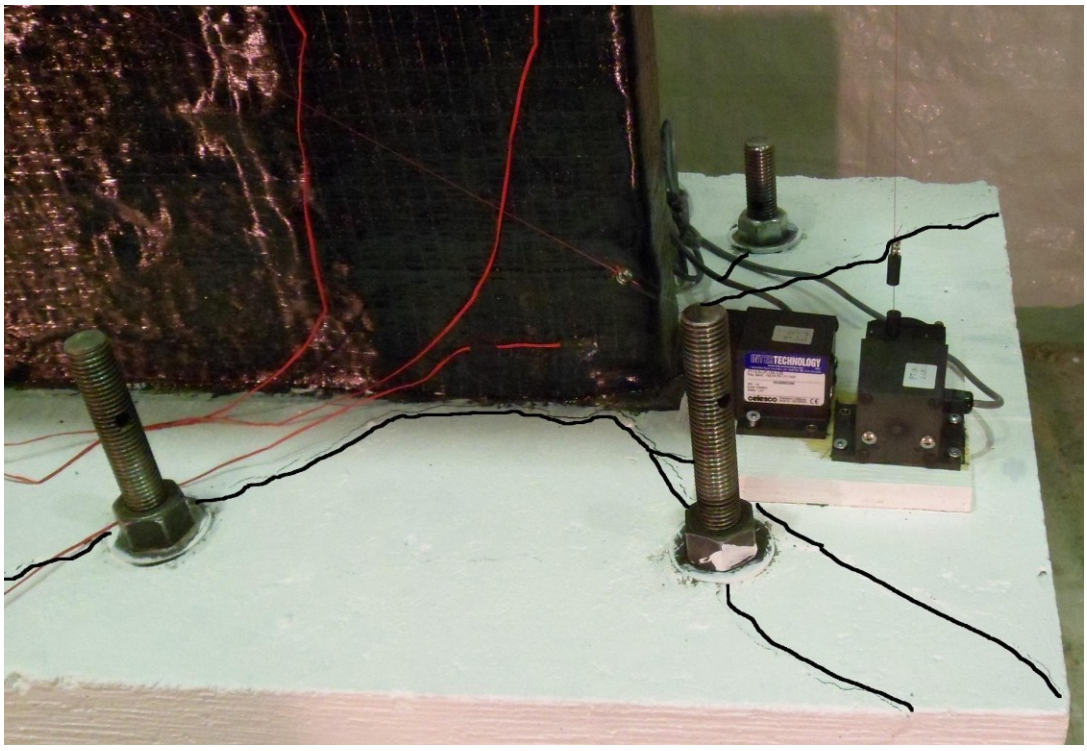

Figure 6.12 Local cracking of the footing of the retrofitted wall RW1 at its maximum load.

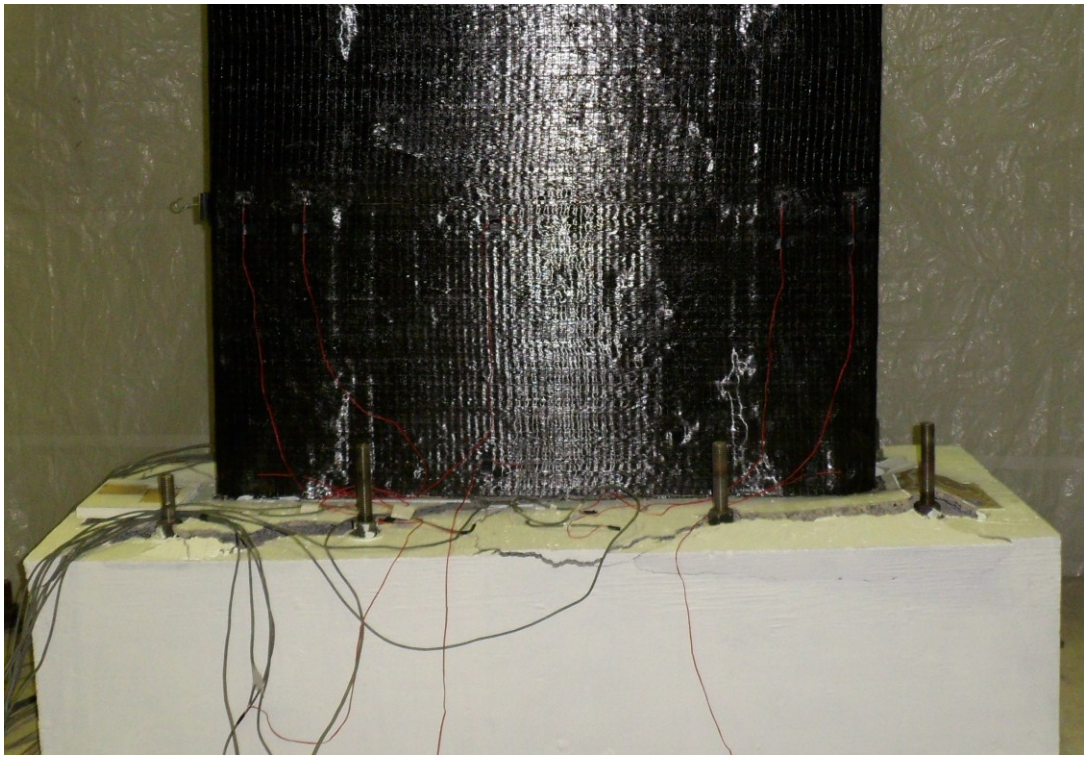

Figure 6.13 Failure of the FRP-retrofitted wall RW1.

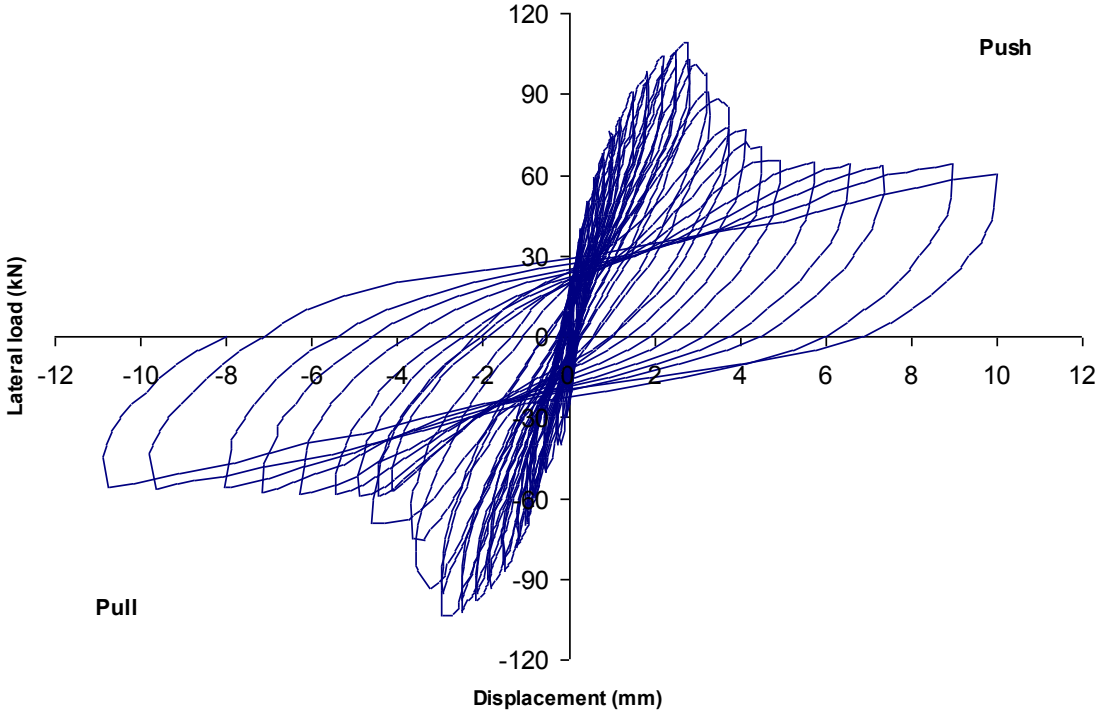

Figure 6.14 Lateral load-mid-height displacement relationship of the retrofitted wall RW1.

6.3.2 Top Rotations of RW1

Figure 6.15 shows the hysteretic lateral load-wall's top rotation relationship of the retrofitted wall RW1. The wall rotation at the yield load was measured to be 0.0017 rad in the push direction and -0.0021 rad in the pull direction. The figure shows that the wall rotation at the peak load was measured to be 0.0067 in the push direction and -0.0077 in the pull direction. The wall rotation at 80% of the wall's ultimate capacity was 0.0072 rad in the push direction and -0.0081 rad in the pull direction. Therefore, the wall was able to sustain a rotational ductility, μ_θ, of 4.2 in the push direction and 3.9 in the pull direction. The displacement transducers that were attached to the wall's footing were removed at a displacement ductility of 6.0 due to local failure of the wall footing which marked the wall's failure limit.

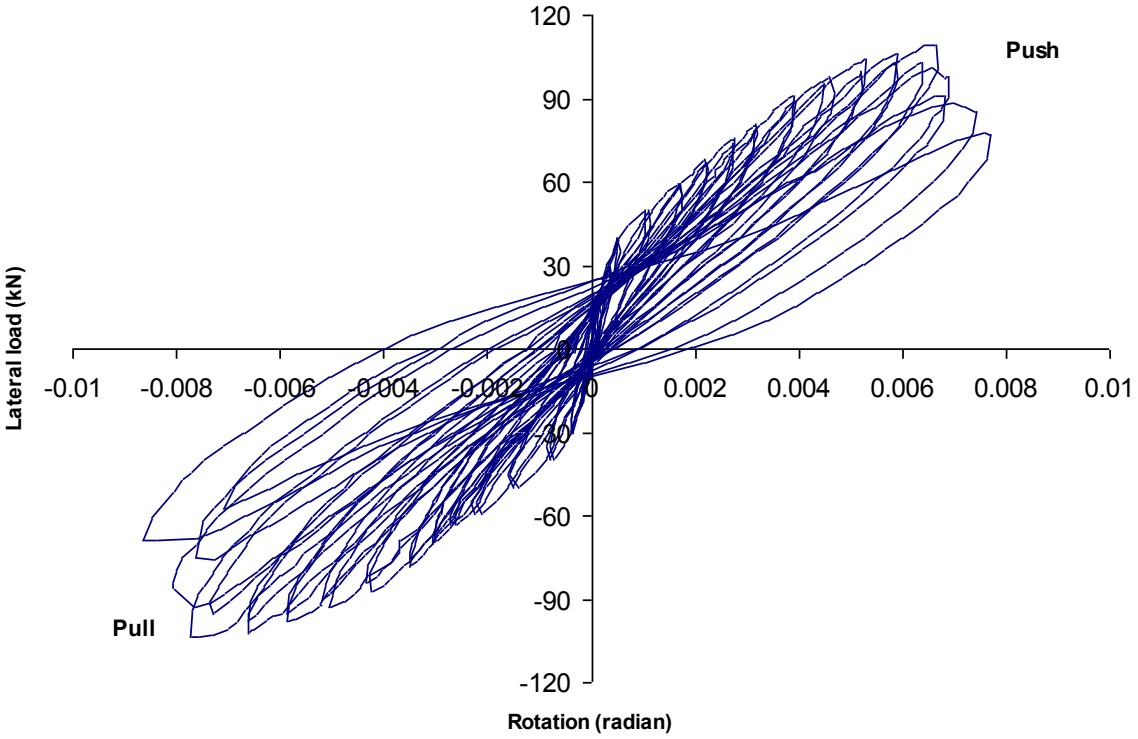

Figure 6.15 Lateral load-top rotation relationship for the retrofitted wall RW1.

6.3.3 Shear Deformation of RW1

Figure 6.16 shows the lateral load-shear displacement (Δ_s) relationship. In the calculation of the wall shear displacement, the values of b and c in Equation 5-4 were measured to be 1360 and 1600 mm, respectively. The wall shear displacement at the ultimate load was measured to be 0.36 mm in the push direction and -0.82 mm in the pull direction. The shear displacement measured at 80% of the maximum load was 1.16 mm in the push direction and -1.70 mm in the pull direction.

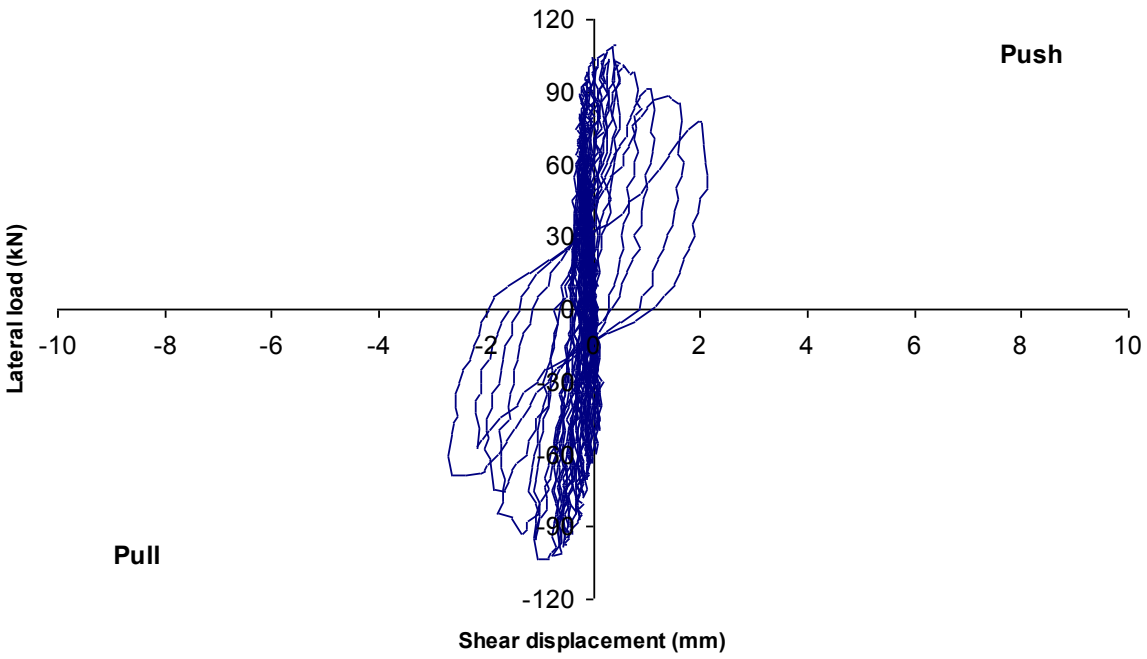

Figure 6.16 Lateral load-shear displacement relationship for the retrofitted wall RW1.

6.3.4 Strains in steel reinforcement of RW1

The maximum strains in the flexural reinforcement of the FRP-retrofitted wall RW1 were recorded from the strain gauges installed on the outermost flexure reinforcement rebars at the wall mid-height, SG5 and SG6, (as depicted in Figure 5.8). The recorded strain readings from SG1 and SG2 at the wall base were smaller than those of SG5 and SG6 due to the presence of FRP anchors that acted as additional local reinforcement at the wall base, which reduced the strain values in the adjacent steel reinforcement at that level. The yield load was determined according to the reading of SG5 and SG6. Figures 6.17 and 6.18 show the measured strains from SG1 and SG5, respectively, plotted versus the applied lateral load. The maximum recorded strain in the horizontal reinforcement bars at SG12 was 624 micro-strain, as shown in Figure 6.19. This small strain value in the shear reinforcement rebars was mainly due to the contribution of the CFRP wraps as shear reinforcement.

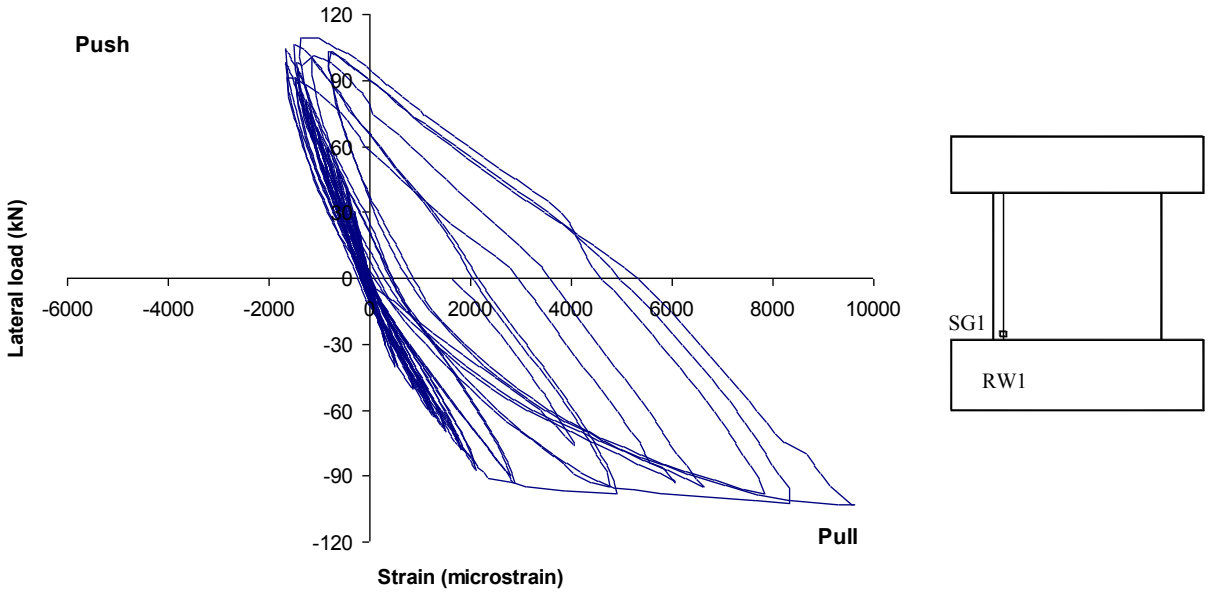

Figure 6.17 Strain gauge SG1 readings for retrofitted wall RW1.

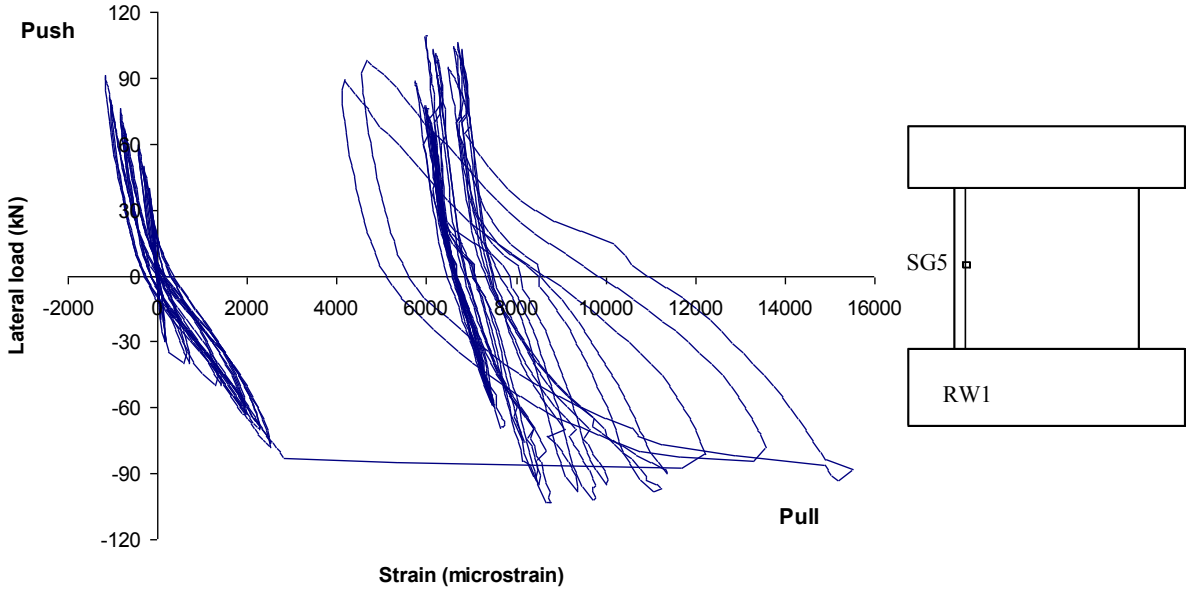

Figure 6.18 Strain gauge SG5 readings for retrofitted wall RW1.

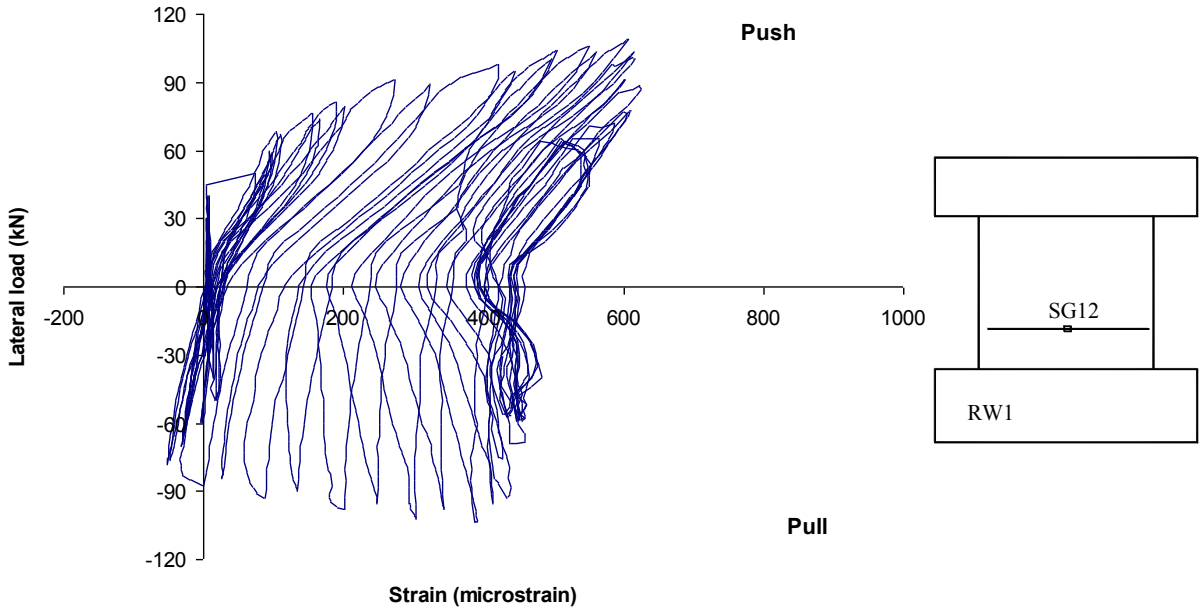

Figure 6.19 Strain gauge SG12 readings for retrofitted wall RW1.

6.3.5 Strains in FRP sheets of RW1

Figures 6.20 to 6.22 show the readings of the strain gauges installed on the vertical FRP strips at different locations. The readings indicated that the pull out of the FRP anchors occurred before the FRP sheets reached their ultimate rupture strain capacity (10500 micro-strain). The maximum recorded vertical strain of the vertical FRP strips was 5300 micro-strain, which is almost half the composite ultimate strain. As can be seen in the figures, the vertical FRP strips stretched when the wall was pushed in one direction, and then the strips were compressed when the load was reversed. By comparing the readings of FRP-SG4 and FRP-SG12, a minor difference in the strain readings can be noticed, which indicates that there was no significant out-of-plane deformations that could have resulted from misalignment or asymmetry. Figure 6.23 shows the horizontal strain reading in the confining CFRP sheet wrapped around the wall's boundary zones. The figure indicates that the maximum horizontal strain recorded near the wall toe was 1230 micro-strain. The strains in the CFRP horizontal wraps were insignificant (maximum of 160 micro-strain), mainly because the wall behaviour was not dominated by shear.

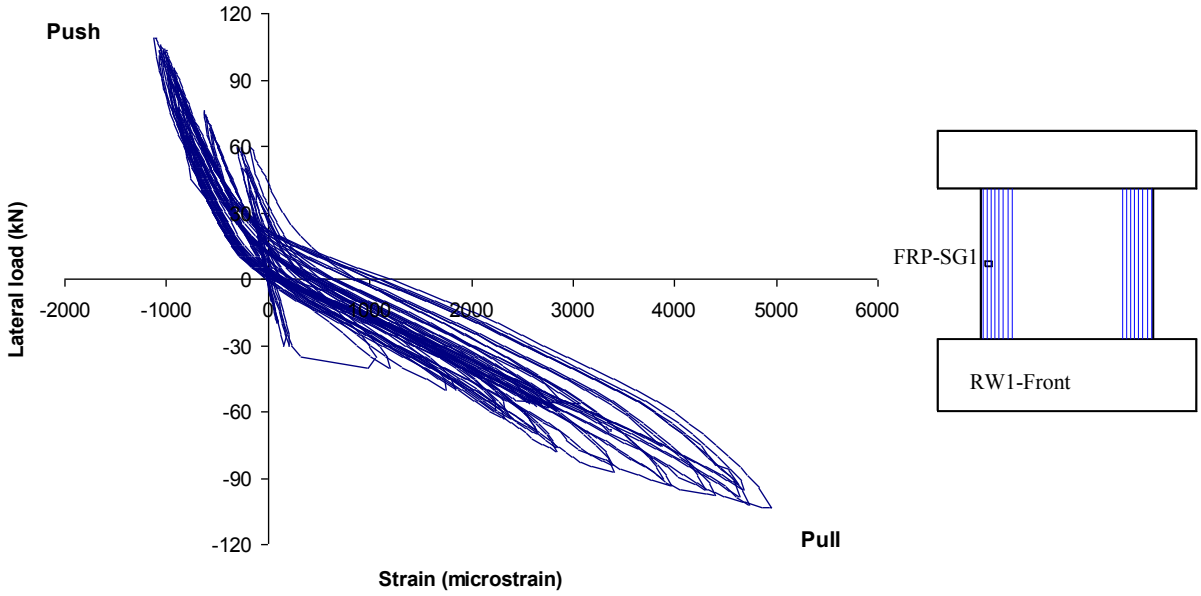

Figure 6.20 Strain gauge FRP-SG1 readings for retrofitted wall RW1.

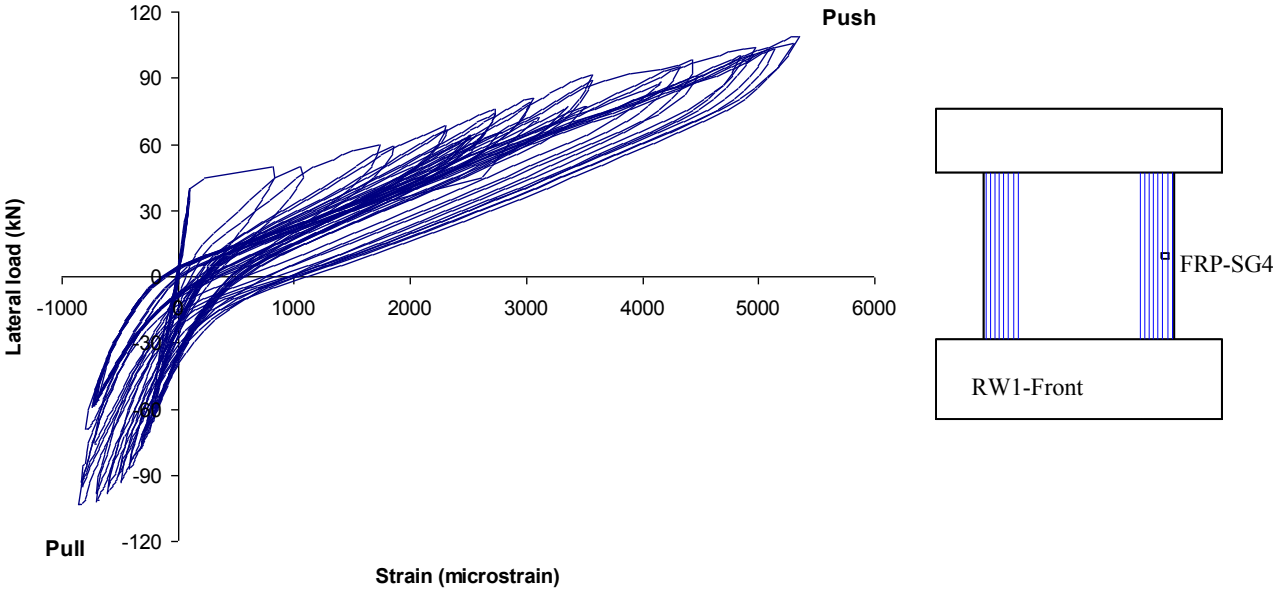

Figure 6.21 Strain gauge FRP-SG4 readings for retrofitted wall RW1.

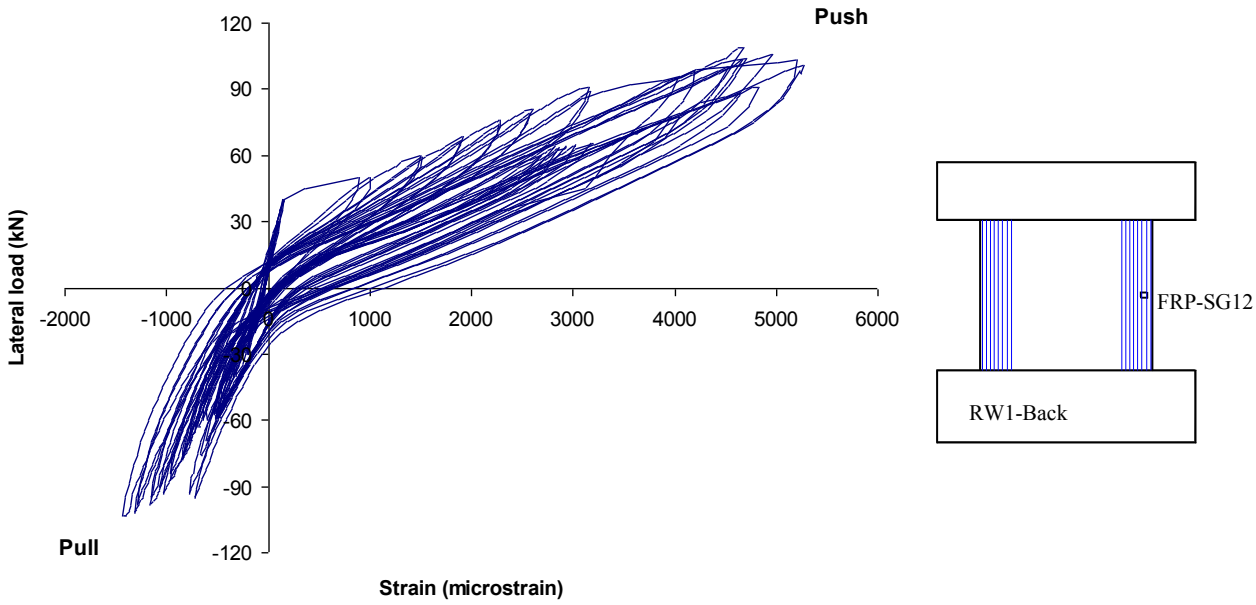

Figure 6.22 Strain gauge FRP-SG12 readings for retrofitted wall RW1.

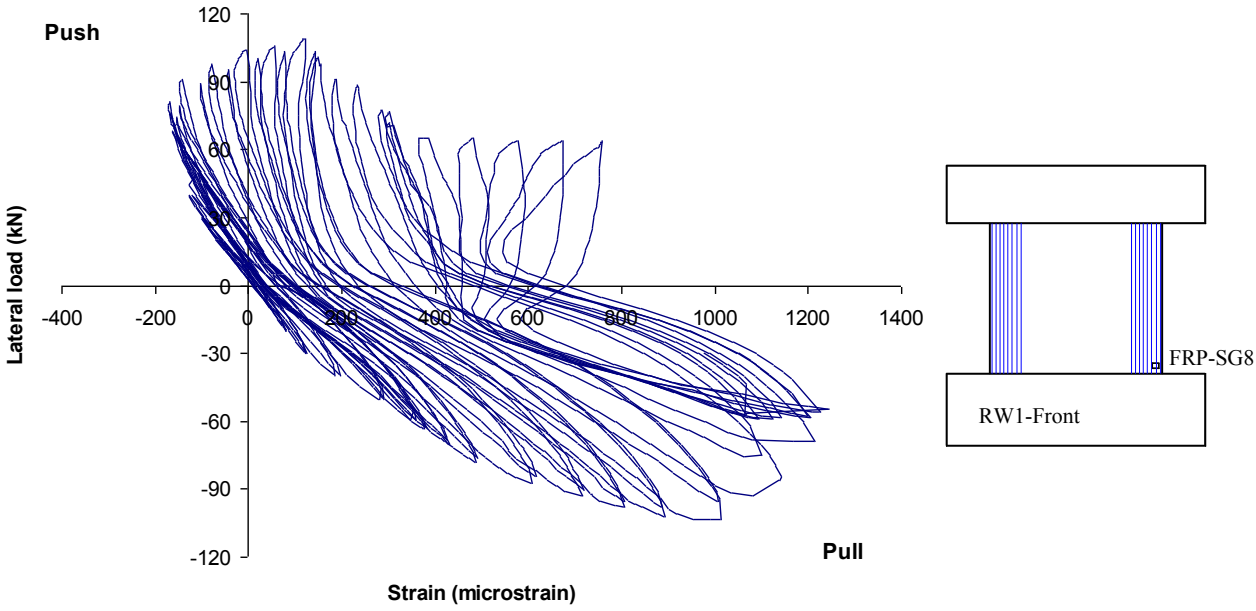

Figure 6.23 Strain gauge FRP-SG8 readings for retrofitted wall RW1.

6.4 RETROFITTED WALL RW2

This untested wall was strengthened by applying diagonal CFRP strips that are anchored to the wall top and bottom blocks, in addition to horizontal C-shaped CFRP strips at the wall top and base. The FRP-retrofitted wall RW2 was tested by applying cyclic force-controlled lateral load excitations at the top of the wall of 20 kN and 40 kN, followed by a load cycle to the yield load. The control mode was then switched to displacement control. The wall's first crack was observed after the pull cycle of -20 kN at almost the mid-height of the wall panel, as can be observed in Figure 6.24. The yield load was determined using the strain gauges installed on the flexure reinforcement at the wall mid-height, SG5 and SG6, (as shown in Figure 5.8) similar to wall RW1. The load at yielding of flexure reinforcement was 48 kN at a lateral displacement of 1.5 mm, which corresponds to a lateral drift ratio of 0.144%. After reaching the yield load, the wall was tested in displacement control mode up to failure. The wall cyclic displacement was increased to displacement ductility levels, μ_{Δ}, of 1.33, 1.67, 2.0, 2.5, 3.0, 3.5, 4.0, 4.5, 5.0, 5.5, 6.0, 6.5, 7.0, 8.0, 9.0 and 10.0, similar to wall RW1. Each cycle was repeated twice until a displacement ductility of 7.0 was reached; each cycle was then applied only once until the test was stopped.

6.4.1 Lateral Displacements of RW2

The hysteretic relationship between the applied lateral load and the wall's top displacement is shown in Figure 6.25. From the figure, it can be seen that after reaching the yield load, the wall continued to gain strength with relatively high stiffness while increasing the lateral displacement due to the contribution of the diagonal FRP strips as

well as the strain hardening of the flexural steel reinforcement. Upon cyclic loading, several cracks were developed in the wall and they continued to propagate until the wall reached a lateral displacement of 3.75 mm (μ_Δ = 2.5) as shown in Figure 6.24. Upon increasing the wall cyclic displacement above this level, no further crack propagation or initiation occurred, but the existing cracks widened especially the crack just above the bottom CFRP wraps. It is believed that widening of the main crack above the horizontal CFRP strip and its opening and closure during successive cycles resulted in maintaining a relatively stable lateral load resistance of the wall while increasing its ductility and energy dissipation capacity. The retrofitted wall was able to resist a lateral load of +92 kN in the push direction and -84 kN in the pull direction at a lateral displacement of 6.75 mm, corresponding to a displacement ductility μ_Δ = 4.5 and lateral drift of 0.65%. The repetition of each load cycle resulted in a strength deterioration and stiffness degradation of about 3 to 4% due to the second cycle. This value is less than the 6% value of the control wall CW, and less than the 4 to 5% for the retrofitted wall RW1. At a lateral displacement of 9.75 mm (corresponding to μ_Δ = 6.5), the CFRP diagonal strips debonded from the concrete surface while they were still properly attached to the top and bottom FRP anchors with no signs of pull out or local cracks at the anchorage zones. At a lateral displacement of 12.0 mm (μ_Δ = 8.0), crushing of the concrete above the well-confined end zones by means of the horizontal CFRP wraps was noticed, and a small portion of the diagonal FRP strip started to rupture. At this displacement level, the wall strength started to degrade in the push direction but the wall was still able to resist more than 80% of its ultimate strength. Therefore, the wall was able to sustain a displacement ductility of 8.0 in the push direction corresponding to a lateral drift ratio of 1.15%. At a lateral displacement of 13.5 mm (μ_Δ = 9.0), the wall strength degraded significantly and more portions of the

diagonal FRP strips resisting the pull cycles ruptured. At this displacement ductility level, cracking of the wall footing was observed at the right side of the wall, which indicated the pull out of FRP anchors at that location, accompanied by a local concrete cone failure of the wall footing. The wall was considered to reach its failure capacity at this level, but the test continued as the wall was still capable of undergoing higher displacement levels. At a lateral displacement of 15.0 mm (μ_Δ = 10.0), a complete rupture of the FRP diagonal strips in one direction occurred and the concrete experienced more damage in both the pull and push directions. However, the wall was able to carry 82% of its ultimate strength in the pull direction at this displacement. This resulted in a displacement ductility of the wall in the pull direction of 10.0 corresponding to a lateral drift ratio of 1.43%. Figure 6.26 shows the rupture of the FRP diagonal sheets of the retrofitted wall RW2. Buckling of the outermost flexure reinforcement bars was observed, as indicated in Figure 6.27. The wall reached 66% of its ultimate strength and the test was stopped at that level due to the severe damage occurred.

The failure mechanism of the retrofitted wall RW2 was identified as a rupture of the diagonal FRP strips resisting the pull cycles and pull out of the FRP anchors resisting the push cycles, as shown in Figure 6.28. The failure was accompanied by concrete crushing above the confined concrete zone wrapped with horizontal CFRP wraps, and buckling of the steel reinforcement bars at both sides of the wall. Figure 6.29 shows the wall's hysteretic lateral load-mid-height displacement relationship. From the figure, it can be seen that the wall displacement at the mid-height was almost 40% of the wall top displacement at different displacement levels.

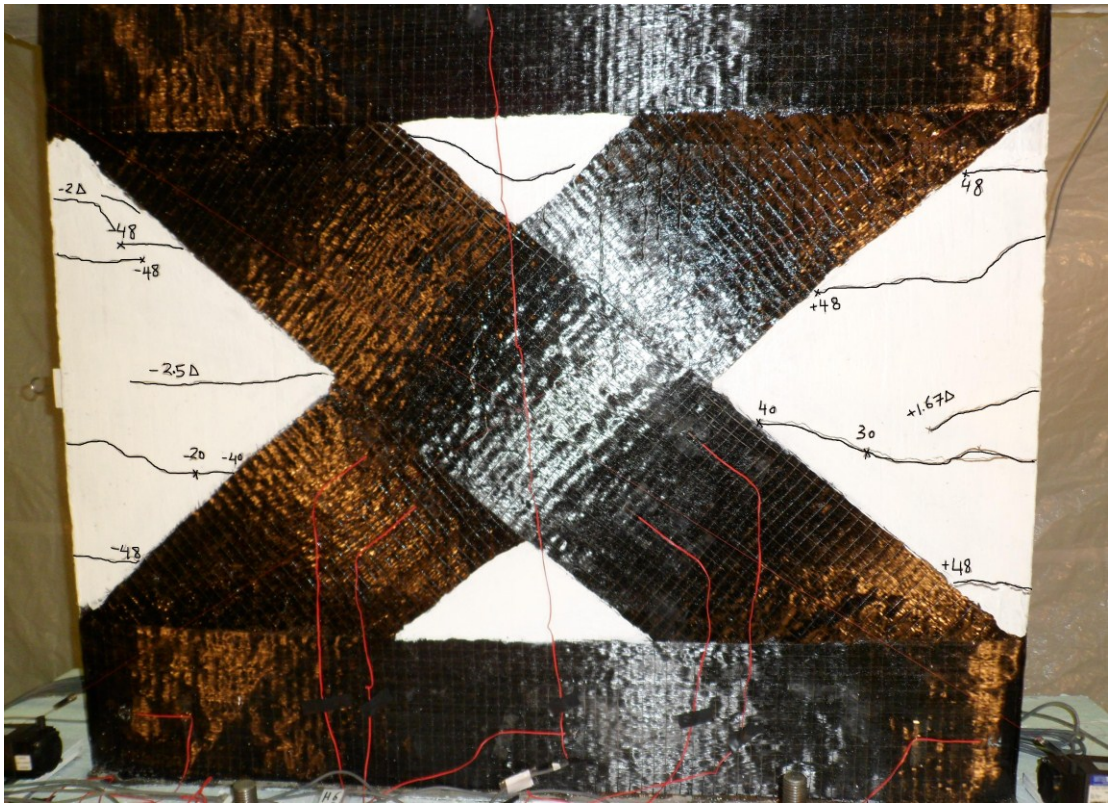

Figure 6.24 Crack pattern of the FRP-retrofitted wall RW2.

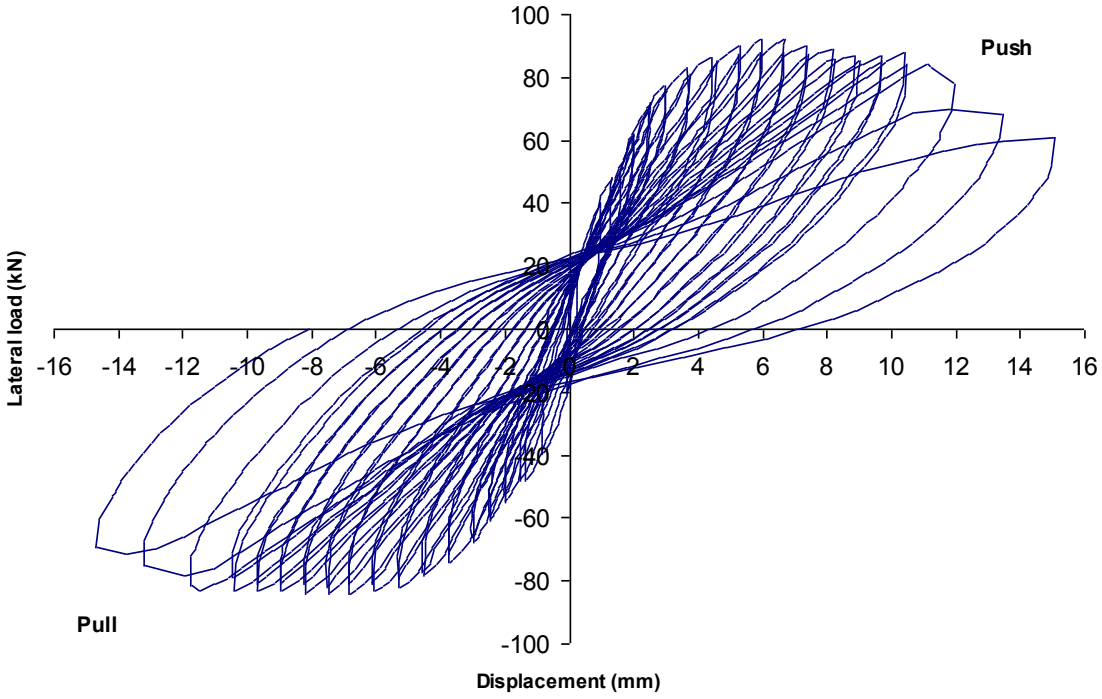

Figure 6.25 Lateral load-top displacement relationship for the retrofitted wall RW2.

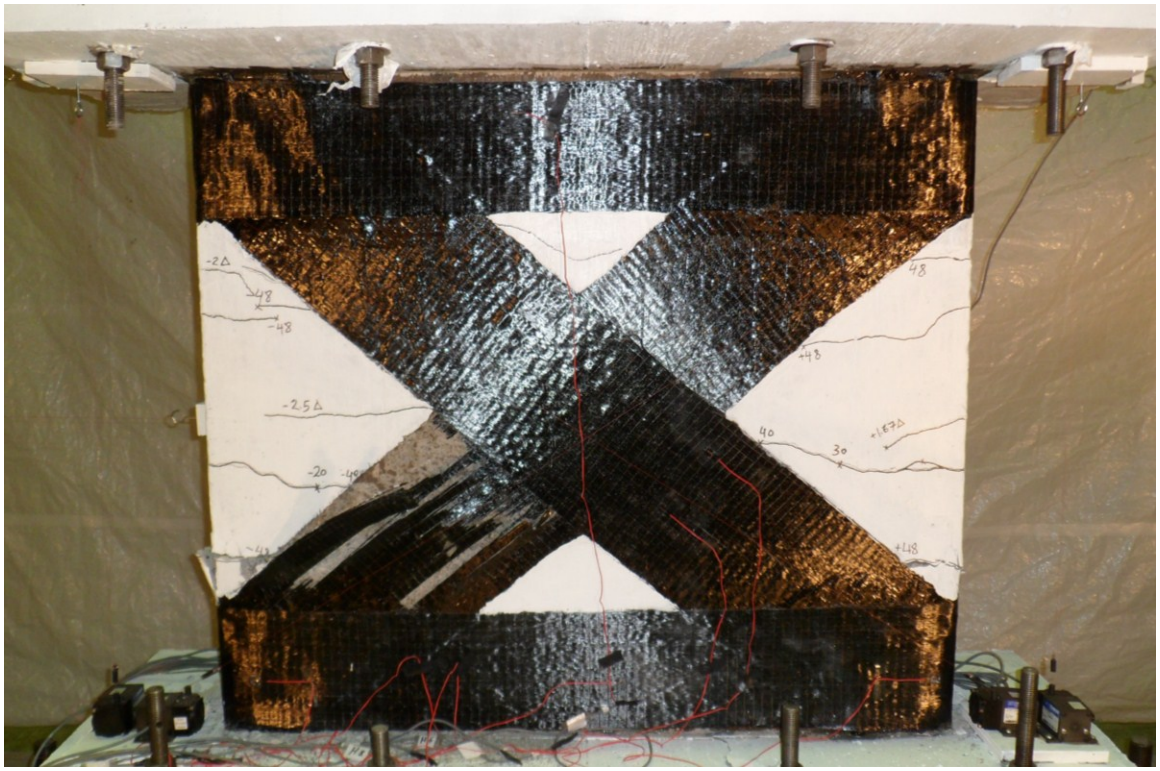

Figure 6.26 Rupture of diagonal FRP sheets of the retrofitted wall RW2.

Figure 6.27 Concrete crushing and buckling of the flexure reinforcement.

Figure 6.28 Pull-out of FRP anchors for the retrofitted wall RW2.

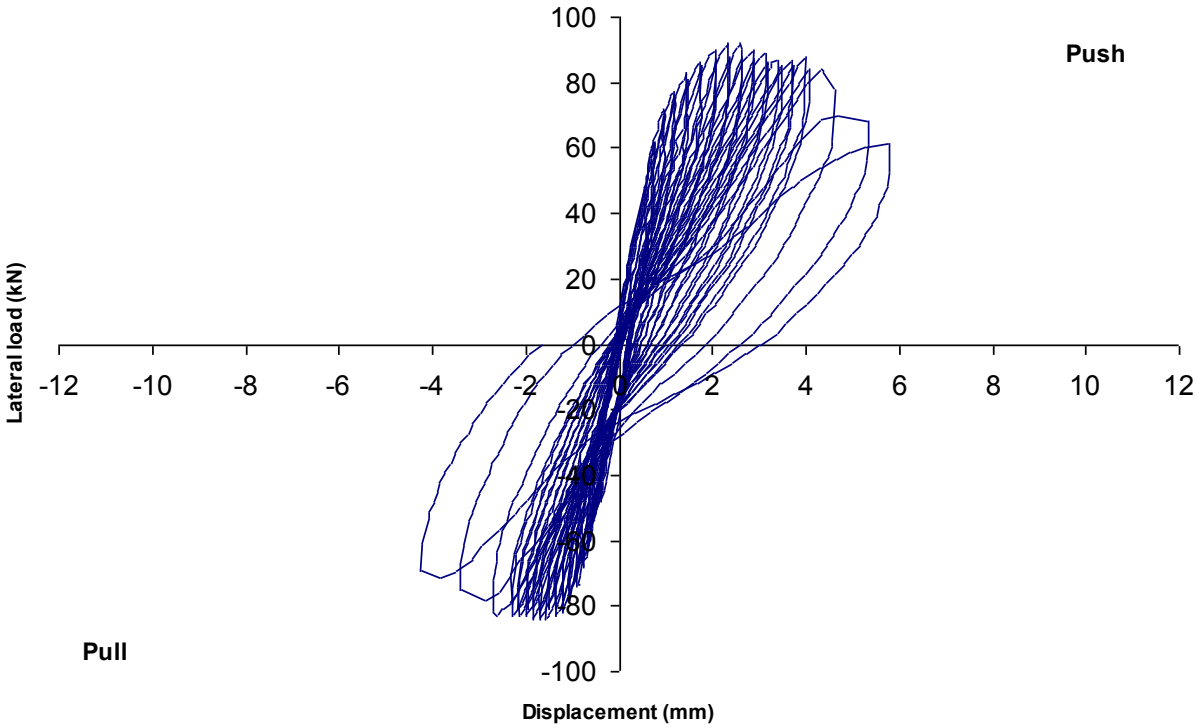

Figure 6.29 Lateral load-mid-height displacement relationship for the retrofitted wall RW2.

6.4.2 Top Rotations of RW2

Figure 6.30 shows the hysteretic lateral load–rotation relationship of the retrofitted wall RW2. The rotation of the wall at the onset of yielding of the longitudinal reinforcement bars was measured to be 0.002 radian in both the push and pull directions. The wall rotation at the ultimate load was measured to be 0.008 in both directions. The wall rotation at 80% of the wall's ultimate capacity was measured to be 0.0132 radian in the push direction and 0.0194 rad in the pull direction. Therefore, the wall was able to sustain a rotational ductility, μ_θ, of 6.6 in the push direction and of 9.7 in the pull direction. The unsymmetrical rotation of the wall occurred at the last two cycles at displacements of 13.5 and 15.0 mm due to the excessive buckling of the wall flexure reinforcement rebar on the wall's right side -- more than the on left side, which resulted in higher rotational demand of the wall during the pull cycle.

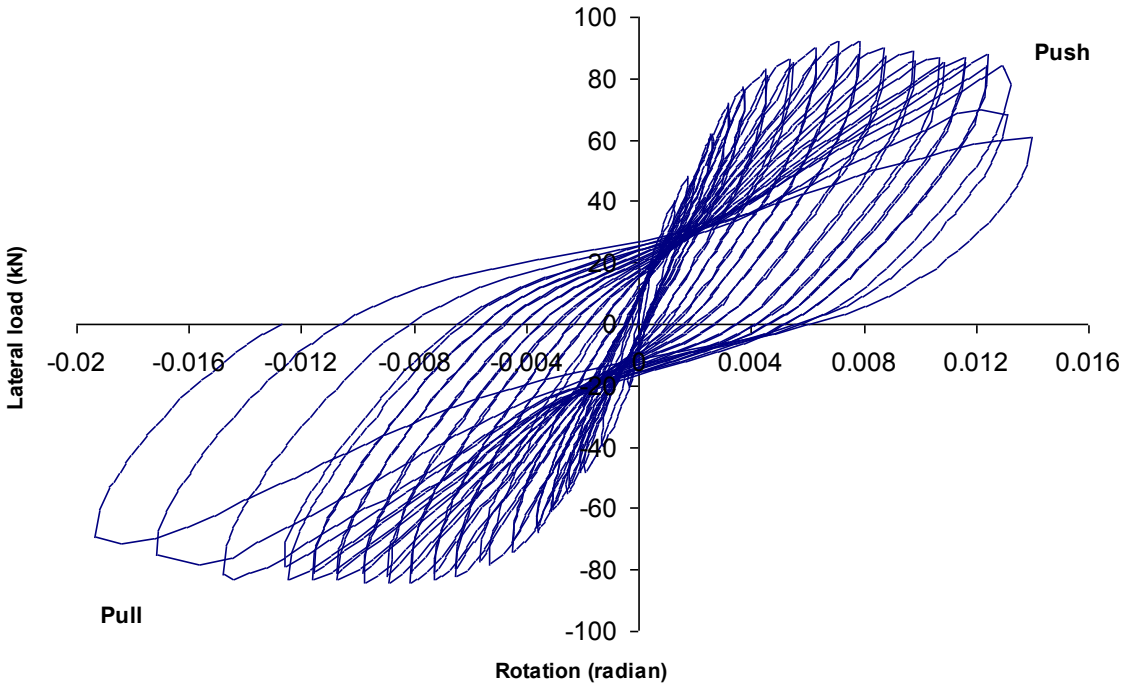

Figure 6.30 Lateral load-top rotation relationship for the retrofitted wall RW2.

6.4.3 Shear Deformation of RW2

Figure 6.31 shows the hysteretic shear displacement, Δ_s, variation with the applied lateral load. In the calculation of the wall's shear displacement, the values of b and c in Equation 5-4 were measured to be 1360 and 1600 mm, respectively. The wall shear displacement at the ultimate load was measured to be 0.15 mm in the push direction and -0.24 mm in the pull direction. The shear deformation measured at 80% of the ultimate load was 1.14 mm in the push direction and -2.10 mm in the pull direction.

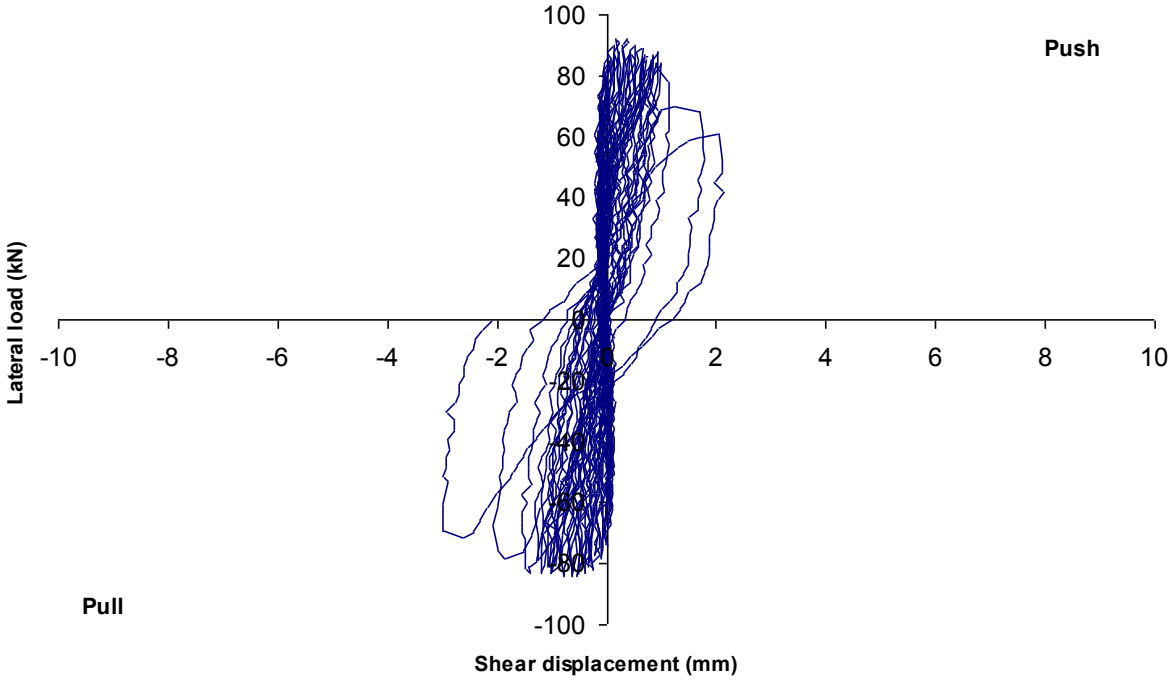

Figure 6.31 Lateral load-shear displacement relationship for the retrofitted wall RW2.

6.4.4 Strains in steel reinforcement of RW2

Similar to the retrofitted wall RW1, the maximum strains in the flexural reinforcement of FRP-retrofitted wall RW2 were recorded from the strain gauges installed on the outermost rebars at the wall mid-height, SG5 and SG6 (Figure 5.8). The strain readings from SG1 and SG2 at the wall base were smaller due to the presence of FRP anchors. The yield load was determined according to the reading of SG5 and SG6. Figures 6.32 and 6.33 show the variation of the measured strains from SG1 and SG5 plotted with the applied lateral load, respectively. From the figures, it can be seen that SG1 recorded a strain value of 2200 micro-strain at the peak load, whereas for SG5, the strain value at the peak load reached 7750 micro-strain. For SG1 and SG5, the operational range of the gauges was exceeded after a lateral displacement of 10.5 mm and 9 mm, respectively. The maximum strain in the horizontal reinforcement bars was recorded at SG13 and was 880 micro-strain. Figure 6.34 shows the variation of the measured strain from SG13 with respect to the applied lateral load.

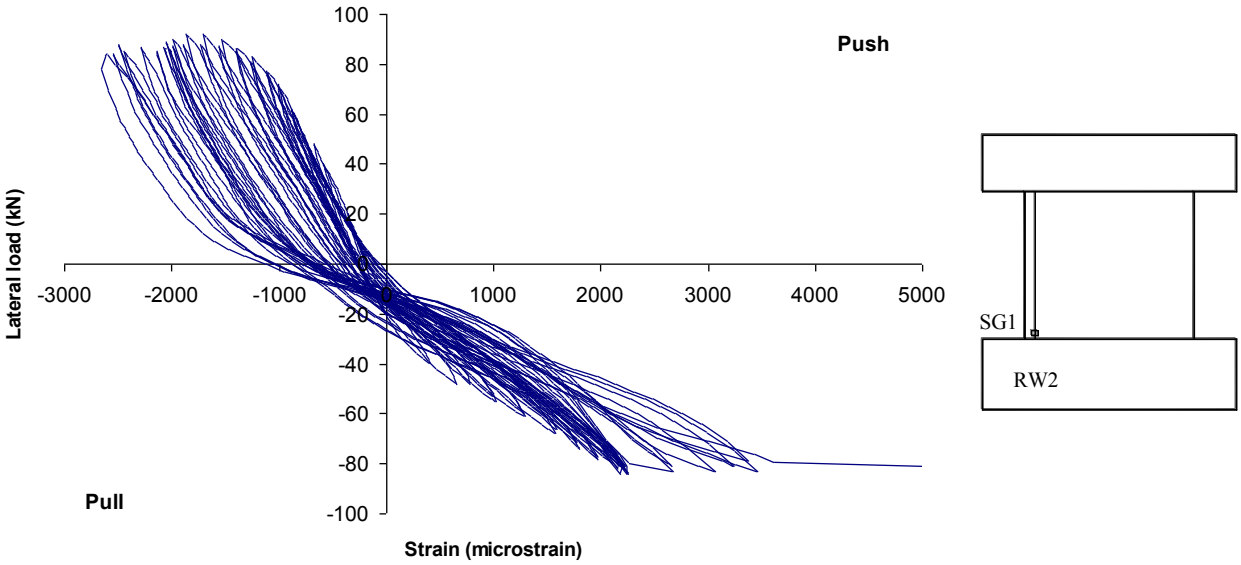

Figure 6.32 Strain gauge SG1 readings for retrofitted wall RW2.

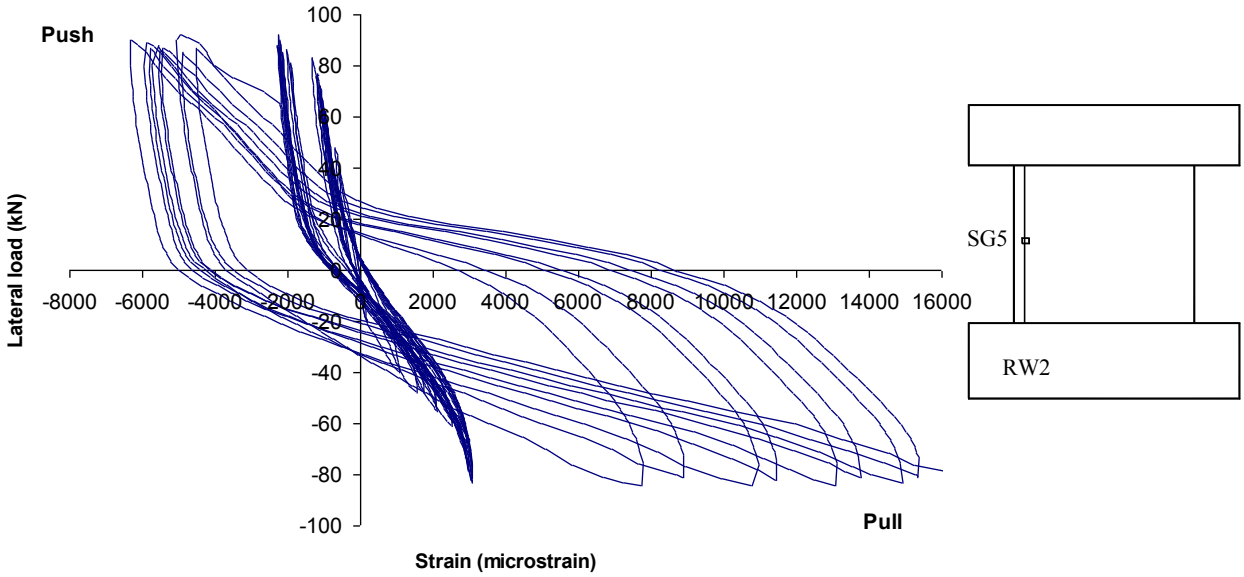

Figure 6.33 Strain gauge SG5 readings for retrofitted wall RW2.

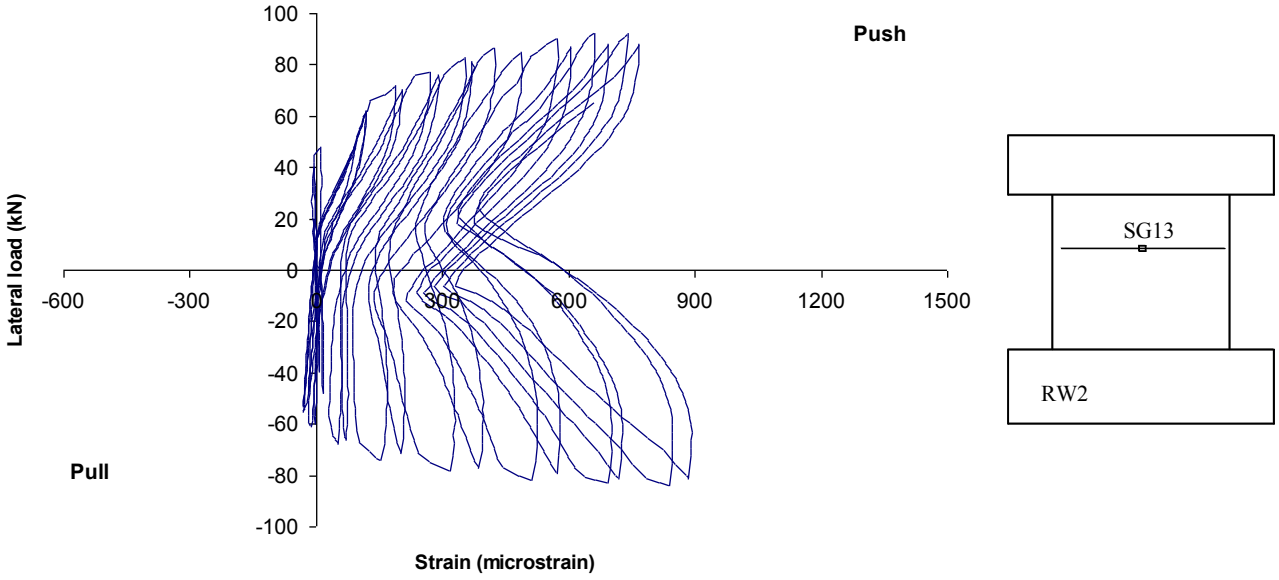

Figure 6.34 Strain gauge SG13 readings for retrofitted wall RW2.

6.4.5 Strains in FRP sheets of RW2

Figures 6.35 to 6.38 show the readings of the strain gauges installed on the diagonal FRP strips at different locations. The readings indicate that the FRP diagonal strips reached a strain of 13500 and 12200 micro-strain for the strips that experienced rupture, which exceeded the manufacturer's typical test value for the composite. The other FRP strips reached a maximum strain of 7300 micro-strain, which is almost 70% of the typical manufacturer test values. As can be seen in the figures, the diagonal CFRP strips were elongated while the wall was pushed in one direction, and then the strips were still elongated with a smaller strain when the load was reversed. This behaviour is different than the behaviour of the vertical CFRP strips observed in the retrofitted wall RW1 (Figures 6.20 to 6.22). A major difference in the shape of load-strain curves of the vertical CFRP strips of RW1 and the diagonal strips of RW2 can be also observed. Figure 6.39 shows the strain reading in the confining CFRP sheet around the wall's boundary zones. The figure indicates that the maximum strain recorded near the wall toe was 1050 micro-strain. The maximum recorded strain in the FRP horizontal wraps was insignificant (160 micro-strain), as the wall behaviour was not dominated by shear.

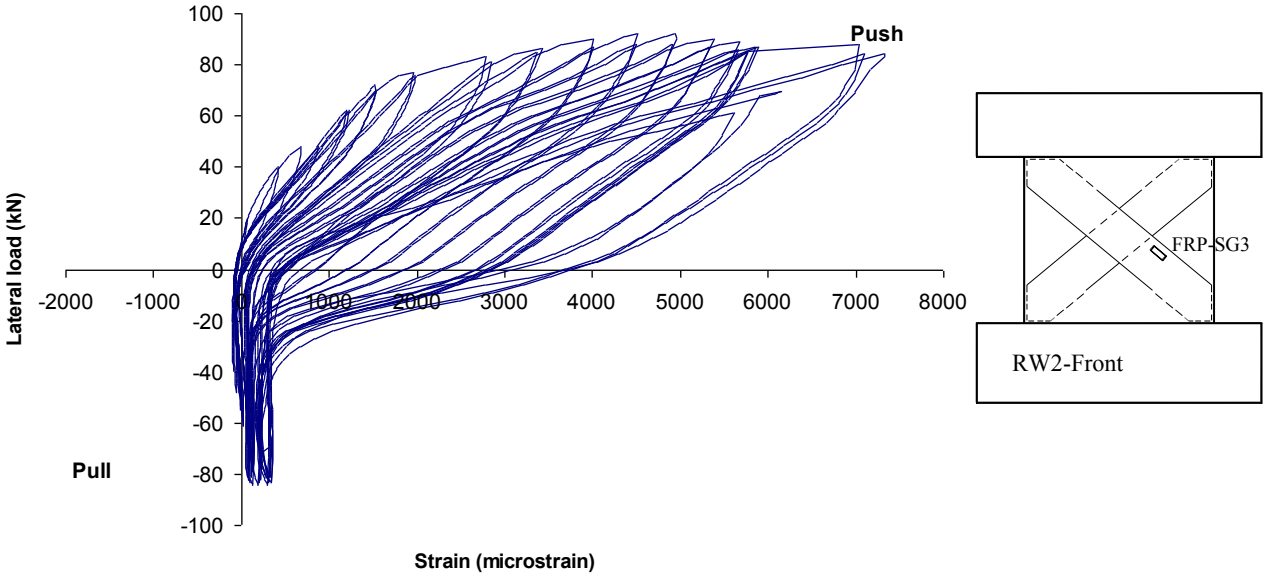

Figure 6.35 Strain gauge FRP-SG3 readings for retrofitted wall RW2.

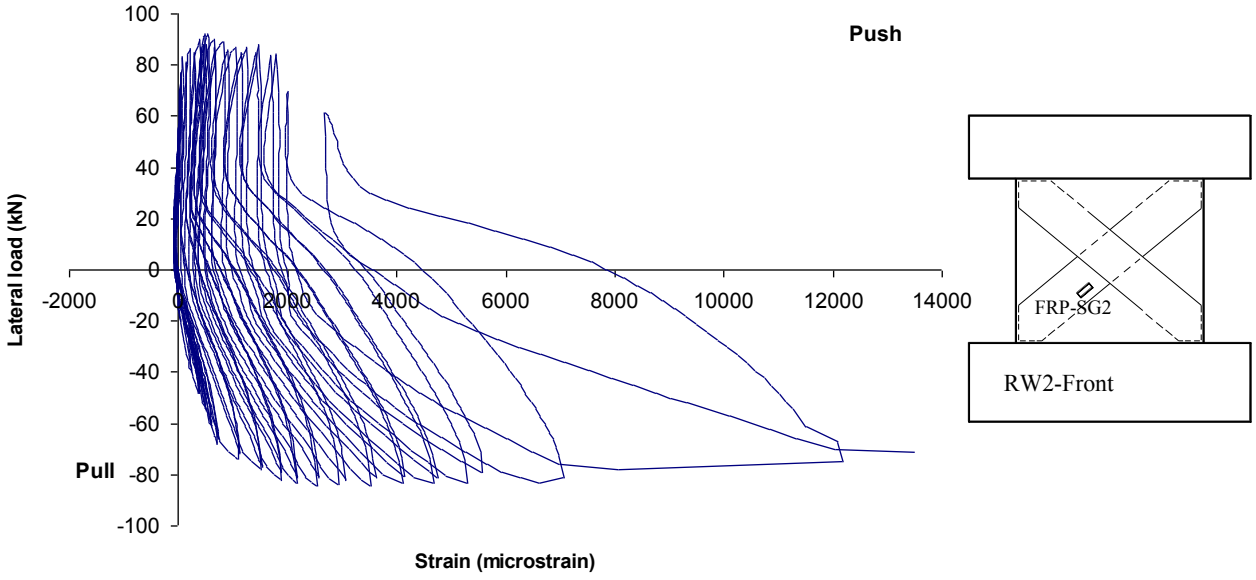

Figure 6.36 Strain gauge FRP-SG2 readings for retrofitted wall RW2.

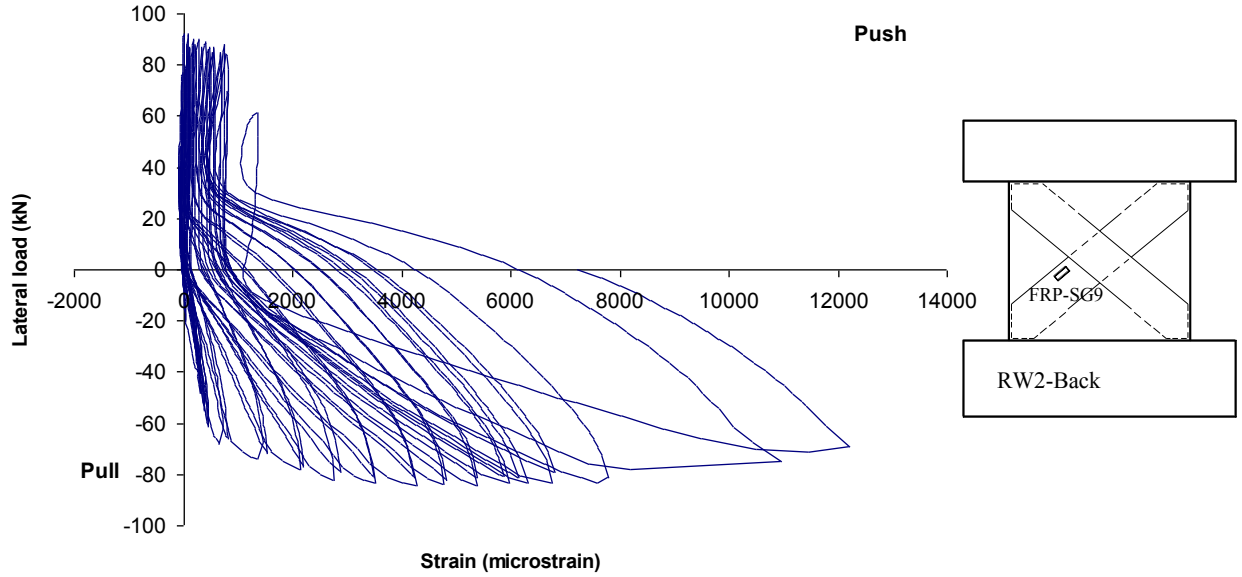

Figure 6.37 Strain gauge FRP-SG9 readings for retrofitted wall RW2.

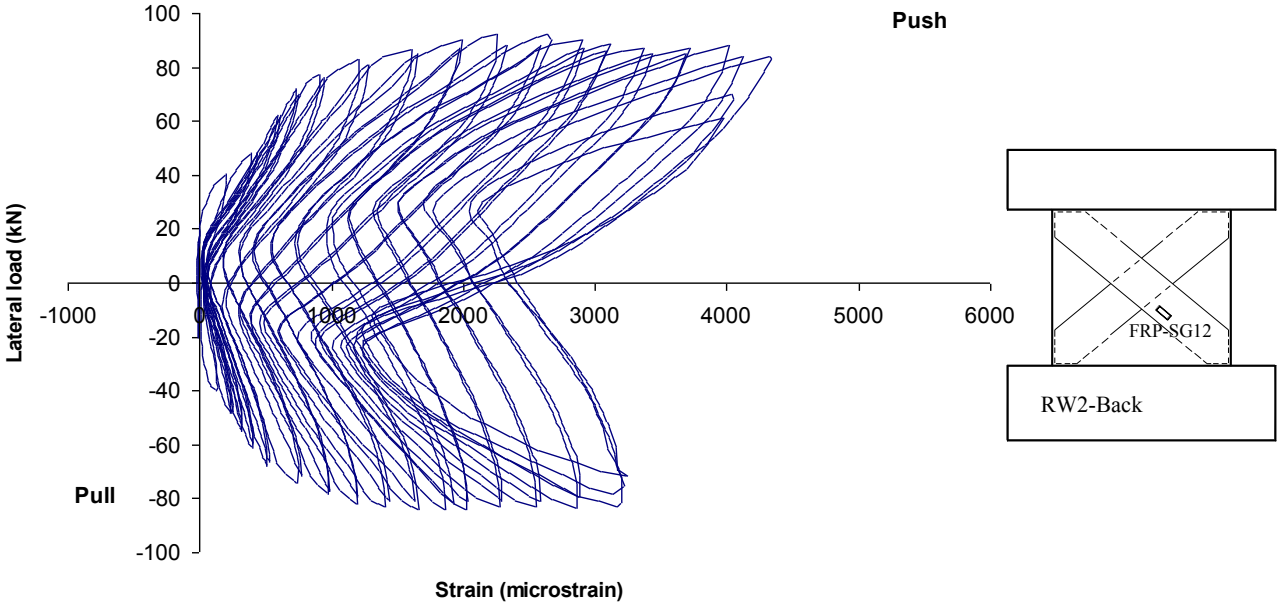

Figure 6.38 Strain gauge FRP-SG12 readings for retrofitted wall RW2.

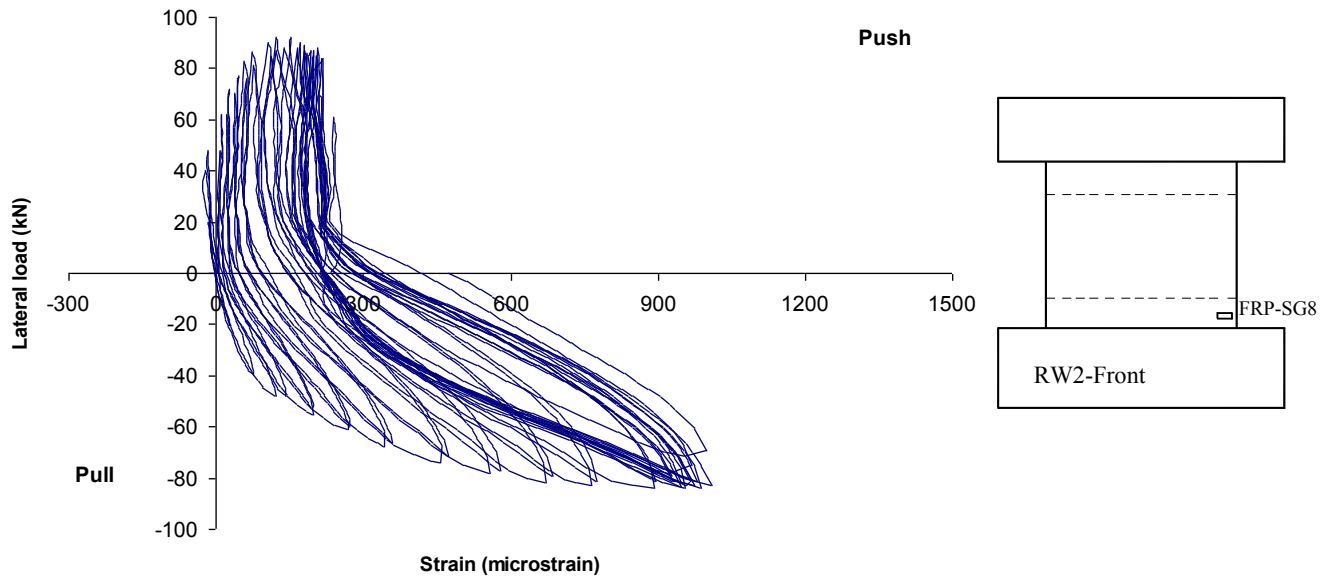

Figure 6.39 Strain gauge FRP-SG8 readings for retrofitted wall RW2.

6.5 COMPARISON OF TEST RESULTS

In the following sub-sections, the measured responses of the three tested wall panel specimens are compared. The seismic performance enhancement of the studied wall panels is evaluated in terms of strength, stiffness, ductility, energy dissipation, displacements, strains and rotations.

6.5.1 Envelope of lateral load-drift relationship

Figure 6.40 shows the envelope of the lateral load-drift ratio relationships for the three tested walls. This envelope shows that the control wall was characterized by ductile behaviour with an average flexural capacity (for both push and pull cycles) of 59 kN and a drift ratio of 1.47%. The control wall was able to reach a displacement ductility value, μ_{Δ}, of 10.0, measured at 20% strength degradation after the peak load. The retrofitted wall RW1 showed an increase of 80% in the flexural capacity compared to the control wall, accompanied by a decrease of the wall's displacement ductility. The retrofitted wall RW1 reached a displacement ductility of 5.5, measured at 20% strength degradation after the peak load. The yield load was measured to be 46% higher than the control wall at a 7% higher yield displacement. The load-drift relationship for wall RW1 is the typical relationship expected for any FRP-retrofitted element where the flexural capacity is to be increased. The sudden post-peak strength degradation could arise from the brittle rupture of FRP sheets, debonding, rupture of FRP anchors, or pull out of FRP anchors accompanied by concrete cone failure, as was the case for wall RW1. The main target of the retrofit scheme for RW1 was to increase the wall flexural capacity at levels that were

subjected to demands higher than the design ones. Therefore, the wall ductility is considered to be a secondary parameter that can be overlooked.

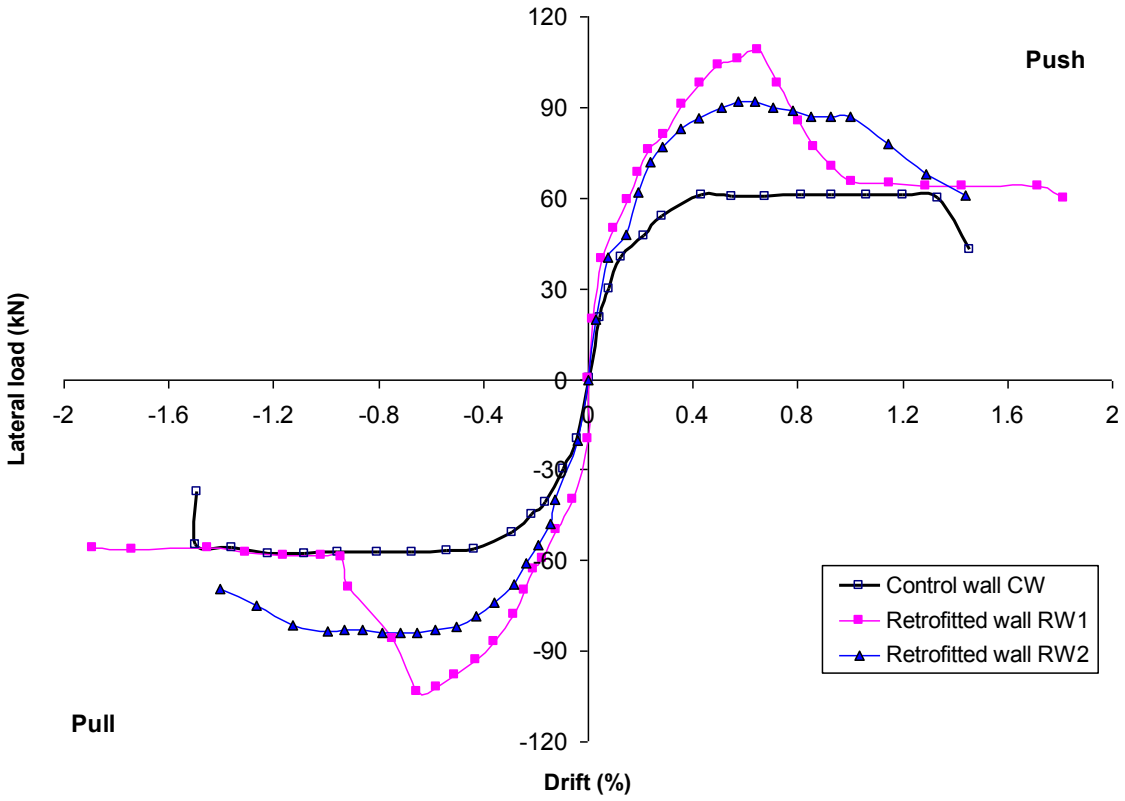

Figure 6.40 Envelope for lateral load-drift ratio relationships for the tested walls.

The retrofitted wall, RW2, showed a 50% increase of flexural capacity compared to the control wall, accompanied by similar displacement ductility. The retrofitted wall RW2 reached a displacement ductility of 9.0 measured at 20% strength degradation after the peak load. The yield load was 19% higher than that of the control wall, at 7% higher yield displacement. The retrofitted wall RW2 was designed to have the same flexural capacity of wall RW1. Interestingly, RW2 was found to have less flexural capacity with much higher displacement ductility, as can be observed in Figure 6.40. This unique behaviour of RW2 combines both the benefits desired; the high strength of wall RW1

and the high ductility of the control wall CW. This observed behaviour serves to promote the adoption of similar retrofit schemes at the plastic hinge regions where higher flexural capacity is required without sacrificing the wall ductility and energy dissipation capacity.

The flexural capacity of wall RW2 was measured to be less than the capacity of RW1 due to the fact that both diagonal FRP strips for RW2 were being stretched while the wall was pushed (or pulled), as can be seen from the strain gauge readings in Figures 6.35 to 6.38. This is different than the behaviour of wall RW1, where the vertical FRP strips were stretched on one side of the wall while being compressed on the other side, as represented in Figures 6.20 to 6.22. This specific behaviour of RW2 is attributed to the wide cracks propagated between the top and bottom horizontal CFRP wraps along the wall height. These wide cracks did not close completely when the load reversed and the concrete came under compression, which resulted in a residual elongation of the FRP diagonal strips. This phenomenon is explained using the schematic diagram in Figure 6.41. The figure shows the relation between the strains of the diagonal FRP strips during a certain load cycle. From the figure, it can be seen that while the diagonal CFRP strip A is being stretched with a high strain value, $\boldsymbol{\varepsilon}_A$, due to the pull cycle shown, the other diagonal strip B is also stretched with a smaller strain value, $\boldsymbol{\varepsilon}_B$, due to the residual elongation in the fibres caused by the wall cracking. This means that the FRP strips were acting against each other and that the net effective FRP contribution, F_{net}, to the total shear force, F, can be obtained using the following formulas:

$$F_A = \varepsilon_{frpA} E_{frp} A_{frp}, \quad (6\text{-}1)$$

$$F_B = \varepsilon_{frpB} E_{frp} A_{frp}, \quad (6\text{-}2)$$

$$F_{net} = F_A \cos\theta - F_B \cos\theta = (\varepsilon_{frpA} - \varepsilon_{frpB})\, E_{frp} A_{frp} \cos\theta, \quad (6\text{-}3)$$

$$F_{net} = \varepsilon_{net} E_{frp} A_{frp} \cos\theta, \quad (6\text{-}4)$$

where ε_{net} is the equivalent net strain of the FRP strips which is equal to the difference between ε_{frpA} and ε_{frpB}, E_{frp} is the elastic modulus of the fibre composite, A_{frp} is the fibre cross sectional area, and θ is the angle between the fibre direction and the horizontal axis.

The maximum average net strain ε_{net} measured for wall RW2 at the maximum load prior to the wall strength degradation was 0.004. However, for RW1, the maximum average strain of the vertical CFRP strips was 0.0054. This resulted in a lower flexural capacity of the retrofitted wall RW2 compared to wall RW1, despite the higher FRP strains observed for RW2. The accumulation of permanent strains in the flexure steel reinforcement, the opening of RW2's horizontal cracks above the horizontal FRP strips, and the ability of the diagonal FRP strips to stretch as the cracks widen allowed the retrofitted wall RW2 to sustain high lateral displacements while maintaining its strength. On the other hand, the vertical CFRP strips of wall RW1 controlled the opening of RW1's horizontal cracks as the cracks were normal to the fibre direction (observed from the control wall specimen), resulting in a lower displacement ductility capacity of the wall. The maximum average strain of the vertical CFRP strips of wall RW1 was 37%

higher than the average net strain of the diagonal FRP strips for wall RW2, and was measured at half the displacement ductility of RW2.

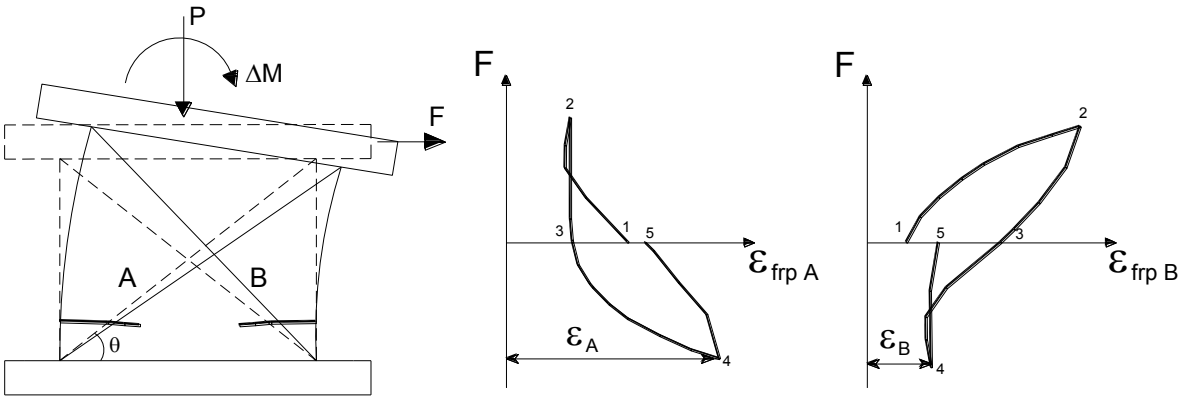

Figure 6.41 The strain in the FRP diagonal strips for the retrofitted wall RW2 at a certain load cycle.

It is also worth noting that the nominal capacities of the retrofitted walls, RW1 and RW2, were measured as higher than those calculated using section analysis and strain compatibility at the same net strain measured during the tests. This is attributed to the mechanical properties of the FRP sheets, which were found to be higher than those provided by the manufacturer. The measured forces and strains of the retrofitted walls showed that the product of fibre cross sectional area A_{frp} times the elastic modulus of the fibre composite E_{frp} was estimated to be 160% higher than the typical value provided by the manufacturer. Table 6.1 shows the calculated nominal capacities of the retrofitted walls using typical manufacturer mechanical properties alongside the proposed ones compared to the experimental nominal capacities.

Table 6.1. Measured and calculated capacities for the retrofitted walls.

Wall	Experimental V_u (kN) *	Experimental FRP net strain (ε_{net})	Analytical V_u (kN) (manufacturer)	Analytical V_u (kN) (proposed)
RW1	106.0	0.0054	70.0	101.0
RW2	88.0	0.004	63.5	85.5

* Average capacity of push and pull cycles

6.5.2 Peak-to-peak lateral stiffness

The peak-to-peak lateral stiffness of the control wall and the FRP-retrofitted walls are shown in Figure 6.42 and Table 6.2, both of which clearly indicate the continuous reduction of the walls' lateral stiffness with the lateral drift increase. Table 6.2 also shows the stiffness degradation that occurred due to the second cycle of loading. The figure shows that the retrofitted wall RW1 had the highest stiffness due to the presence of the vertical FRP strips, up to a lateral drift of 0.71%. It can be seen from the table that the retrofitted wall RW1 had on average a 50% higher stiffness than the control wall CW after the yield load and prior to failure of RW1. This higher stiffness would result in higher seismic forces being attracted to the wall during the ground motion excitation, as was observed during the shake table tests described in Chapter 4. It should be noted that the strengthened walls tested in the cyclic tests had higher stiffness than the rehabilitated ones tested in the shake table tests due to the damage that occurred to the latter walls prior to the rehabilitation process.

It can be also observed that the retrofitted wall RW1 had on average a 15% higher stiffness than wall RW2, which would result in higher seismic forces being attracted to wall RW1 compared to RW2. However, in this study, the retrofitted wall using vertical FRP strips, RW1, attained almost 20% higher strength than the one using diagonal strips RW2, which may be sufficient to withstand the additional forces attracted to the wall due to the higher stiffness.

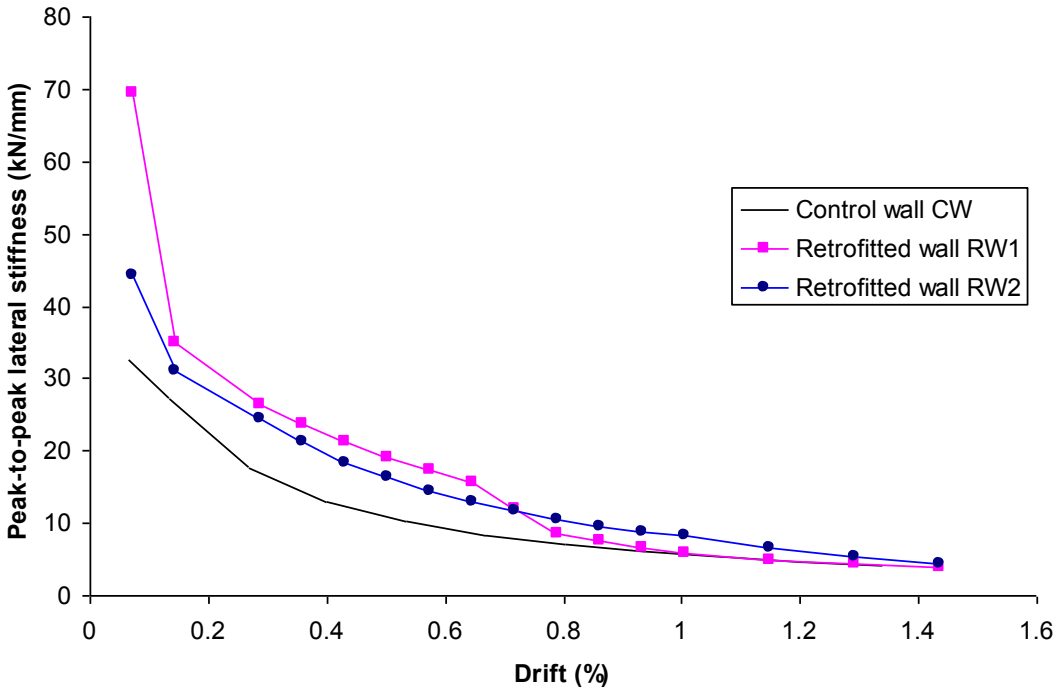

Figure 6.42 Peak-to-peak lateral stiffness-drift ratio relationships of the tested wall panels.

Table 6.2 Experimentally measured peak-to-peak lateral stiffness (kN/mm).

Wall	Cycle	$0.5\Delta_y$	Δ_y	$2\Delta_y$	$2.5\Delta_y$	$3\Delta_y$	$3.5\Delta_y$	$4\Delta_y$	$4.5\Delta_y$	$5\Delta_y$	$5.5\Delta_y$	$6\Delta_y$	$6.5\Delta_y$	$7\Delta_y$	$8\Delta_y$	$9\Delta_y$	$10\Delta_y$
CW	1st	32.6	27.2	17.6		12.9		10.3		8.4		7.0		6.0	5.3	4.7	4.1
	2nd	31.8	26.4	16.8		12.0		9.7		8.0		6.6		5.7	5.0	4.5	3.4
RW1	1st	69.6	35.1	26.5	23.8	21.2	19.1	17.3	15.6	12.0	8.6	7.5	6.6	5.8	5.0	4.4	4.0
	2nd	68.9	34.5	25.9	22.7	20.6	18.6	16.8	14.6	10.8	8.0						
RW2	1st	44.4	31.1	24.4	21.2	18.4	16.3	14.5	13.0	11.7	10.5	9.5	8.8	8.2	6.7	5.4	4.4
	2nd	44.0	30.0	23.4	20.3	17.8	15.7	14.1	12.5	11.3	10.1	9.2	8.6	7.8			

6.5.3 Top Rotations

Figure 6.43 shows the envelope of the lateral load-top rotation relationships for the three tested walls. This figure shows that retrofitted wall RW2 was able to sustain higher rotation at the wall top compared to the control wall CW, whereas the retrofitted wall RW1 was only able to sustain 65% of the rotation of the control wall. This indicates that the retrofit scheme used for RW2 is able to improve the overall rotational ductility capacity of the wall while increasing its flexural capacity. Therefore, such a retrofit scheme will be efficient in the retrofit of multi-storey RC walls at the plastic hinge regions. On the other hand, the retrofit scheme used for wall RW1 is not recommended for cases where the wall rotational ductility capacity is to be maintained.

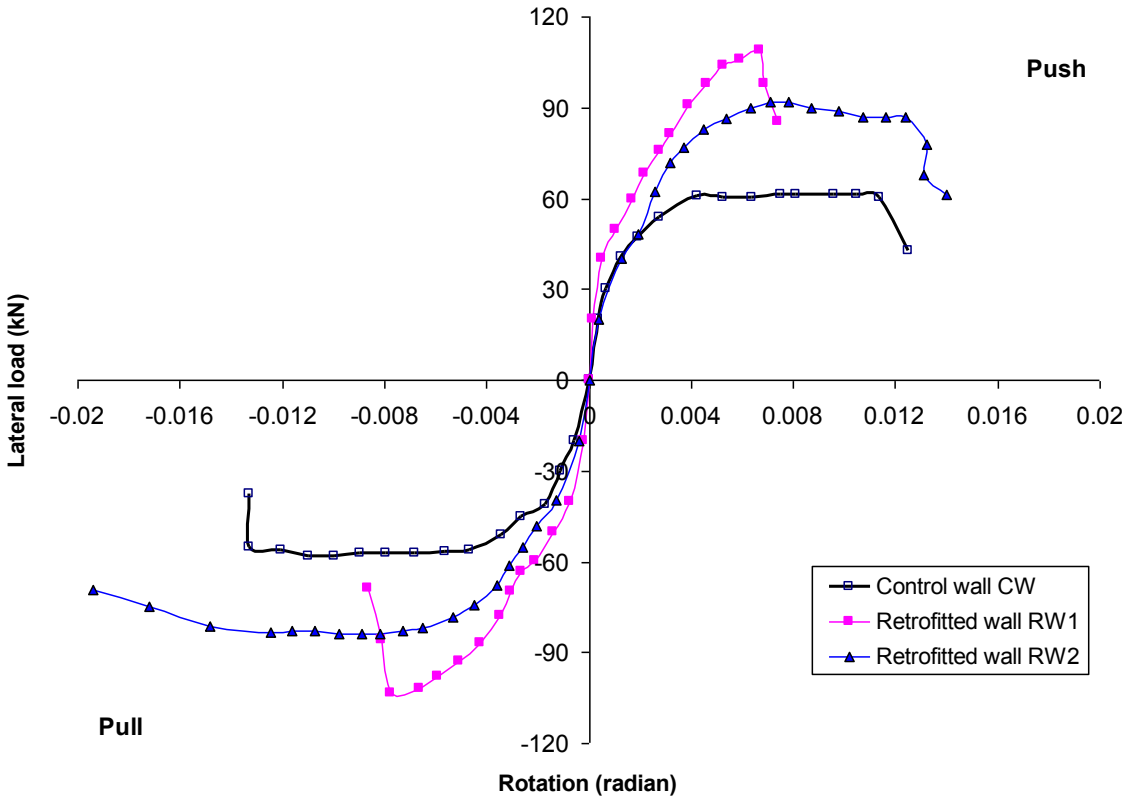

Figure 6.43 Envelope for lateral load-top rotation relationships for the tested walls.

6.5.4 Shear Deformations

Figure 6.44 shows the envelope for the lateral load-shear displacement relationship for the three tested walls. The figure shows that the shear deformations of the retrofitted wall RW2 was almost 30% of the shear deformation of the control wall, although they did reach similar lateral displacement. This result is attributed to the application of the X-FRP strips, which increased the shear resistance of the retrofitted wall and hence reduced its shear deformations. The figure also indicates that the retrofit scheme of RW1 was able to reduce the wall's shear deformation by about 70% compared to the control wall.

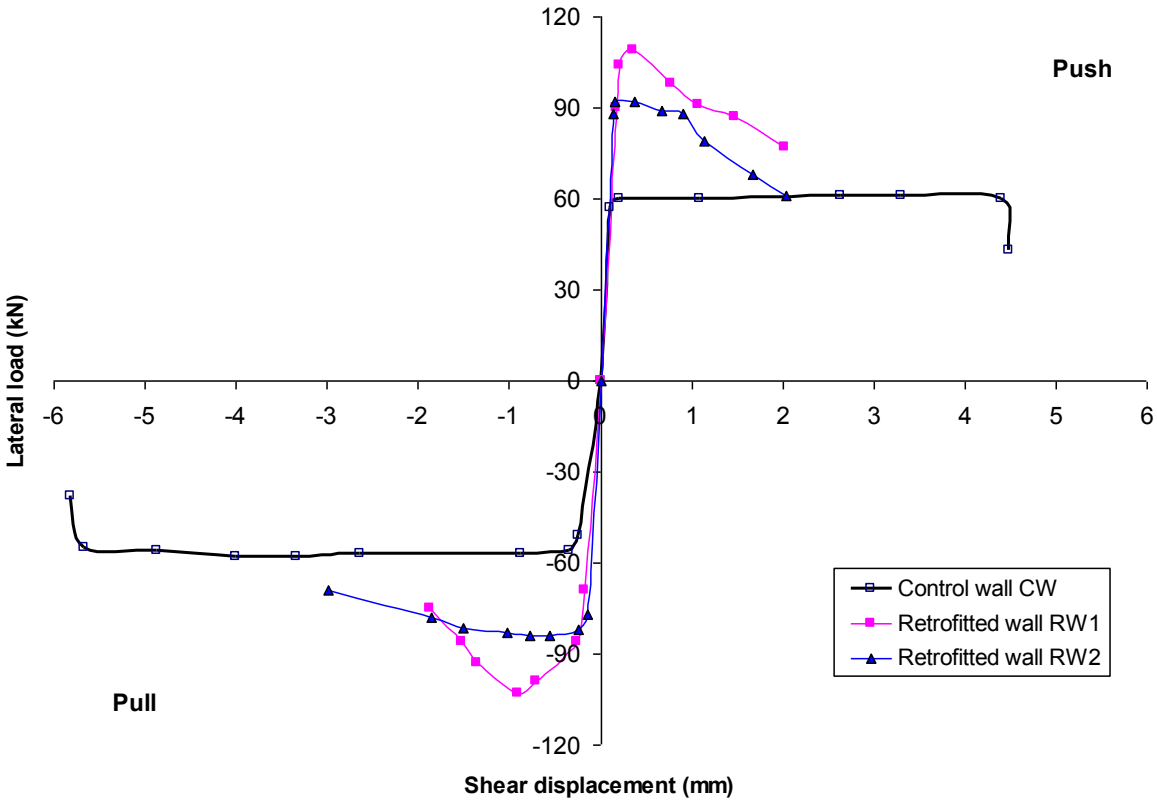

Figure 6.44 Envelope for lateral load-shear displacement relationships of the tested walls.

6.5.5 Energy Dissipation

The energy dissipated by each of the tested walls for each load cycle was calculated using the area enclosed by the load-displacement hysteretic loop. The cumulative energy dissipated by the tested walls was calculated at each displacement level and plotted in Figure 6.45. From that figure, it can be concluded that the three walls dissipated almost the same energy at the same displacement level up to a lateral displacement of 7.5 mm when the retrofitted wall RW1 reached 80% of its maximum load. The retrofitted wall RW2 was able to dissipate almost 3.4 times the energy of wall RW1 when it reached a lateral displacement of 12 mm. At this lateral displacement level, the retrofitted wall RW2 was able to dissipate 92% of the energy dissipated by the control wall CW at the same lateral displacement. Figures 6.46 and 6.47 illustrate the lateral load-top displacement hysteretic loop for one cycle of the retrofitted walls RW1 and RW2 compared to the control wall CW, respectively. These figures show that the hysteretic loops for the FRP-retrofitted walls are narrower due to the elastic behaviour of the FRP composite material, while the peak loads for the FRP-retrofitted walls are higher. This resulted in almost equal energy dissipated for each cycle of the control wall and of the FRP-retrofitted ones. From the figures, it can be also seen that the FRP-retrofitted walls exhibited less pinched behaviour than the control wall. This response is attributed to the application of the vertical or diagonal CFRP strips that controlled the concrete cracking which decreased the pinching effect. In Figure 6.47, some pinching can be observed for the retrofitted wall RW2 due to the closure of the wide concrete cracks observed for RW2 during the test, as was discussed earlier.

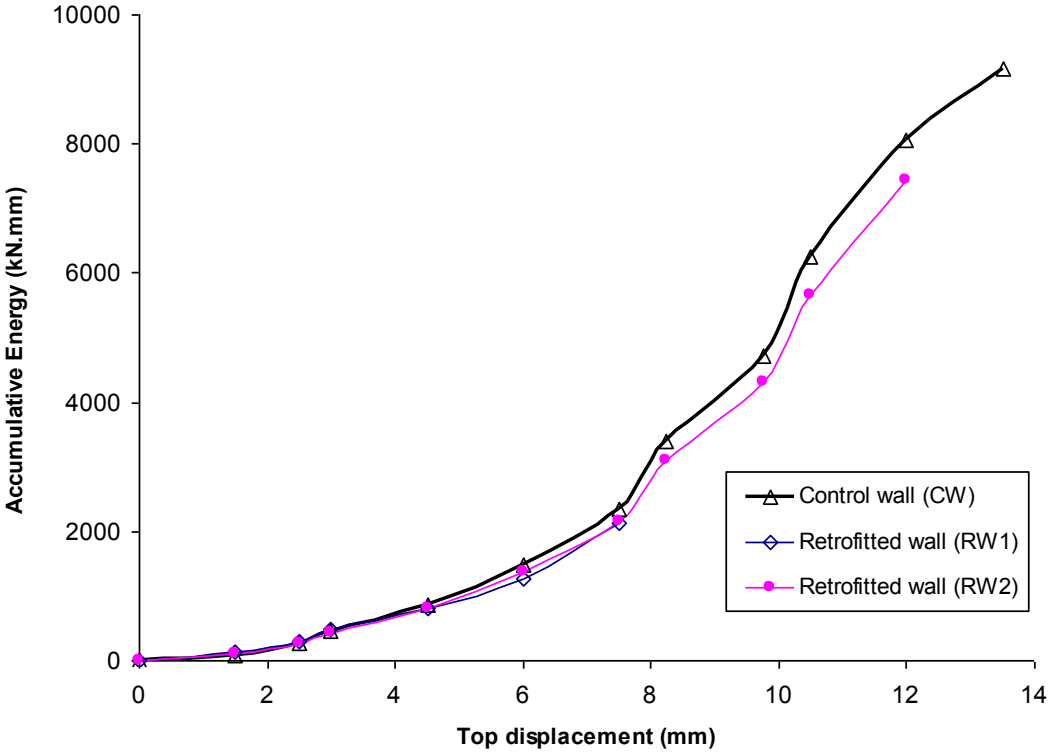

Figure 6.45 Cumulative energy dissipation of the tested wall panels.

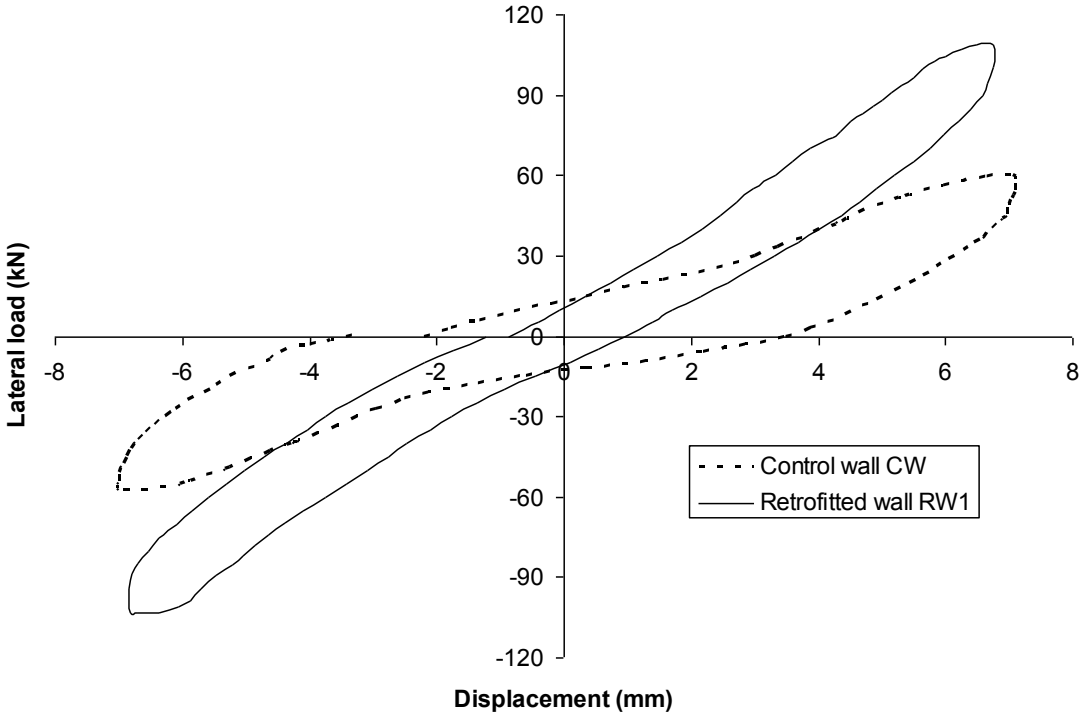

Figure 6.46 Lateral load-top displacement relationship for one cycle of RW1 compared to CW.

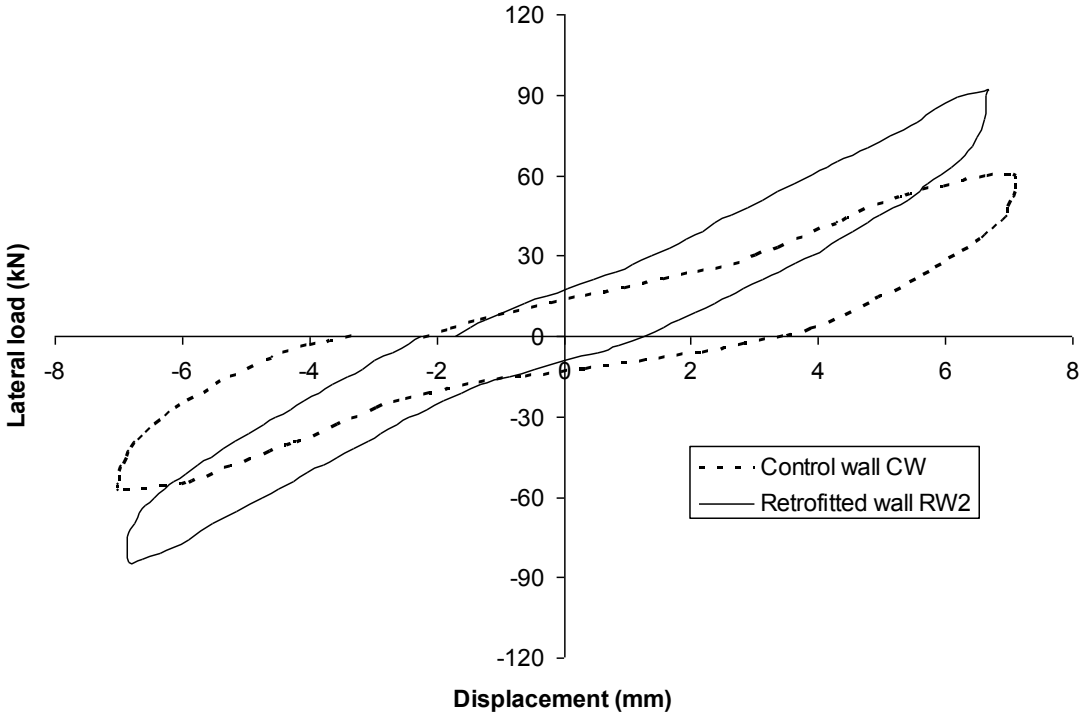

Figure 6.47 Lateral load-top displacement relationship for one cycle of RW2 compared to CW.

6.5.6 Permanent Deformation Control

Controlling the wall's permanent deformations after a severe ground motion is an important aspect of a proper seismic retrofit technique, as was discussed in Chapter 2 (Figure 2.1). By comparing the lateral load-top displacement relationships of the control wall CW and the FRP-retrofitted wall RW2 shown in Figures 6.2 and 6.25, it can be seen that the diagonal FRP braces of RW2 were able to control the wall's residual deformations after reaching a high displacement ductility level. These figures show that the control wall CW had a residual displacement of 8.3 mm (average of pull and push cycles) at the load cycle of 12.6 mm ($9\Delta_y$), whereas the retrofitted wall RW2 had a residual displacement of just 4.8 mm at a similar load cycle of 12.0 mm ($8\Delta_y$). This indicates that the retrofit scheme of RW2 allowed the retrofitted wall to deform well

before failure similar to the control wall but with fewer permanent deformations. On the other hand, it is worth noting that the RW1 retrofit scheme was able to significantly control the wall's permanent deformations but it did not allow the wall to reach the same ductility levels as those of the control wall CW or of the second FRP-retrofitted wall, RW2.

6.5.7 Seismic Force Modification Factors

Seismic force modification factors are being used in several codes to reduce the seismic forces calculated based on the elastic behaviour of a structure. These factors take into account the ductility and the energy dissipation capacities of a structure's seismic force resisting system (SFRS). In the National Building Code of Canada (NBCC 2005), a ductility-related force modification factor, $\boldsymbol{R_d}$, and an overstrength-related force modification factor, $\boldsymbol{R_o}$, are utilized. The equal displacement approach can be used to determine the structure inelastic deformations based on the calculated elastic deformations and the modification factors $\boldsymbol{R_d}, \boldsymbol{R_o}$ (Mitchel et al. 2003). The equal displacement approach is employed in most force-based design codes to calculate the factor $\boldsymbol{R_d}$ according to the displacement ductility level reached experimentally by the SFRS (Priestley et al. 2007). In the calculation of $\boldsymbol{R_d}$, the nonlinear load-displacement relationship of the tested wall can be idealized to a bilinear relationship in order to have a common basis while comparing the walls' behaviour, as shown in Figure 6.48. The $\boldsymbol{R_d}$ value is defined as the ratio of the elastic lateral load V_e to the idealized ultimate wall capacity V_u, which is equal to the ratio of $\Delta_{0.8u}$ and Δ_{ep} by similar triangles as shown in

Figure 6.48, where $\Delta_{0.8u}$ is the lateral displacement measured at 80% of the wall ultimate load and Δ_{ep} is the idealized yield displacement.

The R_o value is defined as the ratio between the wall ultimate load V_u and the design capacity V_d amplified by 5% to account for a conservative design due to restricted dimensions and bar sizes, and which was measured as between 5 to 10% according to Mitchel et al. (2003). The design capacities of the tested walls were calculated according to the CSA A23.3-04 (2004) specifications. The contribution of the compression steel reinforcement to the wall capacity was included in the calculation to reach a conservative estimate of R_o. The concrete and steel material properties were calculated using the concrete cylinder tests and the steel coupon tests described in Chapter 5. The CFRP composite mechanical properties provided by the manufacturer were used in the design. Table 6.3 shows the seismic force modification factors calculated for the three tested walls and the parameters used in their calculation. From the table, it can be seen that the $R_d.R_o$ value for the control wall CW was calculated to be more than three times the value of 2.8 used in the NBCC 2005 for moderately ductile shear walls. This was attributed to the high displacement ductility observed for the control wall during the test which resulted in a high value of R_d. For the retrofitted wall RW1, the $R_d.R_o$ value was 82% higher than the NBCC value for moderately ductile walls. For wall RW2, the $R_d.R_o$ value exceeded the NBCC value for ductile walls, which is 5.6. It should be noted that the displacement ductility, μ_Δ, of the retrofitted walls would have been higher if the walls were subjected to partial damage before the FRP-retrofit, as was the case for the 8-storey walls tested using the shake table. Therefore, it is recommended that more

experiments should be conducted to confirm the values of seismic force modification factors for FRP-retrofitted walls.

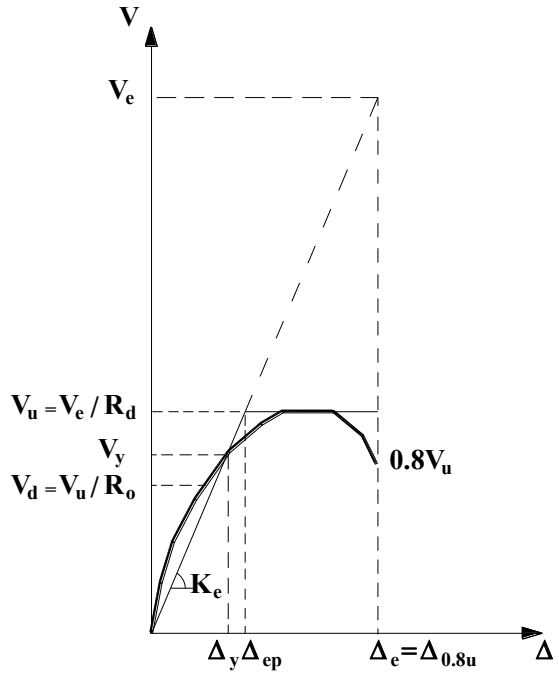

Figure 6.48 Definition of ductility-related and overstrength-related modification factors.

Table 6.3 Seismic response modification factors.

Wall	Design capacity	Experimental results						Force modification factors		
	V_d (kN)	V_y (kN)	Δ_y (mm)	K_e (kN/mm)	V_u (kN)	$\Delta_{0.8u}$ (mm)	$\mu_{\Delta 0.8u}$	R_d	R_o	$R_d.R_o$
CW	47.2	40.5	1.4	28.9	59	14.4	10.3	7.2	1.25	9.0
RW1	57.5	59	1.5	39.3	106	8.0	5.3	2.67	1.94	5.1
RW2	57.5	48	1.5	32.0	88	12.7	8.5	4.33	1.60	6.9

CHAPTER 7

NUMERICAL MODELING OF FRP-RETROFITTED WALL PANELS

7.1 INTRODUCTION

This chapter discusses the numerical macro-model used to simulate the seismic behaviour of the tested control wall panel and the FRP-retrofitted panels. The constitutive material models and the properties of each model are presented along with the modeling assumptions. The numerical model was calibrated using the experimental results of the cyclic loading tests presented in Chapter 6.

7.2 NONLINEAR ANALYSIS OF THE TESTED WALL PANELS

Non-linear static analysis was conducted for the control wall CW and the FRP-retrofitted walls RW1 and RW2. A macro-modeling software for three-dimensional nonlinear static and dynamic structural analysis CANNY (Li 2008) was selected for the analysis. The software was used to simulate the seismic response of existing non-ductile RC frame structures rehabilitated using FRP for increased ductility of members (Galal and El-Sokkary 2008) as well as in the analysis of non-ductile RC frame structures rehabilitated using RC shear walls (El-Sokkary and Galal 2009).

7.2.1 Program description

CANNY (Li 2008) is capable of performing different types of nonlinear analyses, e.g. push over analysis, dynamic analysis, pseudo dynamic analysis, etc. The program has a library of linear and nonlinear models that can represent different types of backbone

curves: linear, bilinear, tri-linear and degradation models. Different hysteretic behaviour can be represented using these models, as well as stiffness degradation, strength deterioration and pinching behaviour. The software is able to account for P-Δ effect in the analysis.

7.2.2 Selected models for analysis

7.2.2.1 Multi-axial spring model (MS model)

The multi-axial spring model is able to represent the interaction of flexural and axial (tension or compression) deformations of column or wall elements. In this model, shear deformations can be represented using a shear spring, in which shear deformations can be linear or nonlinear according to the hysteretic rule used for that spring. A column or wall element is modeled as a linear element with nonlinear multi-axial spring elements at its ends, as shown in Figure 7.1. The spring properties can represent the constitutive material (i.e. concrete and steel) stress-strain relationship. The initial stiffness of the spring is based on equivalent plastic zone stiffness, which can be calculated by:

$$\boldsymbol{K}_0{}^{i} = \frac{\boldsymbol{E}_i \boldsymbol{A}_i}{\eta \boldsymbol{L}_0} \qquad \textit{(for the } i^{th} \textit{ spring)} \qquad \text{……..... (7-1)}$$

$$\boldsymbol{f}_c = \sigma_c \boldsymbol{A}_i , \qquad \textit{(for concrete)} \qquad \text{……..... (7-2)}$$

$$\boldsymbol{f}_{sy} = \sigma_{sy} \boldsymbol{A}_i , \quad \boldsymbol{d}_{sy} = \varepsilon_{sy} \eta \boldsymbol{L}_0 \qquad \textit{(for steel)} \qquad \text{……..... (7-3)}$$

where

$\boldsymbol{K}_0$ is the initial stiffness of the springs;

$\boldsymbol{E}_i$ is the material Young's modulus;

$\boldsymbol{A}_i$ is the area represented by the springs;

σ_c , ε_c are the concrete material compressive strength and corresponding strain;

σ_{sy} , ε_{sy} are the steel material yield stress and strain;

η is the ratio of the plastic zone length to the member clear length, and is taken empirically as half the depth of the member cross-section; and

L_0 is the clear length of the member.

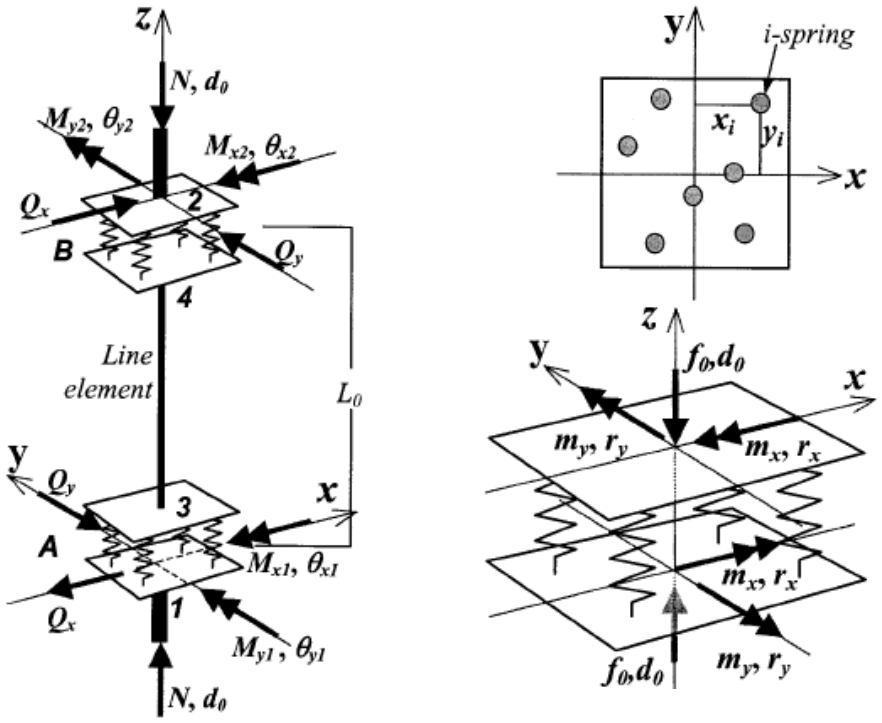

a) Columns with MS element

b) MS element and the forces and displacements (positive)

Figure 7.1 Multi-axial spring model (Li 2008).

7.2.2.2 Linear elastic models (link element)

These models are able to represent the tension/compression force-displacement relationship of a link element with no bending, such as truss or brace members. The link element is modeled as a linear elastic line element with two single-component axial springs. The main input data for this model is the element's force-displacement backbone curve. In this study, the link element was used to represent the FRP vertical or diagonal strips used in the retrofit.

7.2.3 Proposed model

The RC wall panel was modeled using CANNY wall element whereas the FRP strips were modeled using link elements as shown in Figure 7.2. The wall element has four nodes at the corners in addition to an optional node that can be located at the mid points of the top and bottom boundaries. The adjacent panels have compatible deformations at their common three nodes that connect them. A multi-axial spring model is used to represent the flexural and axial tension/compression interaction of the wall elements. The shear deformations can be idealized using a shear spring. Multi-linear curves are used to represent the stress-strain (or force-deformation) relationship for the concrete and steel materials. In the current analysis, the shear deformations were assumed to be linear, as the walls' behaviour was governed by flexure. The moment-to-shear ratio (M/VL) for the tested wall panels was taken into account by adding an additional rigid wall panel that would behave elastically on top of the studied panel. The lateral displacement was applied at the top of the rigid panel, which resulted in a moment at the top of the studied panel corresponding to the top moment applied during the cyclic tests.

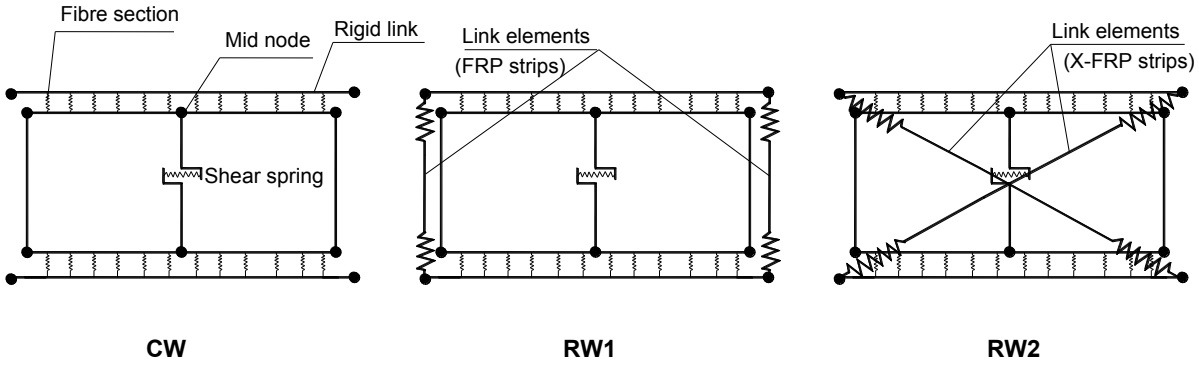

Figure 7.2 The macro-models used for the tested wall panels.

7.2.3.1 Concrete model CS4

Figure 7.3 shows the CS4 model, used to represent the concrete material. This model has a compression ascending part in the linear elastic curve. After reaching the maximum strength, the step-down rule is applied for the descending branch on the compression and on the tension sides to solve for negative stiffness. In this rule, the software uses a very slight positive stiffness (almost equal to zero) and evaluates the element resistance in negative stiffness, and then the unbalanced force which is the difference between the element resistance and the required force for equilibrium is corrected in the next iteration.

The unloading stiffness degradation is calculated as follows:

$$K_5 = \begin{cases} K_{cu}\left(d_c / d_m\right)^{\gamma} & if \quad d_m \rangle d_c \\ K_{cu} & if \quad d_m \le d_c \end{cases} \qquad \ldots\ldots \quad (7\text{-}4)$$

$$K_{cu} = \begin{cases} K_c & if \quad \phi = 0 \\ \dfrac{\varphi . f_c + f_m}{\phi . f_c / K_c + d_m} & if \quad d_m \le d_c \\ \dfrac{\varphi . f_c + f_m}{\phi . f_c / K_c + d_c} & if \quad d_m \rangle \; d_c \end{cases} \qquad \ldots\ldots \quad (7\text{-}5)$$

The tensile strength of concrete is considered only if the tensile strength f_t and the parameter τ are specified. $\tau \geq 3.0$ represents the tension descending portion after reaching the maximum tensile strength f_t.

Our model utilized the following parameters:

- Strain at maximum compressive strength = 0.002 mm/mm
- Ultimate strain/strain at maximum compressive strength ratio $\mu = 1.75$
- Post-peak residual strength/maximum compressive strength ratio $\lambda = 0.4$
- Post-peak unloading stiffness parameter $\gamma = 0.2$
- Tension descending part after tension crack $\tau = 3.0$
- Unloading stiffness parameter before peak stress $\varphi = 2.0$
- Maximum tensile strength $f_t = 4.0$ MPa.

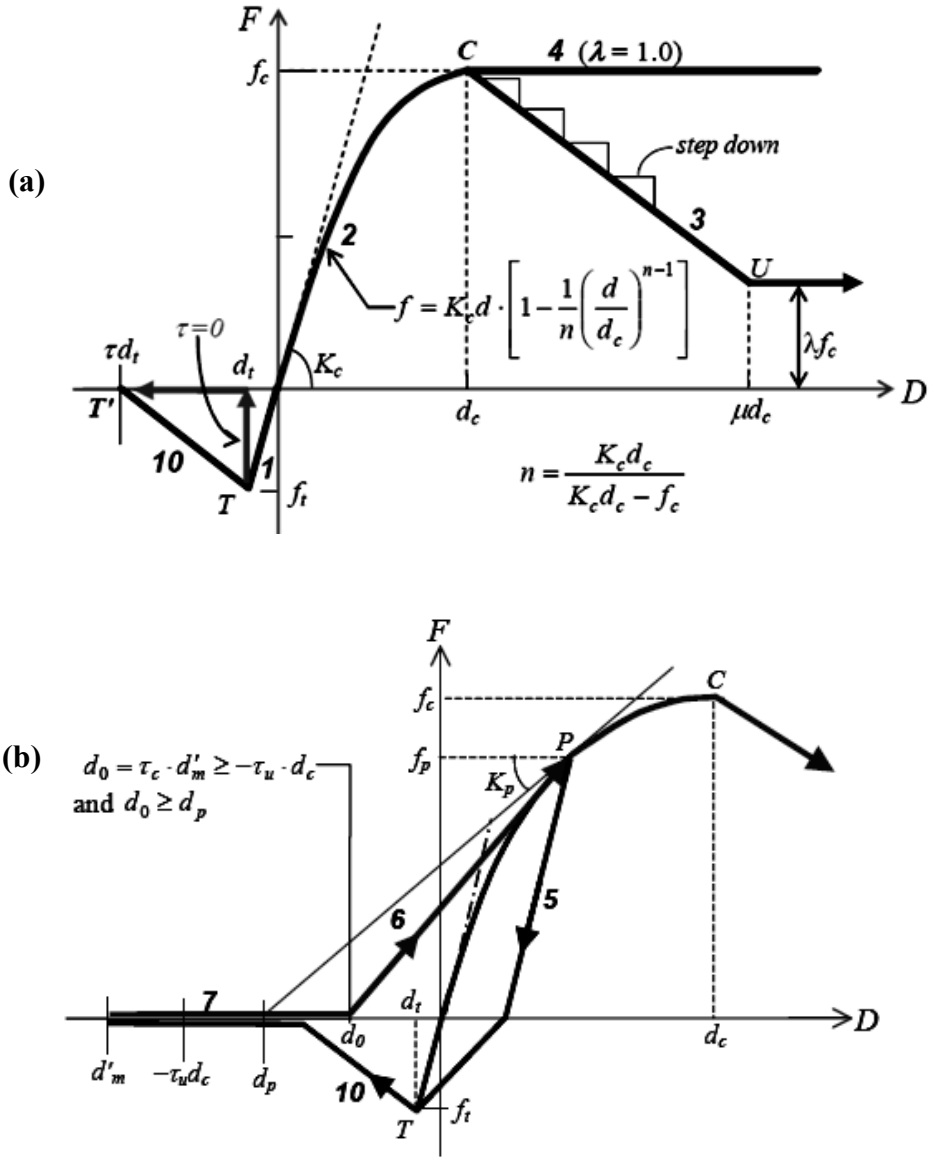

Figure 7.3 Concrete model, CS4, used to represent the concrete material. (a) Skeleton curve, (b) Compression reloading before cracks closing (Li 2008).

7.2.3.2 Steel model SS3

Figure 7.4 shows the trilinear/bilinear model SS3 that is used to represent the steel material. This model is able to represent the stiffness degradation of the whole section before yielding, which can result from cracking or bond slippage of tension reinforcement. The stiffness is reduced before reaching the yielding point by reducing the yielding point from point P_1 to point P_2 and then the curve is connected to point P_3 which corresponds to a spring yield displacement $\kappa\, d_{sy}$, where κ is equal to 1.0 for a bilinear curve. The trilinear model was used to simulate the yielding and strain hardening of the steel material.

The unloading stiffness calculation depends on whether both the tension and compression steel has yielded or not; if yielding has not occurred then:

$$K_u = \begin{cases} \min \text{ of } \dfrac{f_m - \varphi f'_{sy}}{d_m - \varphi f'_{sy}/K_s} \text{ or } \dfrac{f'_m - \varphi f_{sy}}{d'_m - \varphi f_{sy}/K_s} & \text{if } \varphi \rangle 0 \\ K_s & \text{if } \varphi = 0 \end{cases} \quad \ldots\ldots\ldots (7\text{-}6)$$

where ϕ defines the target points A, A' as shown in Figure 7.5. If ϕ is set to zero then no unloading stiffness degradation occurs before yielding. If yielding has occurred in either tension or compression then:

$$K_{uy} = \begin{cases} \min \text{of } \dfrac{f'_{sy} - \varphi f_{sy}}{\kappa' d'_{sy} - \varphi f_{sy}/K_s} \text{ or } \dfrac{f_{sy} - \varphi f'_{sy}}{\kappa d_{sy} - \varphi f'_{sy}/K_s} & \text{if } \varphi \rangle 0 \\ K_s & \text{if } \varphi = 0 \end{cases} \quad \ldots\ldots (7\text{-}7)$$

$$K_u = K_{uy}\left(\frac{\kappa d_{sy} - \kappa' d'_{sy}}{d_m - d'_m}\right)^{\gamma}, \text{ where } d_m \geq \kappa . d_{sy},\ d'_m \leq \kappa' . d'_{sy} \quad \ldots\ldots\ldots (7\text{-}8)$$

When the compression unloading curve passes the horizontal axis and $F < \theta . f_{sy}$, then the loading toward tension maximum point, M', where θ is the factor defining the unloading end point. The parameters taken for this model in our study are as follows:

Skeleton curve parameters ν and κ = 0.8 and 4.0

Post-yielding parameter $\beta = 0.01$

Parameter φ to direct the unloading = 1.0

Unloading stiffness degradation parameter $\gamma = 0.3$

Unloading control parameter $\theta = 0.5$

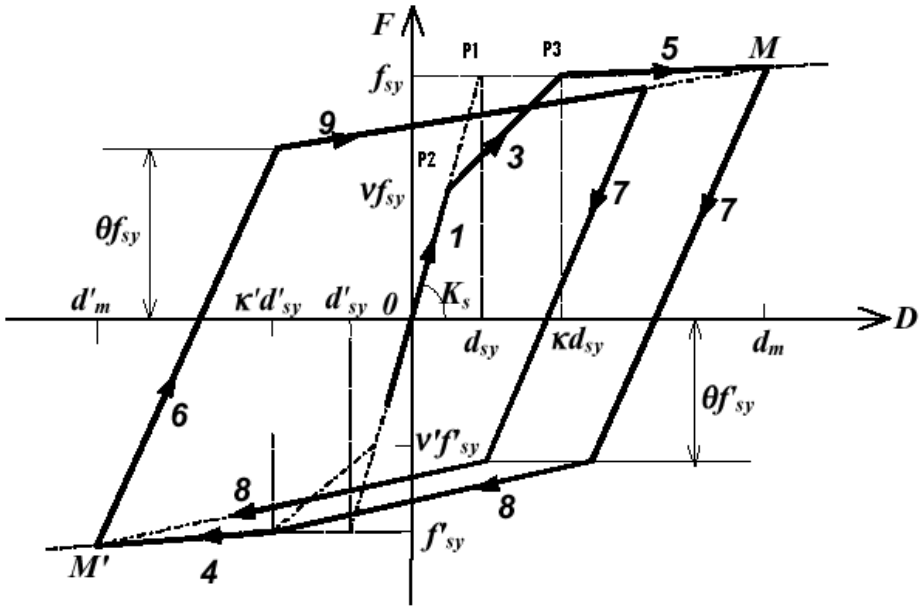

Figure 7.4 Trilinear/bilinear model SS3 used to represent the steel material (Li 2008).

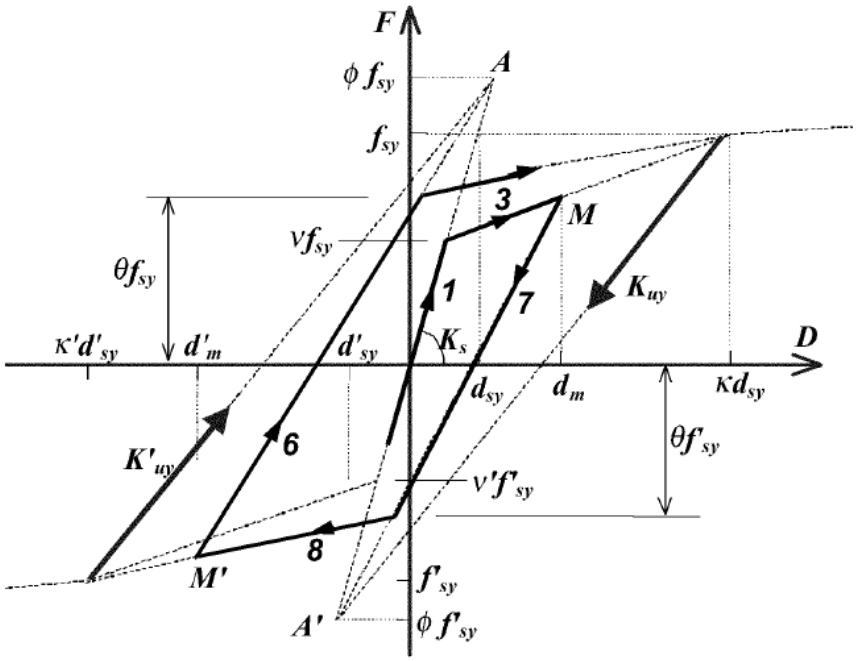

Figure 7.5 Unloading before yielding for steel model SS3 (Li 2008).

7.2.3.3 Model for FRP strips CP4

Figure 7.6 shows the backbone curves for the FRP models used for the retrofitted walls RW1 and RW2. The FRP properties used for the numerical models are the modified ones proposed in the analysis of cyclic test results in Chapter 6 (Table 6.1). Table 7.1 shows the parameters used for the vertical and diagonal FRP strip models of retrofitted walls RW1 and RW2, respectively. The CP4 deterioration model in CANNY was used to represent the FRP vertical and diagonal strips in the nonlinear models of RW1 and RW2. The CP4 model allows the representation of the combined behaviour of the FRP strip and the RC wall that was observed during the cyclic tests due to the wall cracking and the permanent strains of the steel flexural reinforcement. The CP4 model was used to simulate the behaviour of tension only member by adjusting the values of f_c and f_y, shown in Figure 7.7, to zero. The unloading rules for the CP4 model are:

Unloading before yielding:

$$K_{10} = \begin{cases} K_5 & if \ \ |f'_p| \ < \ |f_p| \\ \dfrac{f'_p - f_c}{d'_p - d_c} & if \ \ |f'_p| \ \geq \ |f_p| \end{cases} ; \ K_{11} = \begin{cases} K_4 & if \ \ |f_p| \ < \ |f'_p| \\ \dfrac{f_p - f'_c}{d_p - d'_c} & if \ \ |f_p| \ \geq \ |f'_p| \end{cases} \quad \text{.... (7-9)}$$

Unloading after yielding:

$$K_8, K_{10} = \frac{f'_y - f_c}{d'_y - d_c}\left(\frac{d'_y}{d'_m}\right)^{\gamma} \ ; \quad K_9, K_{11} = \frac{f_y - f'_c}{d_y - d'_c}\left(\frac{d_y}{d_m}\right)^{\gamma} \quad \text{..... (7-10)}$$

$$K_8, K_{10} \geq \frac{f'_m - f_c}{d'_m - d_c} \ ; \quad K_9, K_{11} \geq \frac{f_m - f'_c}{d_m - d'_c} \quad \text{..... (7-11)}$$

where γ is the unloading stiffness degradation parameter (value of 0.7 was assumed)

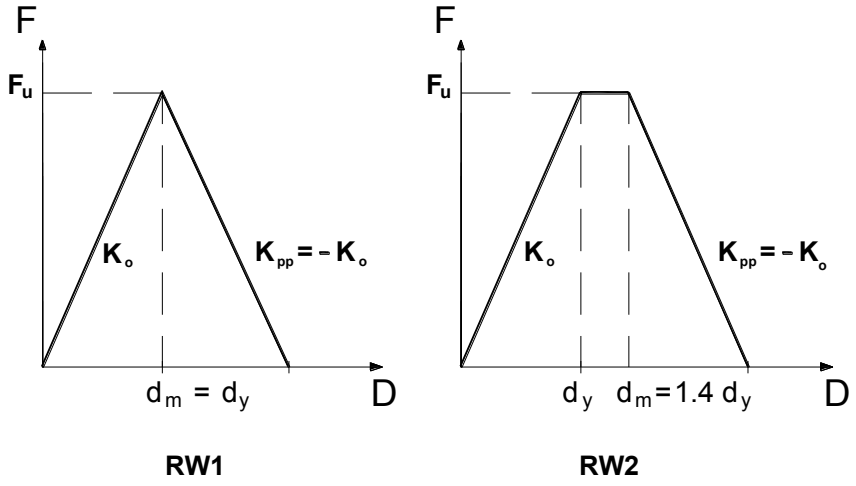

Figure 7.6 The backbone curves for the FRP models of RW1 and RW2.

Table 7.1 Parameters of the FRP models for the retrofitted walls RW1 and RW2.

Wall	RW1	RW2
K_o (N.mm)	33,000	66,000
f_u (kN)	165	173

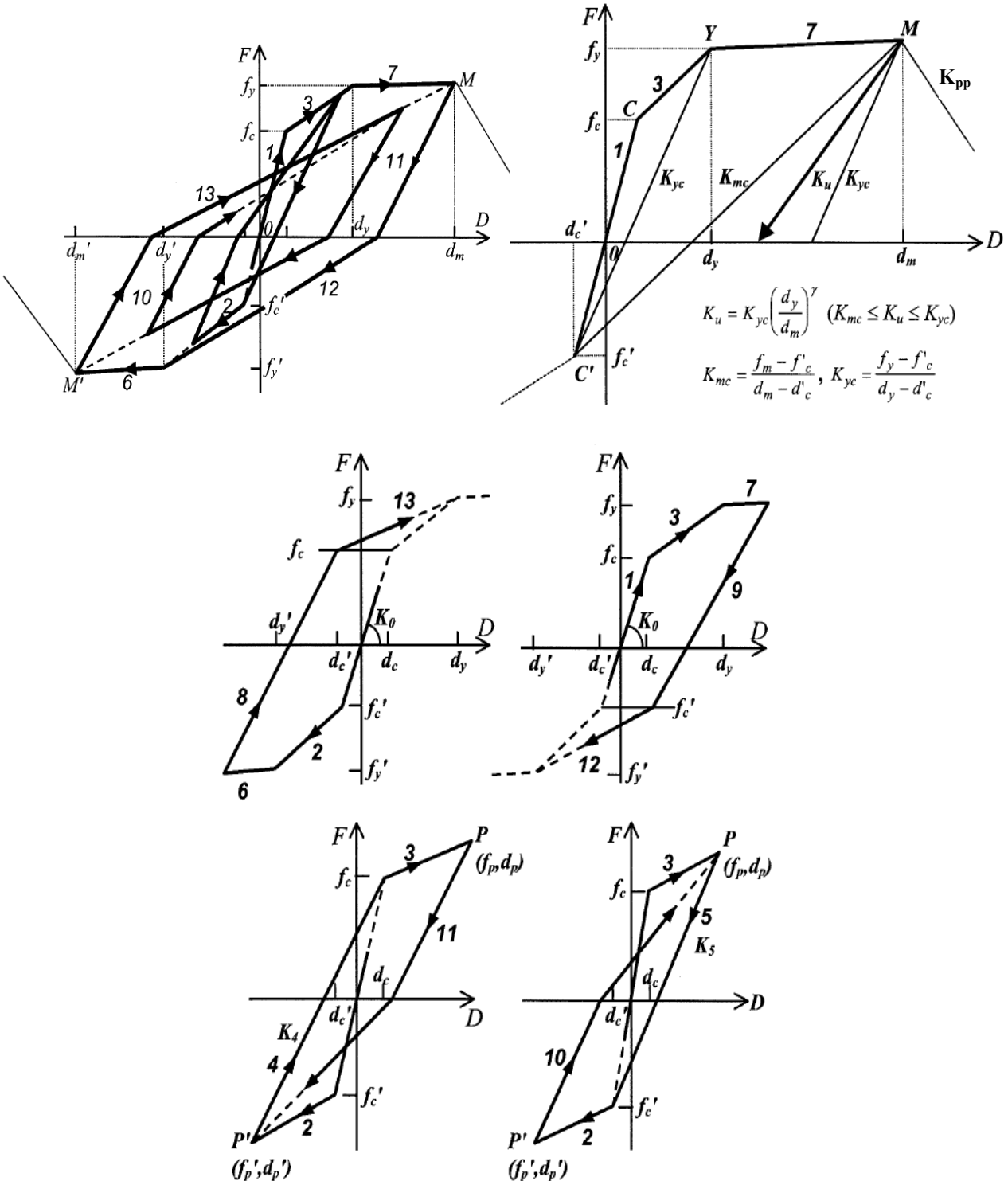

Figure 7.7 Hysteretic behaviour of the CP4 model (Li 2008).

7.3 ANALYSIS RESULTS

The validation and accuracy of the proposed model was checked using the experimental data obtained from the cyclic tests. Figures 7.8 to 7.10 show the experimental hysteretic lateral load-top displacements of the control wall CW and of the FRP-retrofitted walls RW1 and RW2 plotted against the output from CANNY. From the figures, it can be seen that a good agreement between the experimental results and the numerical model has been achieved. Envelopes of the experimental lateral load-top displacement relationships and the numerical ones using CANNY are compared in Figures 7.11 to 7.13. The comparisons showed that the numerical model was able to simulate the monotonic and cyclic behaviour of the tested wall panels with a reasonable accuracy. The numerical model took into account the moment-to-shear ratio of the tested wall panels. Therefore, the proposed model can be used to predict the behaviour of the tested wall panels in multi-storey RC walls when subjected to simulated ground motions. The proposed model would act as a seed for an extensive parametric study that would cover the effect of the wall dimensions, the width of the FRP strips, the number of layers, the FRP composite material properties. It should be noted that such a numerical parametric study could require more experimental tests or nonlinear finite element analysis to validate the findings.

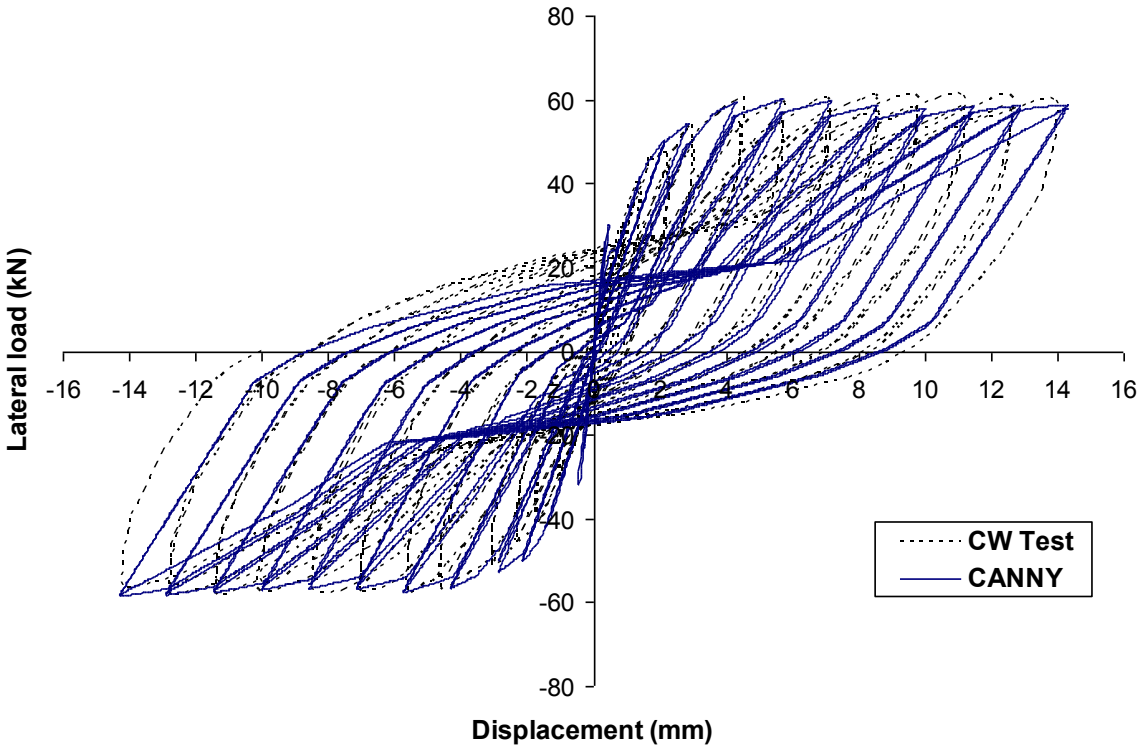

Figure 7.8 Lateral load-top displacement relationship for the control wall CW.

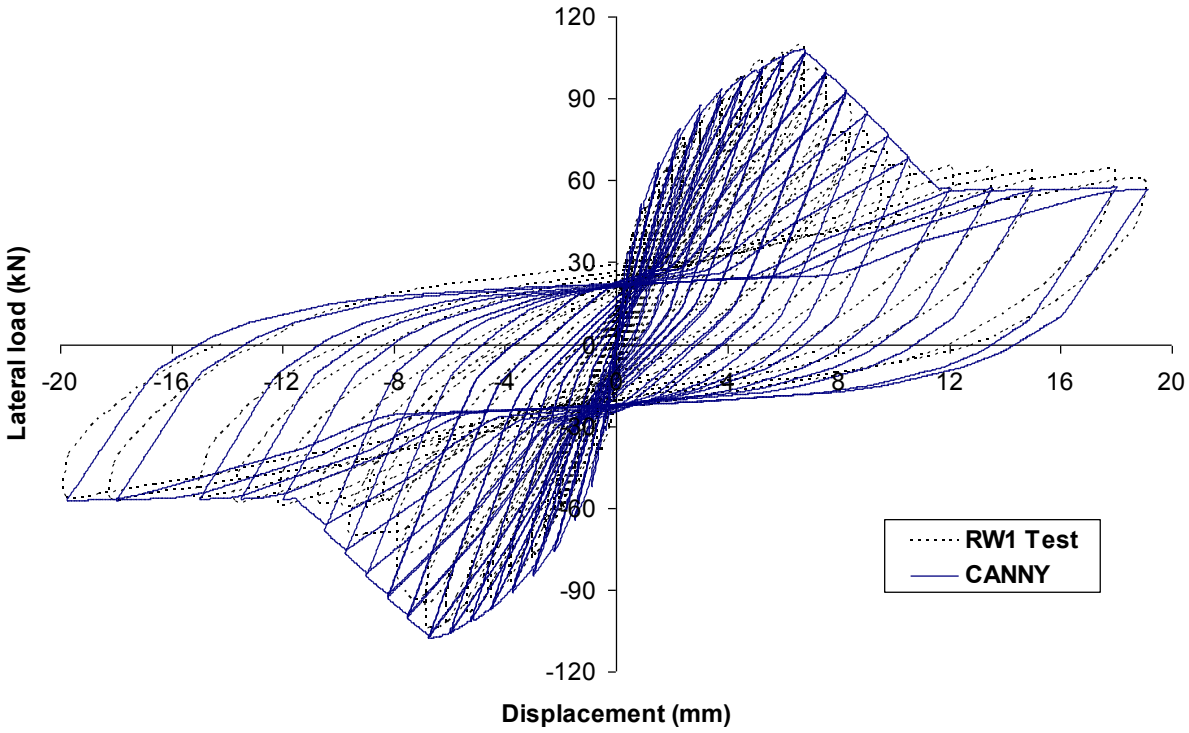

Figure 7.9 Lateral load-top displacement relationship for the retrofitted wall RW1.

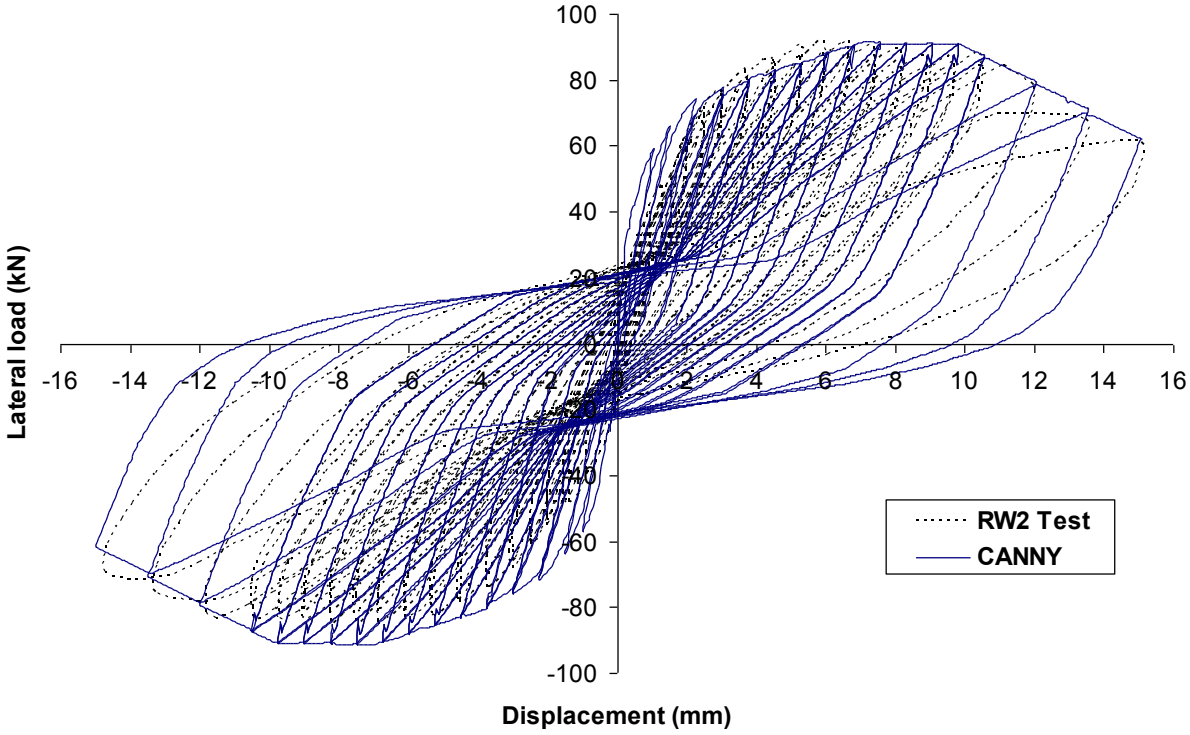

Figure 7.10 Lateral load-top displacement relationship for the retrofitted wall RW2.

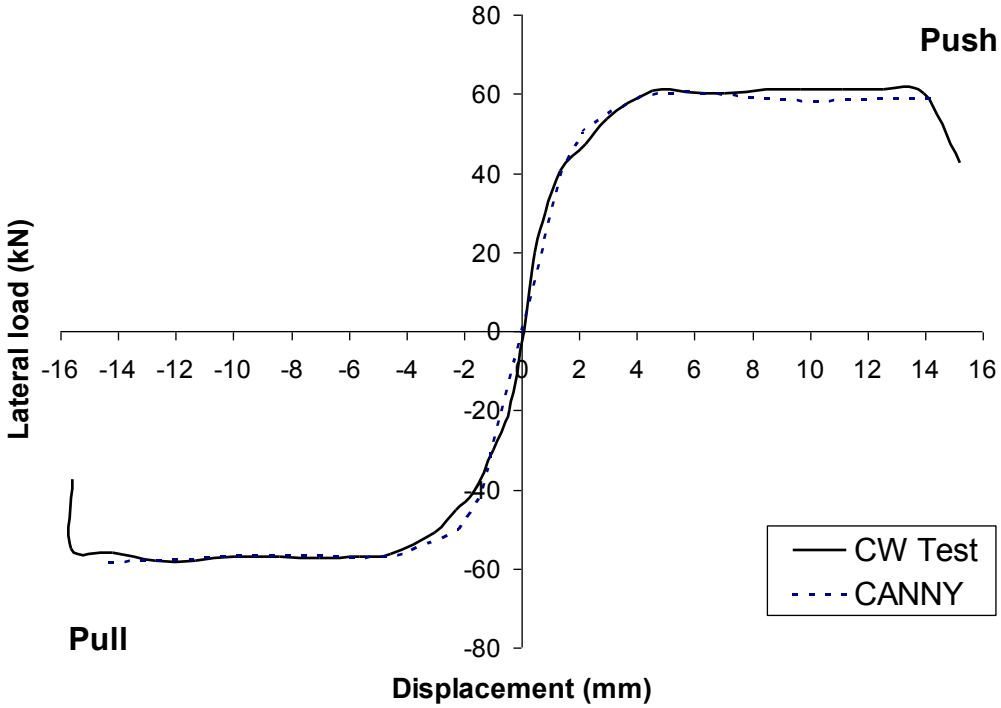

Figure 7.11 Envelope for lateral load-top displacement relationship for the control wall CW.

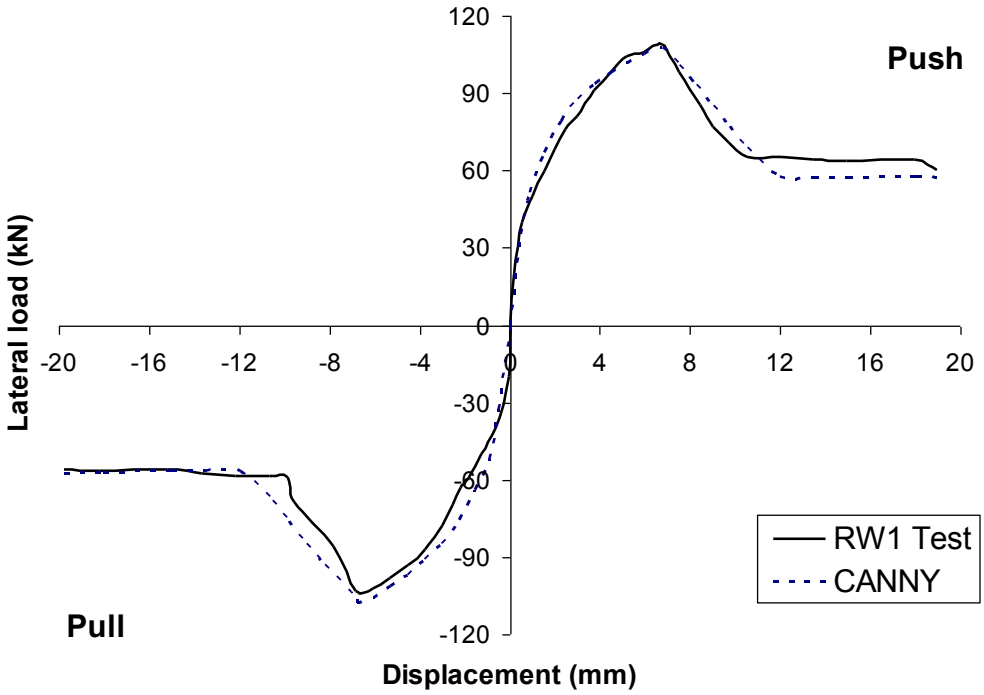

Figure 7.12 Envelope for lateral load-top displacement relationship for the retrofitted wall RW1.

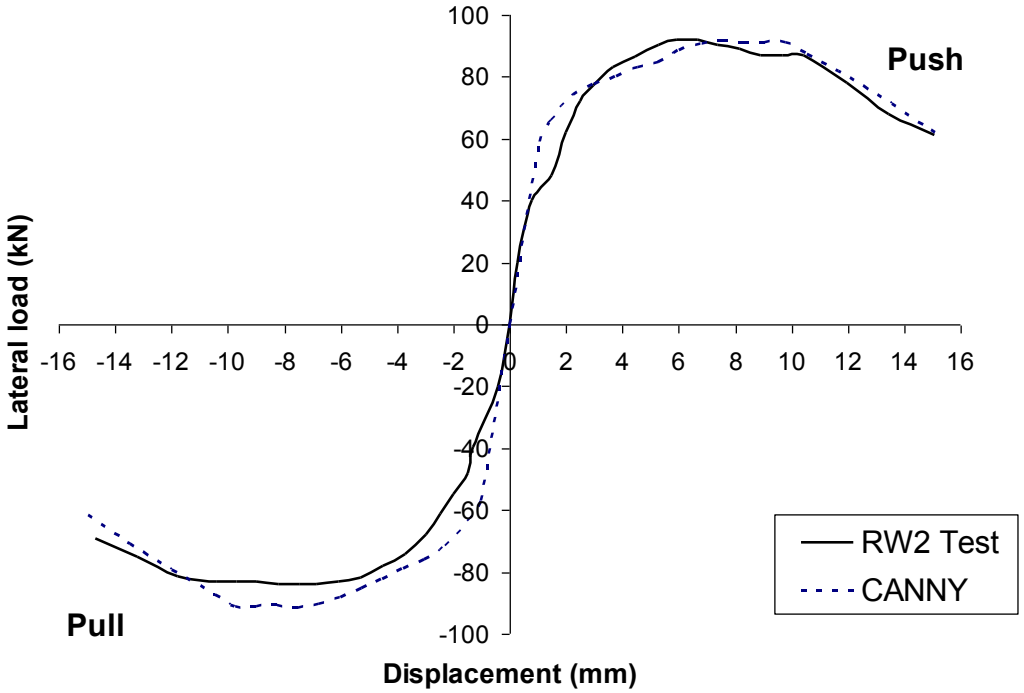

Figure 7.13 Envelope for lateral load-top displacement relationship for the retrofitted wall RW2

CHAPTER 8

SUMMARY AND CONCLUSIONS

8.1 SUMMARY

The seismic behaviour of reinforced concrete (RC) shear walls retrofitted using carbon fibre-reinforced polymers (CFRP) was investigated. The retrofit schemes aimed at increasing the flexural and shear capacities of the retrofitted walls. The experimental program included shake table testing of two FRP-retrofitted 8-storey RC walls under the simulated ground motion excitation from a shake table, as well as cyclic load testing of three RC wall panels. In the first phase of the experimental program, the two 8-storey RC shear walls tested by Ghorbanirenani et al. (2012) were rehabilitated and retested by the author. The original walls were subjected to several levels of ground motion excitation to investigate the effect of higher modes of vibration on the seismic performance of multi-storey shear walls. The damaged walls were rehabilitated and re-subjected to the same intensities of the ground motion excitation. The rehabilitation scheme aimed to increase the flexural and shear capacities of the 6th storey panel (top plastic hinge) by applying vertical and horizontal CFRP strips, whereas the base panel was confined using CFRP sheets to increase the wall's ductility capacity without increasing its strength. The second phase of the experimental program included testing three RC wall panels under lateral cyclic loading up to failure. The walls were subjected to a constant axial load along with synchronized cyclic moment and shear force at the top of each panel. These wall panels were each designed to simulate the 6th storey panel of the 8-storey wall tested under lateral ground motion excitation. The wall panels represent the control wall and two FRP-

retrofitted walls using two different retrofit schemes. The main target of the retrofit schemes was to increase the flexural capacity of the wall section as well as its shear capacity to conform to the capacity design philosophy. The first retrofit scheme was similar to the one used in the rehabilitation of the two 8-storey walls. In the second retrofit scheme, the flexural and shear capacities were increased by applying diagonal CFRP strips as well as horizontal overlapping CFRP wraps. A comparison between the original walls and the FRP-retrofitted walls was presented and the effectiveness of two FRP-retrofit schemes was evaluated in terms of wall strength, deformations, strains, and energy dissipation capacity. A numerical macro-model was proposed to simulate the seismic behaviour of the RC wall panels tested under cyclic loading.

8.2 CONCLUSIONS

The following conclusions were drawn from the results of the experimental and analytical study:

1. The FRP-rehabilitated 8-storey walls performed efficiently, showing an improved flexural behaviour at the top plastic hinge (6^{th} storey panel). The FRP rehabilitation reduced the walls' rotation at this location by about 28% for the first wall (tested at 120% intensity), by 22% for the second wall (tested at 150% intensity) and by 26% for the second wall (at 200% intensity), while the bending moment demands increased slightly at that floor level.

2. The FRP rehabilitation of the two walls reduced the first and second periods of vibration due to the additional stiffness at the top plastic hinge. This resulted in a slight increase of both the base shear and overturning moment due to rehabilitation.

3. The FRP-retrofit of the top plastic hinge decreased the maximum interstorey drift (I.D.) ratio at the 6^{th} storey level. However, the FRP-retrofit scheme did not have a significant effect on the maximum roof drift of the tested walls. On the other hand, the maximum I.D. ratio increased at the lower storeys due to the higher demands as well as the accumulated damage.

4. A noticeable reduction of the longitudinal reinforcement strains at the top plastic hinge region occurred due to the application of the vertical FRP strips at that level, which led to a reduction of the wall rotational demands. On the other hand, the strain values of the longitudinal steel reinforcement at the wall base did not decrease, as no vertical FRP sheets were applied at the base.

5. The vertical FRP strips at the top plastic hinge of the 8-storey FRP-rehabilitated walls reached a strain of about 2000 μ strain (almost 33% of the FRP material's design capacity) at 120% of the ground motion intensity. No FRP anchorage failure or debonding was detected.

6. The FRP-rehabilitated wall was able to achieve the main design target, even at 120% of the design ground motion intensity.

7. The horizontal CFRP sheets applied at the base panel of the 8-storey FRP-rehabilitated walls, where the high shear demands were observed, were able to reduce

the strains in the transverse steel reinforcement at that location by almost 50% compared to the original wall.

8. It is recommended to install FRP anchors similar to those used for the first rehabilitated 8-storey wall, despite the difficulty of drilling holes through the wall thickness. If, however, the anchors must be installed as the detail of the second wall, the designer then has to ensure that the FRP anchor is detailed such that it only elongates in the direction parallel to its axis without any undesired outwards deformations that would waste part of the anchor's longitudinal strains.

9. The bending moment demands increased for some storeys by about 3-13% after rehabilitation at the 150 and 200% intensity. The shear force demands at the base panel increased by about 10-12% after rehabilitation at the 120 and 200% intensity. Therefore, with the flexure rehabilitation of one wall panel, other panels may need to be rehabilitated if the rehabilitation leads to a significant increase in their demands.

10. Three RC wall panels were tested under static cyclic loading. The walls represent the control wall and two FRP-retrofitted walls. The control specimen was able to sustain a lateral displacement of 14 mm with no strength deterioration, which corresponds to displacement ductility, μ_{Δ}, of 10.0 and drift ratio of 1.34% at an average lateral load of 59 kN.

11. The yield load of the retrofitted wall panel using vertical FRP strips was measured to be about 46% higher than the control wall at a 7% higher yield displacement. The tested wall panel showed an increase of the flexural capacity of about 80% compared to the control wall, accompanied by a decrease of the wall's displacement ductility.

The wall panel reached displacement ductility, μ_Δ, of 5.5 measured at 20% strength degradation after the peak load.

12. The vertical CFRP strips of the first retrofit scheme of the tested wall panels controlled the opening of horizontal cracks, as the cracks were normal to the fibre direction (observed from the control wall specimen); this resulted in a lower displacement ductility capacity.

13. The yield load of the retrofitted wall using diagonal FRP strips was 19% higher than the control wall at 7% higher yield displacement. The wall showed an increase of the flexural capacity of about 50% compared to the control wall, accompanied by similar displacement ductility. The wall reached displacement ductility, μ_Δ, of 9.0 measured at 20% strength degradation after the peak load.

14. The failure of the retrofitted wall panel using diagonal FRP strips was due to rupture of the FRP diagonal strips resisting the pull cycles, and to pull out of the FRP anchors resisting the push cycles. The failure was accompanied by concrete crushing above the confined end zones wrapped with horizontal CFRP straps and by buckling of the steel reinforcement bars at both sides of the wall.

15. The wall panel retrofitted using diagonal FRP strips showed less flexural capacity than the wall retrofitted using vertical FRP strips; this was mainly due to the propagation of wide cracks along the wall height. These cracks did not close completely when the load reversed, which caused a residual elongation of the FRP diagonal strips. This led to a situation where the horizontal force components of the

two diagonal FRP strips were acting against each other, which reduced the resultant wall's load capacity.

16. For the wall panel retrofitted using diagonal FRP strips, the opening of horizontal cracks above the bottom horizontal FRP strips and the ability of the diagonal FRP strips to stretch as the cracks widened allowed the wall to sustain high lateral displacements while maintaining its strength.

17. The mechanical properties of the FRP sheets were found to be higher than those provided by the manufacturer, which led to higher measured nominal capacities than those calculated for both retrofitted walls. This also led to the premature pullout of the FRP anchors at the wall base for both retrofitted walls.

18. The wall panel retrofitted using vertical FRP strips had higher stiffness up to lateral drift of 0.71%. On average, the wall panel had about 50% higher stiffness than the control wall after the yield load and prior to its failure, and about 15% higher stiffness than the retrofitted wall using diagonal strips. Therefore, this would result in higher seismic forces attracted to the wall retrofitted using vertical strips.

19. The wall panel retrofitted using diagonal FRP strips was able to sustain higher rotation at the wall top compared to the control wall, whereas the wall retrofitted using vertical FRP strips was only able to sustain 65% of the rotation of the control wall.

20. The vertical FRP strips were able to reduce the wall's shear deformation of the retrofitted wall panel by about 70% compared to the control wall. The shear

deformations of the retrofitted wall panel using diagonal strips were almost 30% of the shear deformation of the control wall, although they reached similar lateral displacement.

21. The retrofitted wall using diagonal strips was able to dissipate almost 3.4 times the energy that the wall with vertical strips could when the former reached a lateral displacement of 12 mm. At this lateral displacement level, the wall with diagonal strips was able to dissipate 92% of the energy dissipated by the control wall CW at the same lateral displacement.

22. The FRP-retrofitted walls showed less pinched behaviour than the control wall. This is attributed to the application of the vertical or diagonal CFRP strips that controlled the concrete cracking which decreased the pinching effect. However, some pinching was noticed for the wall panel retrofitted using diagonal strips due to closure of the wide concrete cracks observed during the test.

23. The retrofit scheme using diagonal strips allowed the retrofitted wall to reach high deformation levels before failure. This response is similar to that of the control wall but with less permanent deformations.

24. The findings of the experimental work prove the viability of using the proposed retrofit schemes, even for older design codes, provided that capacity design concepts are respected.

25. The numerical macro-model was able to simulate the seismic behaviour of the tested wall panels with a reasonable accuracy for both monotonic and cyclic loading. The

numerical model took into account the moment-to-shear ratio of the tested wall panels, and therefore, is able to simulate the seismic behaviour of multi-storey RC walls.

8.3 RECOMMENDATIONS FOR FUTURE WORK

1- More experiments should be conducted to investigate the behaviour of the FRP-retrofitted wall RW1 with smaller areas of vertical FRP strips to examine the FRP rupture mode of failure.

2- More tests should be conducted to examine the effect of complete FRP wrapping along the height of wall RW2 on the concrete confinement at the wall boundary ends.

3- Further experiments should be considered to obtain the seismic force modification factors for FRP-retrofitted walls for both retrofit schemes.

4- The proposed macro-model can be extended to simulate the behaviour of multi-storey RC shear wall structures when subjected to simulated ground motions.

REFERENCES

1. American Society of Civil Engineers, ASCE (2006). "Seismic Rehabilitation of Existing Buildings" ASCE /SEI Standard 41-06, New York.

2. Antoniades, K., Salonikios, T., and Kappos, A. (2003). "Cyclic Tests on Seismically Damaged Reinforced Concrete Walls Strengthened using Fiber-Reinforced Polymer Reinforcement" ACI Structural Journal, 100 (4), 510-518.

3. Bachmann, H. and Linde, P. (1995). "Dynamic Ductility Demand and Capacity Design of Earthquake-Resistant Reinforced Concrete Walls" Proceedings of the Tom Paulay Symposium, La Jolla, Calif., Publication SP 157-06, American Concrete Institute, Detroit, Mich., 117-142.

4. Bakis, C., Bank, L., Brown, V., Cosenza, E., Davalos, J., Lesko, J., Machida, A., Rizkalla, S. and Triantafillou, T. (2002). "Fiber-Reinforced Polymer Composites for Construction—State-of-the-Art Review" Journal of Composites for Construction, ASCE, 6(2), 73-87.

5. Beyer, K., Dazio, A., and Priestley, M. (2011). "Shear Deformations of Slender Reinforced Concrete Walls under Seismic Loading" ACI Structural Journal, 108(2), 167-177.

6. Cho, S., Tubber, B., Cook, W. and Mitchell, D. (2004). "Structural Steel Boundary Elements for Ductile Concrete Walls" Journal of Structural Engineering, 130(5), 762-768.

7. Clough, R. W., Benuska, K. L. and Wilson, E. L. (1965). "Inelastic Earthquake Response of Tall Buildings" Proc. 3rd World Conference on Earthquake Engineering 11, New Zealand.

8. Colotti, V. (1993). "Shear Behavior of RC Structural Walls" Journal of Structural Engineering, ASCE, 119(3), 728-746.

9. Combescure, D. (2002). "IAEA CRP-NFE Camus Benchmark: Experimental Results and Specifications to the Participants" Rapport DM2S. SEMT/EMSI/RT/02-047/A.

10. Canadian Standards Association CSA. (2004). "Design of Concrete Structures A23.3-04", Mississauga, Ont., Canada.

11. De Lorenzis, L., Nanni, A., and La Tegola, A. (2000). "Strengthening of Reinforced Concrete Structures with Near Surface Mounted FRP Rods" International Meeting on composite Materials, PLAST 2000, Milan, Italy, May 9-11.

12. Desroches, R. and Smith, B. (2003). "Shape Memory Alloys in Seismic Resistant Design and Retrofit: A critical Review of their Potential and Limitations" Journal of Earthquake Engineering, 7(3), 1-15.

13. Effendy, E., Liao, W., Song, G., Mo, Y. and Loh, C. (2006). "Seismic Behavior of Low-Rise Shear Walls with SMA Bars" Proceedings of the 10th Biennial International Conference on Engineering, Construction, and Operations in Challenging Environments, Earth and Space (ASCE).

14. Elnashai, A., Pilakoutas, K., and Ambrayses, N. (1990). "Experimental Behavior of Reinforced Concrete Walls under Earthquake Loading" Journal of Earthquake Engineering and Structural Dynamics, 19(3), 387-407.

15. Elnashai, A. and Pinho, R. (1998). "Repair and Retrofitting of RC Walls using Selective Techniques" Journal of Earthquake Engineering, 2(4), 525-568.

16. El-Hacha, R., and Rizkalla, S. (2004). "Near-Surface-Mounted Fiber-Reinforced Polymer Reinforcements for Flexural Strengthening of Concrete Structures" ACI Structural Journal, 101(5), 717-726.

17. El-Sokkary, H., and Galal, K. (2009). "Analytical Investigation of the Seismic Performance of RC Frames Rehabilitated using Different Rehabilitation Techniques" Engineering Structures, 31(9), 1955-1966.

18. El-Sokkary, H., Galal, K., Ghorbanirenani, I., Léger, P., Tremblay, R. (2012). "Shake table tests on FRP-rehabilitated RC shear walls" Journal of Composites for Construction (ASCE), in press, doi: 10.1061/(ASCE)CC.1943-5614.0000312.

19. Emori, K. and Schnobrich, W. C. (1981). "Inelastic Behavior of Concrete Frame-Wall Structures" Journal of the Structural Division, 107(1), 145-164.

20. Fiorato, A., Oesterle, R. and Corley, W. (1983). "Behavior of Earthquake Resistant Structural Walls before and after Repair" ACI Journal, 80(5), 403-413.

21. Fischinger, M., Vidic, T., Selih, J., Fajfar, P., Zhang, H. Y. and Damjanic, F.B. (1990). "Validation of a Macroscopic Model for Cyclic Response Prediction of RC Walls" In Bicanic, N. B. and Mang, H. (eds.), Computer Aided Analysis and Design of Concrete Structures. Vol. 2, Pineridge Press, Swansea, 1131-1142.

22. Fyfe. (2010). "Tyfo® SCH-11UP Composite using Tyfo® S Epoxy User's Guide" Fyfe Company LLC, http://www.fyfeco.com.

23. Galal K. (2008). "Modeling of Lightly Reinforced Concrete Walls Subjected to Near-Fault and Far-Field Earthquake Ground Motions" Journal of the Structural Design of Tall and Special Buildings, 17(2), 295-312.

24. Galal, K., and El-Sokkary, H. (2008). "Analytical Evaluation of Seismic Performance of RC Frames Rehabilitated using FRP for Increased Ductility of Members" Journal of Performance of Constructed Facilities (ASCE), 22(5), 276-288.

25. Ghobarah, A. and Abou Elfath, H. (2001). "Rehabilitation of a Reinforced Concrete Frame using Eccentric Steel Bracing" Journal of Engineering Structures, 23(7), 745-755.

26. Ghorbanirenani, I., Tremblay, R., Léger, P., and Leclerc, M. (2012). "Shake Table Testing of Slender RC Shear Walls Subjected to Eastern North America Seismic Ground Motions" Journal of Structural Engineering, ASCE, in press, doi: 10.1061/(ASCE)ST.1943-541X.0000581.

27. Ghorbanirenani, I., Tremblay, R., El-Sokkary, H., Galal, K., Léger, P., and Leclerc, M. (2010). "Shake Table Tests and Repair of Ductile Slender Reinforced Concrete Shear Walls" Proc. 9th US National and 10th Canadian Conference on Earthquake Engineering, Toronto, ON.

28. Giberson, M. (1967). "The Response of Nonlinear Multi-Story Structures Subjected to Earthquake Excitation" Tech. report, Earthquake Engineering Research Laboratory, California Institute of Technology, Pasadena, California.

29. Greifenhagen, C. and Lestuzzi, P. (2005). "Static Cyclic Tests on Lightly Reinforced Concrete Shear Walls" Journal of Engineering Structures, 27(11), 1703-1712.

30. Hiraishi, H. (1984). "Evaluation of Shear and Flexural Deformations of Flexural Type Shear Walls" Bulletin of the New Zealand Society for Earthquake Engineering, 17(2), 135-144.

31. ISIS Design Manual 4. (2008). "FRP Rehabilitation of Reinforced Concrete Structures". ISIS Canada Corporation, The Canadian Network of Centers of Excellence on Intelligent Sensing for Innovative Structures, Canada.

32. Jiang, Y. and Saiidi, S. M. (1990). "Four-Spring Element for Cyclic Response of R/C columns" Journal of Structural Engineering, ASCE, 116(4), 1018-1029.

33. Kabayesawa, T. H., Shiohara, S., Otani, S. and Aoyama, H. (1982). "Analysis of the Full-Scale 7-Story R.C. Test Structure" Proceedings, 3rd Joint Technical Coordinating Committee, U.S. Japan Cooperative Earthquake Research Program, Building Research Institute, Tsukuba.

34. Kanakubo, T., Aridome, Y., Fujita, N. and Matsui, M. (2000). "Development of Anchorage System for CFRP Sheet in Strengthening of Reinforced Concrete Structures" Proceedings of 12th World Conference on Earthquake Engineering, (CD-ROM), paper No. 1831.

35. Khalil, A., and Ghobarah, A. (2005). "Behaviour of Rehabilitated Structural Walls" Journal of Earthquake Engineering, 9(3), 371-391.

36. Kim, T. and Foutch, D.A. (2007). "Application of FEMA Methodology to RC Shear Wall Buildings Governed by Flexure" Journal of Engineering Structures, 29(10), 2514-2522.

37. Kunnath, S. K., Reinhorn, A., M. and Park, Y. J. (1990). "Analytical Modeling of Inelastic Seismic Response of R/C Structures" Journal of Structural Engineering, ASCE, 116(4), 996-1016.

38. Lai, S. S., Will, G. T. and Otani, S. (1984). "Model for Inelastic Biaxial Bending of Concrete Member" Journal of Structural Engineering, ASCE, 110(11), 2563-2584.

39. Lefas, I. and Kotsovos, M. (1990). "Strength and Deformation Characteristics of Reinforced Concrete Walls under Load Reversal" ACI Structural Journal, 87(6), 716-726.

40. Li, K. (2008) "Three Dimensional Nonlinear Static and Dynamic Structural Analysis Computer Program" User's Manual, CANNY Structural Analysis, Vancouver, BC, Canada.

41. Li, K. N. and Otani, S. (1993). "Multi-Spring Model for 3-Dimensional Analysis of RC Members" Journal of Structural Engineering and Mechanics, 1(1), 17-30.

42. Linde, P. and Bachmann, H. (1994). "Dynamic Modelling and Design of Earthquake-Resistant Walls" Journal of Earthquake Engineering and Structural Dynamics, 23(12), 1331-1350.

43. Lombard, J., Lau, D., Humar, J., Foo, S., and Cheung, M. (2000). "Seismic Strengthening and Repair of Reinforced Concrete Shear Walls" Proc. 12th World Conference on Earthquake Engineering, Auckland, NZ (CD-ROM), Paper No. 2032.

44. Lopes, M. (2001). "Experimental Shear-Dominated Response of RC Walls, Part I: Objectives, Methodology and Results" Journal of Engineering Structures, 23(3), 229-239.

45. Mitchell, D., Tremblay, R., Karacabeyli, E., Paultre, P., Saatcioglu, M., and Anderson, D. (2003). "Seismic Force Modification Factors for the Proposed 2005 Edition of the National Building Code of Canada" Canadian Journal of Civil Engineering, 30(2), 308-327.

46. Moncarz, P., and Krawinkler, H. (1981). "Theory and Application of Experimental Model Analysis in Earthquake Engineering" Report No. 50, John A. Blume Earthquake Engineering Center, Department of Civil and Environmental Engineering, Stanford University, Stanford, CA, USA.

47. Mosalam, K., Mahin, S. and Rojansky, M. (2003). "Evaluation of Seismic Performance and Retrofit of Lightweight Reinforced Concrete Shear walls" ACI Structural Journal, 100(6), 693-703.

48. MTS Systems Corporation (2011). "Multi-purpose System Software" MTS, Minneapolis, USA. www.mts.com

49. NBCC (2005). "National Building Code of Canada, 12th ed." National Research Council of Canada, Ottawa, ON.

50. Orakcal, K. and Wallace, J. W. (2006). "Flexural Modeling of Reinforced Concrete Walls-Experimental Verification" ACI Structural Journal, Vol. 103, No. 2, p 196-206.

51. Ozbakkaloglu, T., and Saatcioglu, M. (2009). "Tensile Behaviour of FRP Anchors in Concrete" Journal of Composites for Construction, ASCE, 13(2), 82-92.

52. Panneton, M., Léger, P., Tremblay, R. (2006). "Inelastic Analysis of a Reinforced Concrete Shear Wall Building According to the National Building Code of Canada 2005" Canadian Journal of Civil Engineering, 33(7), 854-871.

53. Paterson, J. and Mitchell, D. (2003). "Seismic Retrofit of Shear Walls with Headed Bars and Carbon Fiber Wrap" ASCE Journal of Structural Engineering, 129(5), 606-614.

54. Paulay, T., Priestley, M. and Synge, A. (1982). "Ductility in Earthquake Resisting Squat Shear walls" ACI Journal, 79(4), 257-269.

55. Priestley, M., Seible, F., and Calvi, G. (1996). "Seismic Design and Retrofit of Bridges" Wiley, New York.

56. Priestley, M., and Amaris, A. (2002). "Dynamic Amplification of Seismic Moments and Shear Forces in Cantilever Walls" Research Report ROSE – 2002-01, Rose School of Engineering, Pavia, Italy.

57. Priestley, M., Calvi, G., and Kowalsky, M. (2007). "Displacement-Based Seismic Design of Structures" IUSS Press, Pavia, Italy.

58. Riva, P., Meda, A. and Giuriani, E. (2003). "Cyclic Behaviour of a Full Scale RC Structural Wall" Journal of Engineering Structures, 25(6), 835-845.

59. Sabnis, G., Harris, H., White, R., and Mirza, S. (1983). "Structural Modeling and Experimental Techniques" Prentice Hall, Inc.

60. Taghdi, M., Bruneau, M. and Saatcioglu, M. (2000). "Seismic Retrofitting of Low-Rise Masonry and Concrete Walls using Steel Strips" Journal of Structural Engineering 126(9), 1017-1025.

61. Takayanagi, T. and Schnobrich, W. C. (1976). "Computed Behaviour of R/C Coupled Shear Walls" Civil Engineering Studies, SRS 434, University of Illinois, Urbana.

62. Takeda, T., Sozen, M. A. and Nielsen, N. N. (1970). "Reinforced Concrete Response to Simulated Earthquake" Journal of the Structural Division, 96(12), 2557-2573.

63. Takizawa, H. (1976). "Notes on Some Basic Problems in Inelastic Analysis of Planar R/C Structures (Part I and II)". Transactions of the Architectural Institute of Japan, **240**, 51-62, **241**, 65-77.

64. Tremblay, R. and Atkinson, G. (2001). "Comparative Study of the Inelastic Seismic Demand of Eastern and Western Sites" Journal of Earthquake Spectra, 17(2), 333-358.

65. Tremblay, R., Léger, P. and Tu, J. (2001). "Inelastic Seismic Response of Concrete Shear Walls Considering P-delta Effects" Canadian Journal of Civil Engineering, 28(4), 640-655.

66. Vecchio, F., Haro de la Pena, O., Bucci, F. and Palermo, D. (2002). "Behavior of Repaired Cyclically Loaded Shear Walls" ACI Structural Journal, 99(3), 27-334.

67. Vulcano, A. and Bertero, V. V. (1986). "Nonlinear Analysis of RC Structural Walls" Proceedings, 8th European Conference on Earthquake Engineering, V. 3, Lisbon, Portugal, pp 6.5/1-6.5/8.

68. Vulcano, A., Bertero, V. V. and Colotti, V. (1988). "Analytical Modeling of RC Structural Walls" Proceedings, 9th World Conference on Earthquake Engineering, V. 6, Tokyo-Kyoto, Japan, 41-46.